NTNU

Norwegian University of
Science and Technology

Measuring Negative Pore Pressures in Partially Frozen Saturated Soils

Johannes Gaspar Holten

Civil and Environmental Engineering
Submission date: June 2017
Supervisor: Gustav Grimstad, IBM
Co-supervisor: Steinar Nordal, IBM

Norwegian University of Science and Technology
Department of Civil and Environmental Engineering

NORGES TEKNISK-
NATURVITENSKAPELIGE UNIVERSITET
INSTITUTT FOR BYGG OG MILJØTEKNIKK

Thesis Title: **Measuring Negative Pore Pressures in Partially Frozen Saturated Soils**	Date: **19.06.2017** Number of pages: **155**	
	Master thesis	x
Name: Johannes Gaspar Holten		
Supervisor: Gustav Grimstad		
Co-supervisors: Steinar Nordal		

Abstract:

Freezing of soil is an issue which has many implications on modern infrastructure, in which frost heave plays a pivotal role. During freezing the behavior of the soil and the flow of water is altered. In an engineering perspective, it is important to grasp the driving forces behind these behavioral changes. The main contributor to frost heave is the development of a large negative pore pressure in the unfrozen water in partially frozen fine-grained soil. This negative pore pressure is termed cryosuction. The suction leads to an inflow of water to the frozen areas.

In this thesis, a freezing cell has been constructed for measurements of pressure change in a saturated soil column exposed to one-dimensional unsteady heat flow. The cell is designed, built and tested at the *Geotechnical Division* at the Norwegian University of Science and Technology. The freezing cell consists of four pressure sensors and temperature transducers. The cell was tested in an ice lab holding -3°C, and was heated from the bottom up by a cryostat holding +4°C. Multiple tests were performed using the cell, in which three yielded complete results. All tests showed good continuity in the water phase through the sample, as a clear communication of pressure were present.

The measured pressure change is the macroscopic pressure, which correlates to the suction in the thin water films adsorbed by ice and soil particles through the unfrozen water content. The largest measured suction is 8.5 kPa. Adjusted for unfrozen water content, with an estimated unfrozen water content of 10%, this equals approximately 85 kPa of cryosuction. The theoretically estimated suction is 560 kPa, which yields a large gap between calculated and measured suction. It is noted that the measured suction of 8.5 kPa equals a pressure reduction of almost 1 meter water column height, which in engineering terms is very significant, even though it is lower than the expected value.

The sample size of tests performed in this thesis is quite small as only three tests has been successfully performed. However, the general trend in the results from the tests are promising, and further tests should be performed with the cell to properly evaluate its ability to measure the cryosuction.

Stikkord:

1. Cryosuction
2. Partially frozen soils
3. Frost heave
4. Premelting

Johannes G. Holten

NTNU
Faculty of Engineering Science and Technology
Institute of Civil and Environmental Engineering

MASTER DEGREE THESIS

Spring 2017
for
Johannes Gaspar Holten

Measuring negative pore pressures in partially frozen saturated soils

BACKGROUND

Freezing of soil is a complicated process which has many implications on modern infrastructure. During freezing the unfrozen water in partially frozen soils will experience a large decrease in pore pressure, termed cryosuction. The development of negative pore pressures gives rise to an increase in water flow to the frozen areas. In an engineering perspective, it is useful to measure and quantify the cryosuction, and its effect on the water flow. Measurements on the cryosuction is also essential for use and verification of numerical simulations on the freezing of soils, such as the *Frozen and Unfrozen Soil Model* in Plaxis. The thesis is written in conjunction with the *Sustainable Arctic Marine and Coastal Technology* project.

TASK

The aim of the thesis is to:

- Perform a literature study in which the theory behind freezing soil is outlined. The study should especially focus on the development of negative pore pressures, and the behavior of water, in partially frozen soils. It should also discuss the frost susceptibility of soils and issues connected with the measurement of pore pressures.
- Design and construct a freezing cell capable of measuring negative pore pressures developed in the unfrozen water in partially frozen saturated soils.
- Perform testing of the freezing cell. Any results should be evaluated by theoretical solutions.

Professor in charge: Gustav Grimstad

Other supervisors: Steinar Nordal

Department of Civil and Transport Engineering, NTNU
Date: 15.06.2017

Gustav Grimstad

Preface

The present thesis is carried out at the Geotechnical Division at the Department of Civil and Transport Engineering at NTNU, as part of the MSc in Civil and Environmental Engineering. It was carried out during the spring semester of 2017. The thesis was written for NTNU in conjunction with the SAMCOT project for *Sustainable Arctic Marine and Coastal Technology*, in the work package *Coastal Technology*. The idea and initial design for this thesis came from prof. Gustav Grimstad at NTNU.

Trondheim, 2017-06-11

Johannes Gaspar Holten

Acknowledgment

I would like to thank my supervisor Prof. Gustav Grimstad for great help on this thesis, both in form of the idea and design for the cell produced, and also for his advice and knowledge.

I would also like to thank Prof. Steinar Nordal and Seyed Ali Ghoreishian Amiri for good discussions and guidance on this thesis. Per Asbjørn Østensen has contributed with installation and calibration of all equipment, as well as design of the computer program used. Frank Stæhli has been a great help with the construction of the cell, both in form of practical help and discussions about materials and methods. I would also like to thank my fellow geotechnical students, and especially Christian Strømme Ofstad, for the many discussions we have had, and the impact it has made on the progress on this thesis.

Lastly I would like to thank my wife Silje for her continuing support during the work on this thesis. You always brighten up my day, and I'm forever thankful you're in my life.

J.G.H.

Summary

Freezing of soil is an issue which has many implications on modern infrastructure, in which frost heave plays a pivotal role. During freezing the behavior of the soil and the flow of water is altered. In an engineering perspective, it is important to grasp the driving forces behind these behavioral changes. The main contributor to frost heave is the development of a large negative pore pressure in the unfrozen water in partially frozen fine-grained soil, termed cryosuction. The suction leads to an inflow of water to the frozen areas. It is important to be able to estimate the cryosuction to predict the inflow of water, and also to quantify its impact on the stress state in the soil.

In this thesis, an apparatus has been constructed for measurements of pressure change in a saturated soil column exposed to one-dimensional unsteady heat flow, called a freezing cell. The cell is designed, built and tested at the *Geotechnical Division* at the Norwegian University of Science and Technology. The freezing cell consists of four pressure sensors and temperature transducers. The cell was tested in an ice lab holding -3°C, and was heated from the bottom up by a cryostat holding +4°C. Multiple tests were performed using the cell, in which three yielded complete results. All tests showed good continuity in the water phase through the sample, as a clear communication of pressure were present.

The soil used for testing was a silt. 6% of the material was larger than $74\mu m$, and 2.5% was smaller than $2\mu m$. The soil was deemed to be medium to very frost susceptible by inspecting mineralogy, grain-size distribution, void ratio and overburden pressure.

The measured pressure change is the macroscopic pressure, which correlates to the suction in the thin water films adsorbed by ice and soil particles through the unfrozen water content. The largest measured suction is 8.5 kPa. Adjusted for unfrozen water content, with an estimated unfrozen water content of 10%, this equals approximately 85 kPa of cryosuction. The theoretically estimated suction is 560 kPa, which yields a large gap between calculated and measured suction. It is noted that the measured suction of 8.5 kPa equals a pressure reduction of almost 1 meter water column height, which in engineering terms is very significant, even though it is lower than the expected value.

The sample size of tests performed in this thesis is quite small as only three tests has been successfully performed. However, the general trend in the results from the tests are promising, and further tests should be performed with the cell to properly evaluate its ability to measure the cryosuction.

Sammendrag

Frostdannelse i jord er en stor utfordring knyttet til moderne infrastruktur, hvor telehiv spiller en sentral rolle. Når jord fryser endres oppførselen og vannstrømningsmønsteret. I et ingeniørperspektiv er det viktig å forstå drivkraften bak endringene. Den viktigste bidragsyteren til telehiv er utviklingen av et stort negativt poretrykk, kalt kryogenisk sug, i det ufrosne vannet i den delvis frosne jorden. Suget fører til en tilførsel av vann til de frosne områdene. Det er nødvendig å kunne estimere det kryogeniske suget for å kunne forutse den økte vanntilførselen til jorden, og også for å kunne kvantifisere sugets påvirkning på spenningstilstanden i jorden.

Det er konstruert et apparat for måling av trykkendring i vannmettet delvis frossen jord utsatt for endimensjonal ikke-stasjonær varmestrøm, kalt en frysecelle. Cellen er designet, bygget og testet ved Geoteknisk Avdeling ved Norges teknisk-naturvitenskapelige universitet. Frysecellen består av fire trykk- og temperatursensorer. Cellen ble testet i en is-lab som holdt -3°C, og ble oppvarmet fra bunnen ved et varmeelement som holdt +4°C. Flere tester av cellen ble gjennomført, hvorav tre ga fullstendige resultater. Alle tester viste god kontinuitet i vannfasen i jordsøylen.

Jorden som ble brukt til testing var en silt. 6% av materialet var større enn 0,074 mm, og 2.5% var mindre enn 0,002 mm. Jorden ble ved inspeksjon av mineralogi, kornfordeling, poretall og vertikal belastning, ansett å være medium til veldig frost-mottakelig.

Den målte trykkendringen i cellen er det makroskopiske trykket, som korrelerer med det kryogeniske suget i vannfilmene adsorbert av is og jordpartikler gjennom det ufrosne vanninnholdet. Det største målte suget var 8.5 kPa. Justert for et estimert ufrossent vanninnhold på 10%, tilsvarer dette omtrent 85 kPa kryogenisk sug. Det teoretisk estimerte suget var 560 kPa, hvilket som gir et stort sprik mellom beregnet og målt sug. Det bemerkes at det målte suget på 8.5 kPa tilsvarer en trykkreduksjon på nesten 1 meter vannsøyle, noe som i geotekniske termer er signifikant, selv om det er lavere enn forventet verdi.

Da antallet tester som er utført i forbindelse med denne masteroppgaven er relativt få er det vanskelig å si noe definitivt om frysecellens kapasitet. Den observerte generelle trenden i resultatene fra testene er derimot lovende. Ytterligere tester av frysecellen bør utføres for å evaluere dens evne til å måle kryogenisk sug.

Contents

List of Tables

List of Figures

Nomenclature

Letters

A	Area
c_v	Consolidation coefficient
d_{50}	Mean particle sizes
d_{50}(FF)	Mean particle sizes of the fines fraction
e	Internal Energy
e_0	Void Ratio
e_{min}	Minimum Void Ratio
e_{max}	Maximum Void Ratio
F_F	Amount of fines
F_V	Amount of fines at porosity n_F required to fill the pore space of a coarser sand structure at a porosity n_C
g	Gravitational constant
G	Gibbs free energy
h	Enthalpy
h_v	Henry's volumetric coefficient of air solubility
i	Potential gradient
i_c	Critical potential gradient
k	Permeability
$\overline{K}_f$	Overall permeability of the frozen fringe
l	Latent heat of fusion
L	Length
m_s	Mass of solid
m_w	Mass of water
M	Oedometer Modulus
n	Porosity

n_c	Porosity of fines
n_f	Porosity of coarse material
N	Number of freeze-thaw cycles
p	vapor pressure on water column
p_0	vapor pressure on free water
p_i	Ice pressure
p_w	Water pressure
P	Pressure
P_e	Overburden pressure
q	Water Flow
q_h	Heat Flow
r	Curvature radius
r_f	Relative fines content
R	Gas constant
R_p	Pore radius
R_s	Filter pore radius
s	Entropy
S	Cryosuction
S_f	Suction at the frost front
S_i	Suction at the ice lens
$S_{measured}$	Measured suction
S_{sat}	Degree of saturation
SP	Segregation Potential
t	Time
T	Temperature
T_0	Temperature at a given pressure
T_F	Temperature at freezing front
T_m	Bulk freezing temperature at 1 atm
T_s	Segregation-freezing temperature
T_{sf}	Segregation-freezing temperature at initiation of new ice lens
T_{sm}	Segregation-freezing temperature when the ice lens stops growing
ΔT_f	Temperature gradient within the frozen fringe
u	Pore pressure
$\overline{u}$	Average pore pressure

u_{alt}	Altered measured pore pressure
u_c	Air entry value
$u_{hydrostatic}$	Hydrostatic pore pressure
$u_{measured}$	Measured pore pressure
v	Specific Volume
$\tilde{v}$	Average water influx
v_u	Velocity of the pore water entering the unfrozen soil
V	Volume
V_p	Volume of pores
V_s	Volume of solids
w	Water content
w_L	Liquid limit
w_m	Mechanical work
w_s	Work performed in a system
W	Weight
W_w	Weight of water
W_S	Weight of solid material
z	Depth

Greek Symbols

β	Compressibility of pore air-water mixture
β_w	Compressibility of water
$\Delta\beta$	Added tertiary compressibility
ϵ	Strain
γ	Soil unit weight
γ'	Adjusted soil unit weight
γ_d	Dry unit weight
γ_w	Unit weight of water
λ	Thermal conductivity
ρ_d	Dry density
$\rho_{d,max}$	Maximum dry density
ρ_i	Ice density
ρ_s	Solid particle density

σ	Total stress
σ'	Effective stress
σ^*	Solid phase stress
σ_s	Surface tension of hydraulic fluid
σ_t	Surface tension of water
Ψ	Soil Water Potential
Ψ_g	Gravitational Potential
Ψ_m	Matric Potential
Ψ_o	Osmotic Potential
Ψ_p	Pressure Potential
θ_{uf}	Unfrozen water content

Mathematical denotation

d	Change
Δ	Incremental change
∂	Partial differentiate

Chapter 1

Introduction

Freezing of soil is an important subject with great implications on the modern infrastructure. Several issues arises as a consequence of freezing, such as frost heave, which causes difficulties on roads and foundations all over Norway. The primary cause of frost heave is often prescribed to the volume increase of freezing water. However, experiments dating back as far as 1914 shows that the development of a negative pore pressure in the soil is the main contributor to frost heave. This process is termed cryosuction and occurs when parts of the pore water is unavailable to freeze due to interfacial forces between the soil particles and the pore water. Cryosuction leads to a inflow of water to the freezing ground which leads to vertical expansion of the ground.

Measurements of the cryosuction has previously been performed, but not without difficulty. When measuring large negative pore pressures in the unfrozen water in partially frozen soils cavitational issues often arise. The systems are often prone to develop air bubbles which may disturb the measurements. There is also an issue with measuring pressure in the thin layers of unfrozen water, which is at the nano-scale.

Measurements of cryosuction is performed in apparatus in which a soil sample is subjected to a thermal gradient. Such an apparatus is called a freezing cell. For this thesis a freezing cell was constructed by the author. The cell was designed with inspiration from similar cells. The cell was tested on fine-grained soil material, and the results evaluated by theoretical solutions based on constitutive models. The freezing cell were constructed in collaboration with the *Geotechnical Laboratory*, the *Road and Transportation Laboratory* and *Fellesverkstedet* at the department of Civil and Transport Engineering at the Norwegian University of Science and Technology (NTNU).

The thesis is written considering use with the *Frozen and Unfrozen Soil model* in PLAXIS. The soil model describes the mechanical behavior of frozen soils. The model is produced

as a collaboration between NTNU and PLAXIS. The thesis is written in conjunction with the *SAMCoT* project (Sustainable Arctic Marine and Coastal Technology), under the work package *Costal Technology*.

1.1 Objectives

The main objectives of this project are to:

1. Perform a literature study in which the theory behind freezing soil is outlined. The study should especially focus on the development of negative pore pressures, and the behavior of water, in partially frozen soils. It should also discuss the frost susceptibility of soils and issues connected with the measurement of pore pressures.

2. Design and construct a freezing cell capable of measuring negative pore pressures developed in the unfrozen water in partially frozen saturated soils.

3. Perform testing of the freezing cell. Any results should be evaluated by theoretical solutions.

1.2 Structure of the Report

The thesis is structured as follows. ***Chapter 2*** gives an introduction to the theory of freezing soil, which involves a physical interpretation of cryosuction, soil parameters governing the behaviour of freezing soils and the propagation of the freezing front through a soil column. ***Chapter 3*** describes the freezing cell produced in this thesis in detail and presents the design and materials used, in addition to the procedure used during testing. ***Chapter 4*** describes the soil used for testing the freezing cell. ***Chapter 5*** presents the results from the performed tests of the freezing cell. ***Chapter 6*** gives a discussion and evaluation of the results from the tests. ***Chapter 7*** concludes the findings and suggests further work to be done.

Chapter 2

Theory

In this chapter, the processes which are measured in the freezing cell are described, and the theoretical background for freezing of soil is presented. This includes the background for the development of negative pore pressures, and the behavior of water, in partially frozen soils, an assessment of pore pressure behavior and the formation of ice lenses in the soil, as well as discuss the frost susceptibility of soils and issues connected with the measurement of pore pressures.

2.1 Freezing of Soil

Freezing of soil is an important subject for many reasons. From elementary courses in geotechnics it is well know that the distribution of stresses in soil is a product of the overburden stress, the grain-size, void ratio, water content and more. As a soil is exposed to a freezing environment it is then imperative to understand how the freezing of pore water changes the pore pressure and effective stresses in the soil, and how it impacts the water flow. The primary cause of frost heave is often prescribed to the volume increase of freezing water. However, experiments dating back as far as 1914 shows other important contributing factors. In 1914 Simen Johansson proved experimentally that water flows towards the freezing front, and that this accumulation of water was a large contributor to frost heave (Beskow, 1935). Other experiments performed by Taber (1930, 1929) and Casagrande (1932) showed that even if the water is substituted by a liquid with constant or decreasing volume upon solidification frost heave still occurs due to the water flow to the freezing front. From what we know of pore pressures, water flow and soil behavior this inflow of water must be due to a decrease of pore pressure, or suction in the free water. This will be explored further in the coming section.

2.2 Relevant Properties of Partially Frozen Soils

2.2.1 Thermal Conductivity

Thermal conductivity is an important parameter when discussing thermodynamics of soil moisture. The thermal conductivity of a material is a measure of the rate at which heat energy, or molecular kinetic energy, flows across a unit area of the soil due to a unit temperature gradient (Farouki, 1986). Thermal conductivity is highly dependent upon the saturation and dry density of the soil, as well as the temperature itself. Soil grains, water vapor, ice and liquid water have different thermal conductivity. The proportion of each component has a great impact on the combined thermal conductivity of the material. Figure 2.1 shows the thermal conductivity of a frozen peat as a function of dry density and water content, and illustrates the dependence upon dry density saturation.

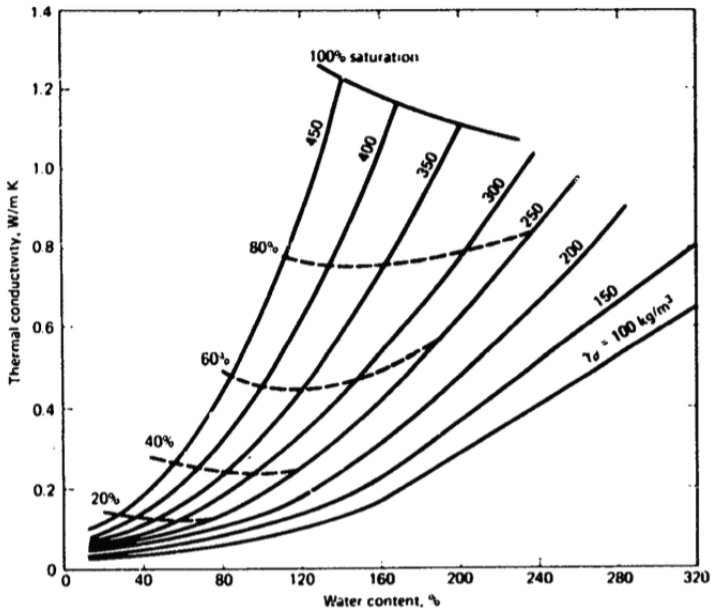

Figure 2.1: Variation in thermal conductivity with respect to water content and dry density (Andersland and Anderson, 1978)

Heat is transferred either as convection, conduction, or radiation. The most important heat transfer in soil is conduction, but convection is also important, as water and air may circulate in the soil. Air-convection is assumed not to be important in this thesis as we assume fully saturated soils. Water flow, and thereby transportation of heat within the soil by convection, is relevant for the one-dimensional unsteady heat flow, but is hard to quantify as the water flow is dependent upon both pressure and temperature. Ice has a greater thermal conductivity than water, see figure 2.2, and a decreasing unfrozen water content in the soil leads

to an increasing thermal conductivity (Fredlund et al., 1991). Water-convection decreases as the unfrozen water content decreases. The total effect of increased conduction due to ice content and decreased convection is not implicitly given by investigating at a principal level. Specified thermal properties for water and ice are given in appendix A.

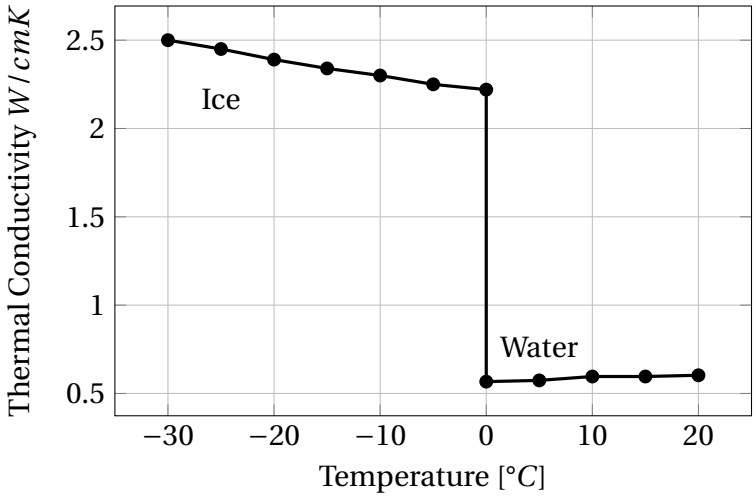

Figure 2.2: Thermal conductivity of water and ice at various temperatures (Van Wijk et al., 1963)

2.2.2 Unfrozen Water Content

Unfrozen water content is the amount of water in frozen soils that has not crystallized as ice. As the temperature decreases below 0°C the unfrozen water exists as free water held by the soil particles (Williams, 1964). The amount of unfrozen water content is directly associated with the suction in the free pore water. Figure 2.3 shows a characteristic relationship between temperature and unfrozen water content in silt and clay. The unfrozen water content is given as the volumetric ratio between unfrozen water on the unfrozen and frozen water (Ghoreishian Amiri et al., 2016).

2.3 Cryosuction

As mentioned earlier the effects of frost heave can largely be contributed to a suction in the pore water in the soil which leads to accumulation of water. This suction is often referred to as cryosuction. In other words, cryosuction is a term for the negative pore pressures induced by a negative thermal gradient in partially frozen soils (Konrad and Morgenstern, 1980). The negative pore pressure is dependent upon several soil parameters such as permeability, temperature, and continuity of pore water (Hohmann, 1997). Thermodynamically it can be as-

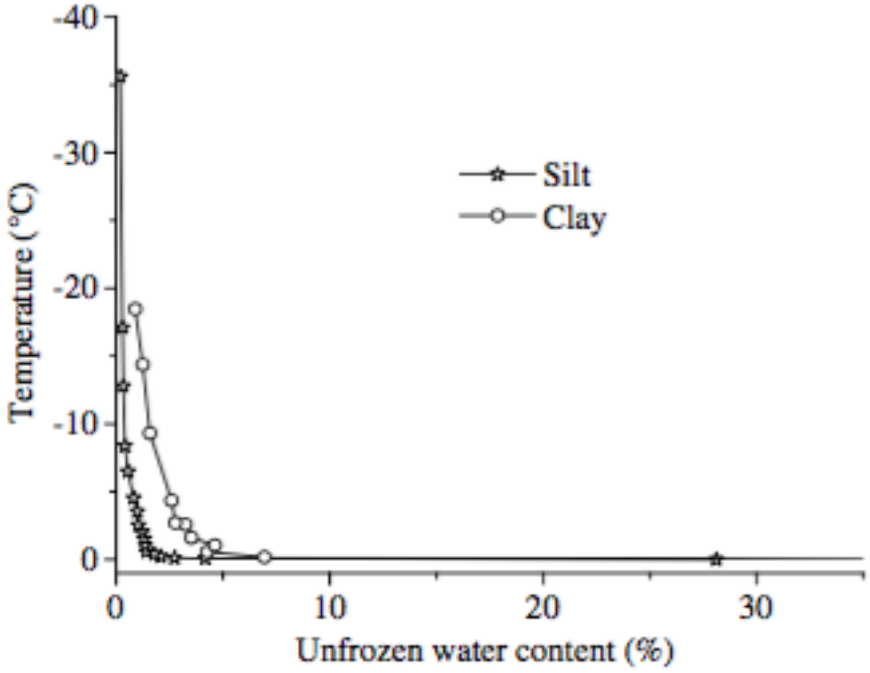

Figure 2.3: Soil freezing characteristics (Ma et al., 2015)

cribed to difference in free energy within the pore water, and the depression of the freezing temperature of water, which will be presented more in depth in section 2.3.2.

To give a sufficient physical account of cryosuction it is necessary to investigate what happens in the pore water at a micro level. It is useful to use concepts as free energy and soil water potential to describe the process.

2.3.1 Soil Water Potential

It is useful to establish a concept for expressing the pressure in the pore water, relative to free water. The pressure condition of the pore water in soil is complicated and depend upon several factors., and introducing temperature as a variable complicates matters further. It is common to use the soil water potential as an equipment to describe the pore pressure. Several factors determine the total soil water potential such as the attraction of soil particles and gravitational effects. In the general case, the total soil water potential is, according to Hohmann (1997), defined as:

$$\Psi = \Psi_g + \Psi_p + \Psi_o + \Psi_m \tag{2.1}$$

where Ψ_m is the matric potential, Ψ_g is the gravitational potential, Ψ_p is the pressure potential and Ψ_o is the osmotic potential.

As a reference for the establishment of soil water potential, we define a reference body of water. The reference body consists of free, pure, and unbound water at the same temperature and elevation as the pore water in question. The soil water potential is then the required alteration in pressure necessary to bring the reference body and pore water in equilibrium. There is no flow between points of equal potential, which indicates that the equilibrium condition requires $\Delta\Psi = 0$. Flow only occurs between points of different potential, and will always move in the direction of lesser potential, as can be seen from equation 2.2 (Hohmann, 1997).

$$q = kA\frac{\Delta\Psi}{\Delta z} \tag{2.2}$$

where q is water flow, A is cross-sectional area, k is permeability and $\Delta\Psi/\Delta z$ is the gradient of potential. An evident consequence of equation 2.2 is the important role of permeability on development of pressure gradients, as a small permeability k requires a larger gradient to induce water flow.

Gravitational Potential

Gravitational potential is a contribution to the total soil water potential due to gravitational effects on the water. The gravitational potential is caused by difference in elevation, or head, between different points of the soil water (Hohmann, 1997), and can be compared to potential energy.

Pressure Potential

The pressure potential appears due to the overlying masses. Given hydrostatic pore pressure under drained conditions at approximately constant temperature the pore pressure at a given depth z, and for given water density γ_w, is given by equation 2.3 (Emdal, 2014).

$$\Psi_p(z) = \gamma_w z \tag{2.3}$$

Osmotic Potential

The osmotic potential contribution is given by effects of ions and other solutions in the soil water (Edlefsen et al., 1943). By definition, the osmotic pressure of pure water is zero. Solutions in the water will have a negative effect on the pore water potential, i.e. $\Psi_o \leq 0$.

Matric Potential

Matric potential is a pressure potential which is characteristic to the material itself, and is often referred to as capillary potential. The potential is a result of molecular forces, i.e. the adsorptive forces between soil particles and soil moisture in the pores. The matric potential is the sum of capillary forces and adsorptive-force-field attractions.

The classic example of matric suction is water rising within a tube of very small diameter, connected to a pool of water with a free surface. Since the water molecules are more strongly attracted to the tube walls then they are to the other water molecules, the surface tension between the water and the vapor within the tube allows the water to climb up into the tube. The soil water potential is equal throughout the liquid after the water has risen into the tube. It is evident that the surface tension has a negative contribution on the pressure, which makes the water rise to equalize the pressure difference. The relation between the vapor pressure and water pressure is given by equation 2.4 (Edlefsen et al., 1943).

$$ln\frac{p}{p_0} = \left(\frac{v}{RT}\right)\frac{2\sigma_t}{r} \tag{2.4}$$

where σ is the surface tension of the water, r is the radius of curvature, p_0 is the vapor pressure on the free water, p is the vapor pressure on the water column, v is the specific volume, R is the gas constant and T is the temperature in kelvin.

Consider water trapped within the pores separating soil grains in a partially saturated soil, as the one given in figure 2.4. The dotted line f illustrates the adsorptive force field which surrounds the soil particles. These force fields attract the water. Point k might then be subjected to a negative pressure, relative to 1 atm. Water at point s will be subjected to compression.

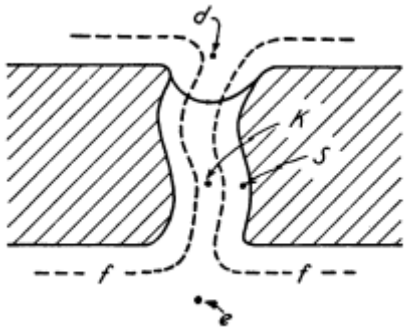

Figure 2.4: Water adsorbed by soil grains (Edlefsen et al., 1943)

The attraction the soil water experiences from the soil grains is the capillary potential. The definition of this potential is the work required to pull a unit mass of the water away

from a unit mass of the grains (Farouki, 1986).

2.3.2 Gibbs Free Energy

In explaining the negative pore pressure that arises in freezing soil, the theory of soil water potential is lacking. Changes in potential due to temperature changes cannot be described through the soil water potential theory. It is therefore useful to introduce a concept of thermodynamic potential which takes temperature and pressure into account, and at the same time is less general than entropy (Hohmann, 1997). Gibbs free energy, hereafter referred to as free energy, is such a thermodynamic potential. In the most general case free energy is defined as:

$$G = h - Ts = e + Pv - Ts \tag{2.5}$$

where h is the enthalpy of the system, T is the temperature, e is internal energy, v is the specific volume and s is the entropy (Edlefsen et al., 1943). One of the main uses of free energy is to predict whether a reaction or process will be spontaneous (Brady, 1990). By definition, a process is spontaneous if the change in free energy is negative, i.e. $dG < 0$ (Edlefsen et al., 1943). Differentiating equation 2.5 we get:

$$dG = de + Pdv + vdP - Tds - sdT \tag{2.6}$$

where $de = dq_h - dw_s = Tds - dw_s$ for any reversible process according to the first law of thermodynamics (Clausius, 1867). q_h is heat flow and w is work in the system. We further use that total work performed on a system is equal to the contributions from the work of expansion against a pressure, and the mechanical work, i.e. $dw_s = Pdv + dw_m$, which when inserted into equation 2.6 yields:

$$dG = -sdT + vdP - dw_m \tag{2.7}$$

Comparison of Free Energy and Soil Water Potential

Comparing the notion of free energy with soil water potential there are many similarities, according to Edlefsen et al. (1943), which result, among other things, in the spontaneous movement of soil moisture from wet soils to drier soils, given constant temperature and pressure, and continuity in soil moisture.

1. *Equilibrium condition:* Both notions share the equilibrium condition which requires

that for any infinitesimal change of the system the change in potential must be zero, i.e. $\Delta G = 0$ and $\Delta \Psi = 0$.

2. *Spontaneous change:* Both notions also requires a negative change in potential for spontaneous change to transpire, i.e. $\Delta G < 0$ and $\Delta \Psi < 0$. Any spontaneous change must lead to a reduction of the total energy, and equilibrium is not reached until there is no path for the free energy or the potential to be reduced further.

Free Energy in a System Consisting of Multiple Phases of the Same Substance

In this section, we assume that no work is performed on the system ($dw_m = 0$), and that energy is dissipated as heat. In an isolated system consisting of a substance in multiple phases it is necessary to specify that the free energy term G refers to absolute specific free energy per unit mass of the substance in a single phase (Edlefsen et al., 1943).

For two phases coexisting in equilibrium, such as water and ice, any change of free energy in either phase must equal the change in the other phase. This is under the condition of constant temperature and pressure. For a finite change of energy due to, for example, the melting of 1 gram ice, the change in free energy will be given as:

$$dG = G_2 - G_1 = 0 \tag{2.8}$$

which, if rewritten, gives:

$$G_1 = G_2 \tag{2.9}$$

Considering water and ice in a closed system, where the substances are in equilibrium at $0°C$ and 1 atm. pressure. We want to explore what effect a change in temperature or pressure has on the free energy, if we require equilibrium between the two phases. We associate G_1, s_1 and v_1 with the ice phase, and G_2, s_2 and v_2 with the water phase. For a system in equilibrium equation 2.9 results in:

$$dG_1 = dG_2 \tag{2.10}$$

Since the free energy is perfectly differential (Edlefsen et al., 1943), the change in the free energy is given as:

$$dG_1 = \left(\frac{\partial G_1}{\partial P}\right)_T dP + \left(\frac{\partial G_1}{\partial T}\right)_P dT \tag{2.11}$$

$$dG_2 = \left(\frac{\partial G_2}{\partial P}\right)_T dP + \left(\frac{\partial G_2}{\partial T}\right)_P dT \tag{2.12}$$

Remembering equation 2.7 and 2.10 this is reduced to:

$$v_1 dP - s_1 dT = v_2 dP - s_2 dT \tag{2.13}$$

The second law of thermodynamics state that the entropy of an isolated system can never decrease, which yields $ds = dq/dT$, and directly relates into:

$$s_2 - s_1 = \frac{\Delta h}{T} \tag{2.14}$$

Inserting this into equation 2.13 yields

$$\frac{dP}{dT} = \frac{\Delta h}{T\Delta v} \tag{2.15}$$

For water Δh can be substituted with l which is the heat of fusion of ice. Then the expression is:

$$dP = \frac{l}{\Delta v}\frac{dT}{T} \tag{2.16}$$

This equation is readily known as the Clausius-Clapeyron equation. The Clausius-Clapeyron equation is a direct product of the second law of thermodynamics. The equation describes a discontinuous transition between two phases of the same substance. Phase diagram for water is given in figure 2.5. The diagram indicates which phase corresponds to different combinations of temperature and pressure. The Clausius-Clapeyron equation mathematically determines the tangent of the line of coexistence in the diagram, i.e. the conditions in which two or more phases can coexist.

By Clausius-Clapeyron equation, equation 2.16, it's clear that the freezing temperature of pore water in a confined volume is dependent upon the pressure and temperature of the water, when water is present as both a liquid and a solid. For the given situation $dT = T_M - T_0$ is the change in freezing temperature, where T_M is the bulk freezing temperature at 1 atm. pressure, and T_0 is the freezing temperature at given pressure. T is the absolute temperature of the system. Δv is the volumetric contraction of ice per unit mass upon melting.

To estimate the suction that develops in the free water when equilibrium is required between ice and free water, we rewrite equation 2.16. The suction is given as the difference in pressure between the ice phase and water (Thomas et al., 2009).

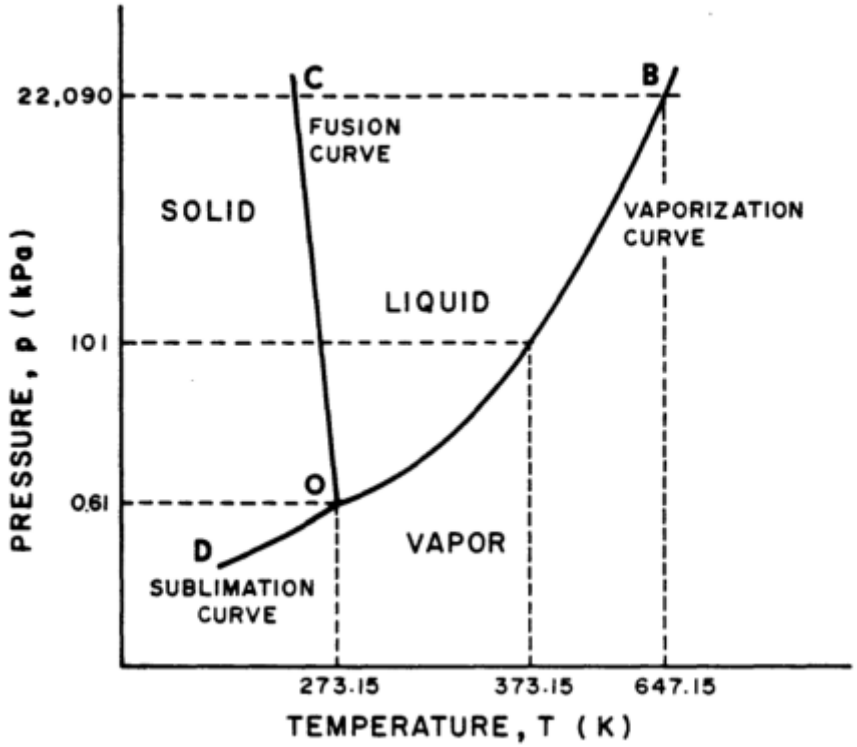

Figure 2.5: Water phase diagram (Fredlund et al., 1991)

$$S = p_i - p_w = -\rho_i l \ln \frac{T}{T_0} \tag{2.17}$$

where p_i is ice pressure, p_w is water pressure, ρ_i is ice density (which is the inverse of the specific volume). One could assume a situation where the pressure on the ice remains constant, while the pore water pressure is lowered. This assumption is somewhat false as the stress condition in the pore ice is quite complicated (Konrad and Morgenstern, 1980). However, the pressure change in free water and ice will not be equal and a suction develops.

Concluding from the mentioned theory of free energy it is evident that a situation where unfrozen water in pores are being confined in progressively smaller spaces the free energy of the water will decrease. The equilibrium between the ice and unfrozen-water is contained by water of higher free energy flowing to the pores.

2.4 One-Dimensional Unsteady Heat Flow

The specific case of one-dimensional unsteady heat flow in soil will be presented in this section. An unsteady heat flow indicates that the soil goes from a initial temperature condition and distribution to a steady state distribution. The one-dimensional example is the basis for

the freezing cell established for this thesis, and is inspired by Konrad and Morgenstern (1980) mechanistic theory of ice lens formation.

2.4.1 Assumptions

The theory presented is based on the in-situ situation of ground freezing where the ground freezes from the surface, and holds a higher temperature further down. This can be simulated by a model of a vertical soil column exposed to a one-dimensional unsteady heat flow in the vertical direction. In this section, we assume homogeneous soil regarding permeability, thermal conductivity, moisture distribution and soil properties at the initial state, as well as uniform grain-size distribution. We also assume a fully saturated soil sample, incompressibility of the soil skeleton and no overburden pressure on the soil column. The case of one-dimensional unsteady heat flow is shown in figure 2.6.

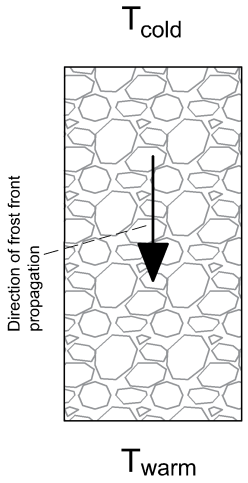

Figure 2.6: One dimensional unsteady heat flow in soil column

2.4.2 Freezing at a Macro Level

In this section, the overall freezing of a soil column will be discussed, and how this, on a macro level, changes the disposition of the soil.

As the soil is exposed to subzero temperatures freezing of the soil is initiated. It is useful to define a freezing front, in which all soil above this point has temperatures below zero, and all soil below this point has a temperature above zero. In other words, the freezing front is defined by $T_F = 0°C$. This freezing front will propagate downwards into the soil in the direction of the heat loss (Konrad and Morgenstern, 1980). The rate of freezing will be restricted by the heat flow from the ground, the transportation of heat away from the freezing front and the

latent heat released from the freezing of water. Observations and experiments have shown that in the frozen parts of the soil, i.e. above the freezing front, unfrozen water is present as adsorbed films on the soil particles. Unfrozen water exists as a result of the free energy of the water. Somewhat behind the freezing front an ice lens is formed due to the accumulation of water. Some water will lie unfrozen on this ice lens. The water flux to this ice lens comes from the unfrozen parts below the ice lens. The temperature at the base of the ice lens is denoted as T_s, and is called the *Segregation-freezing temperature*.

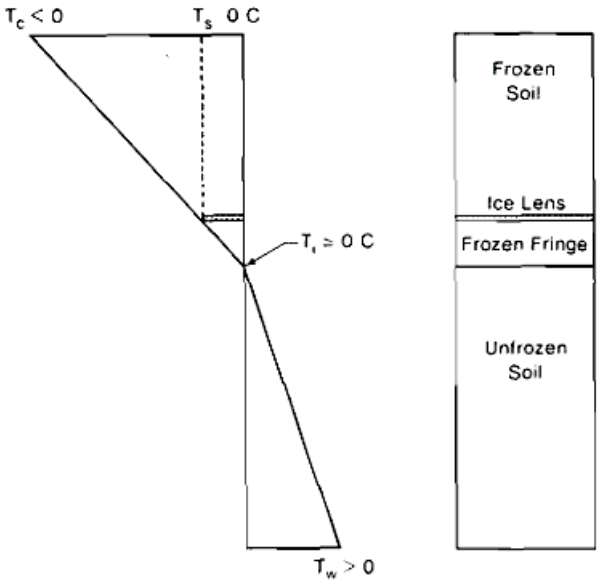

Figure 2.7: Temperature variation in soil sample with a thermal gradient (Konrad and Morgenstern, 1980)

Figure 2.7 shows a cross-section of a soil sample exposed to a freezing environment. The*frozen fringe* shown in the figure is defined as the area between the freezing front and the ice lens. In the frozen fringe the unfrozen water content decreases as one gets closer to the ice lens. The sample can be divided into a passive and an active zone. In the passive zone moisture transfer is greatly reduced due to low permeability. The passive zone has an almost negligible contribution to the total frost heave. The active zone consists of the Frozen Fringe and *Unfrozen Soil*. The characteristic property of the active zone is that most of the moisture transport takes place in this zone.

The aforementioned suction at the base of the ice lens can be approximated with equation 2.17, the Clausius-Clapeyron equation, when the ice pressure is assumed to equal atmospheric pressure for the case of zero overburden stress (Konrad and Morgenstern, 1980). It is expected that this suction will decrease the further away from the ice lens one measures. Figure 2.8 shows how characteristic parameters vary within the frozen fringe during an ad-

vancing freezing front. The temperature varies linearly within the fringe. It is interesting to observe the exponential decrease in the permeability profile as you get closer to the ice lens. There is a clear correlation between the increasing suction, and the decreasing permeability.

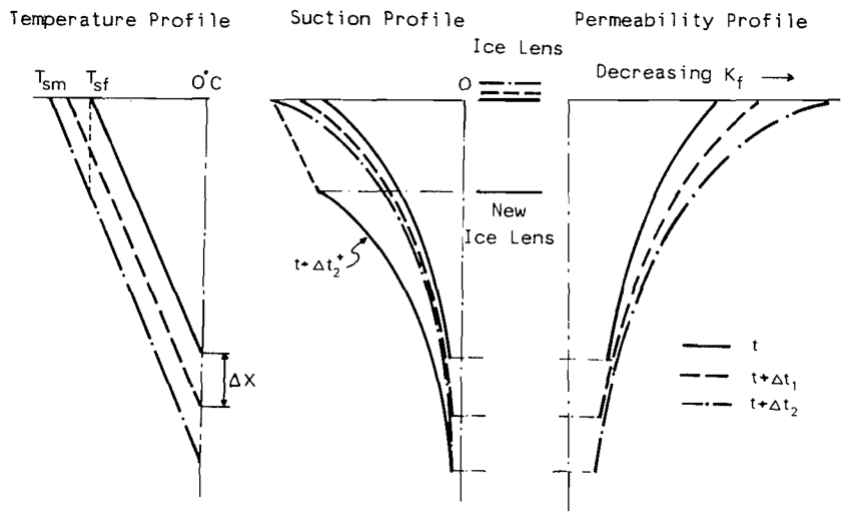

Figure 2.8: Characteristics within the frozen fringe (Konrad and Morgenstern, 1980)

Ice Lenses

The ice lens and the unfrozen water film beneath it will be in equilibrium with respect to free energy. Since it is in equilibrium at $T_s < T_F$, and the free energy is lower than that of the water in the reservoir further down, water flows towards the ice lens. The growth of the ice lens will continue until the frozen fringe permeability is reduced below a critical value. Konrad and Morgenstern (1980) estimates that the accumulation of water through the frozen fringe leads to an ice lens with a thickness of $1.09\tilde{v}\Delta t$, where $\tilde{v}$ is the average water influx during time interval Δt. Once the thickness requirement is met the ice lens growth will end. A new ice lens will start at a new point where the conditions are such that water accumulates. At this point a segregation-freezing temperature at the initiation of the ice lens, T_{sf}, can be determined. When the ice lens stops growing the temperature at the base of the ice lens is T_{sm}. Figure 2.9 shows how ice lenses are developed throughout the profile. Ice lenses will appear until the steady-state condition is reached, i.e. linear temperature variation throughout the entire profile.

Rhythmic ice lens formation will continue throughout the sample. The deeper and slower the freezing front moves, the ice lenses will become increasingly thick, as the time interval of water accumulation increases. Rhythmic ice lens formation is shown in figure 2.9.

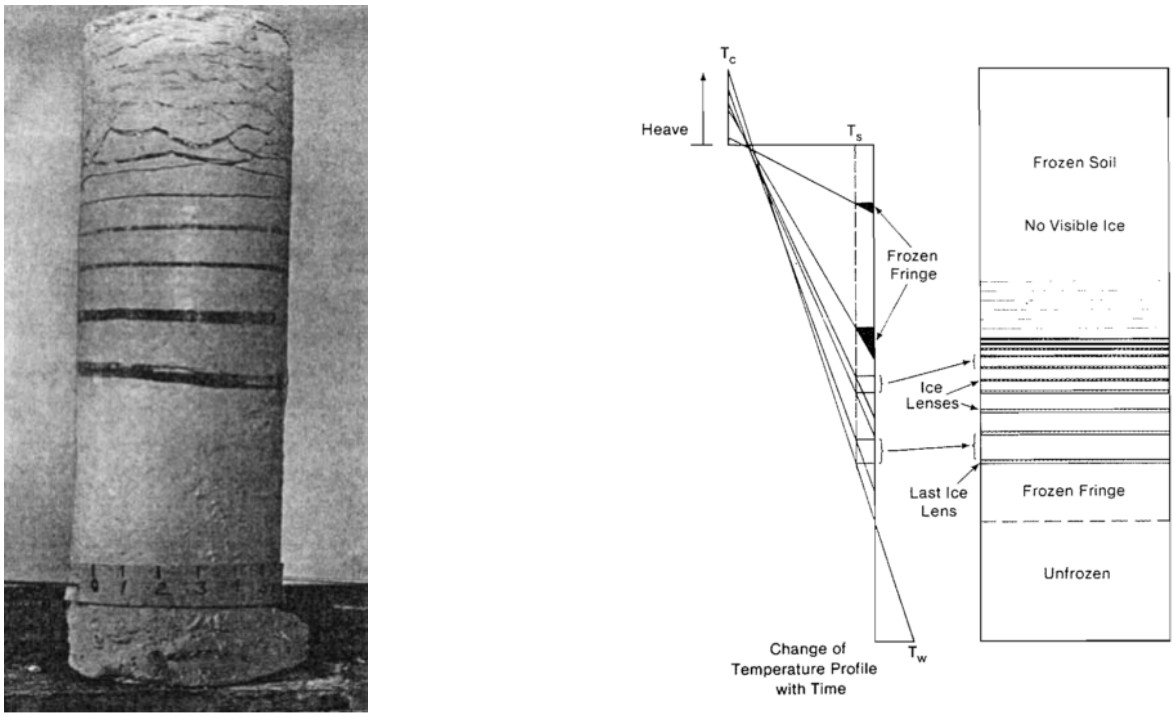

(a) Soil cylinder

(b) Schematic

Figure 2.9: Examples of rhythmic ice lens formation. Figure (a) is from Taber (1930). Figure (b) is from Konrad and Morgenstern (1980)

2.4.3 Freezing at a Micro Level

In this section, the processes that occur within the pores of a freezing soil will be discussed in detail. The freezing pattern within the soil governs how the suction is developed. The properties of water confined in partially frozen pores is also discussed. As mentioned earlier difference in free energy is the driving force of the water flow to the ice lens. Within a pore one must however look at the interfacial effect which leads to cryosuction.

Water Behavior in Confined Spaces

As water is confined and absorbed by granular particles the individual behavior changes within the water with respect to density and freezing temperature. The freezing behavior of water confined to pores of small diameters can be divided into two different areas, depending on the relative placement with respect to the soil grains. We separate the free water in the middle of the pores, and the water that is bound to the soil particles by adsorptive force fields. The freezing patterns of these two types of pore water will be quite different (Morishige and Kawano, 1999).

Water density increases with increasing distance from soil particle (Farouki, 1986), i.e. the water film around soil particles has a higher density than free water, as seen figure 2.10.

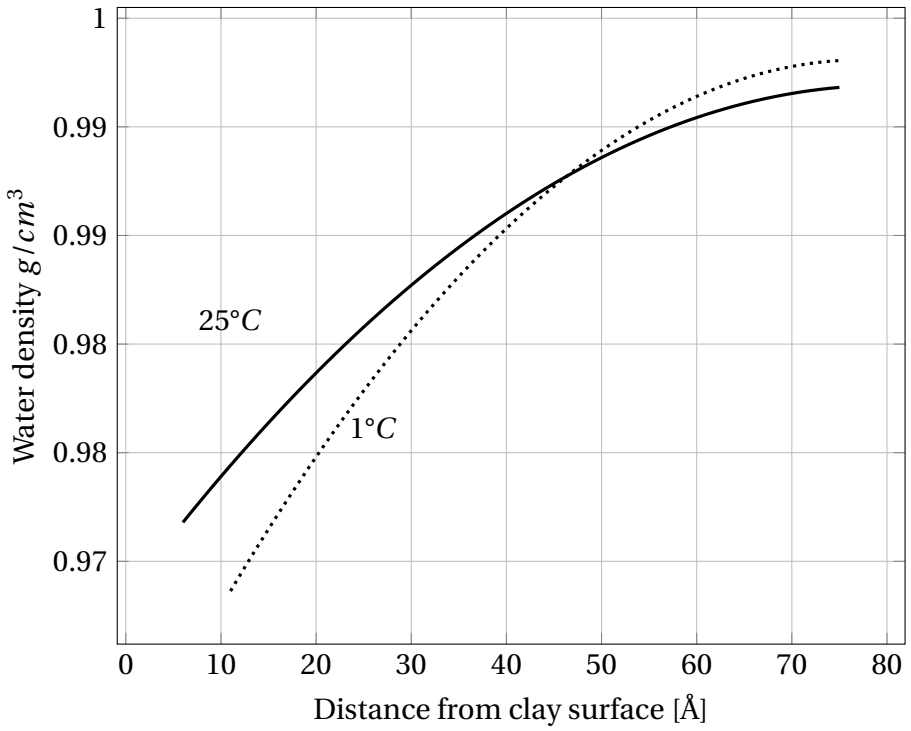

Figure 2.10: Water density for pure water at different temperatures (Low and Lovell, 1959)

It is also known to have a lower latent heat of freezing than the free water.

Kudryavtsev et al. (1978) visualized the transition from the adsorbed water to the free water through a division into three zones, as seen in figure 2.11. The figure shows the decreasing activation energy water particles are exposed to with increasing distance to the mineral surface. Zone I is referred to as *hot ice*. Water in zone II experiences dramatic changes in thermal properties. There is a depression of freezing temperature, and an increase in thermal conductivity and heat capacity. Zone III is characterized by almost free water, with nearly negligible adsorption effects. Water in zone III will crystallize when exposed to freezing temperature, while water in zone I will remain liquid. Decreasing the temperature below $0°C$ increases the surface activity (Kudryavtsev et al., 1978).

Experiments support Kudryavtsev et al. (1978) hypothesis that the absorbed water freezes at a lower temperature than the free water. Morishige and Kawano (1999) shows that there exists a linear relationship between the pore radius and the depression of the freezing temperature. The bound water is interfacially confined between the surface of the soil particles and the frozen phase of the free water. This often results in development of quasi-liquid water, or metastable cubic ice, instead of the ordinary hexagonal ice. This discovery led Morishige and Kawano (1999) to speculate that the non-freezable, bound water might exist due to the incommensurability of the crystalline structure of frozen water when it interacts with the wall surface.

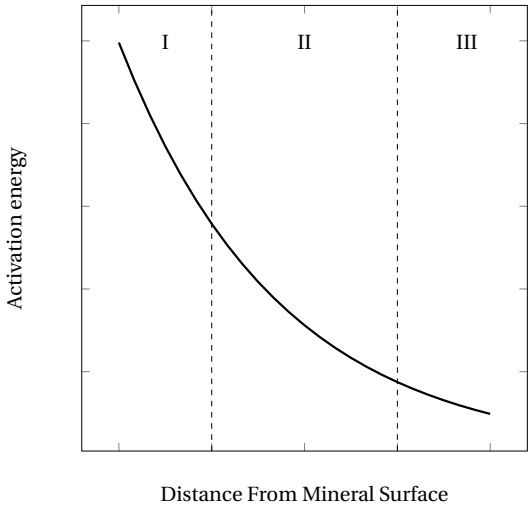

Figure 2.11: Zone structure of adsorbed water, based on Kudryavtsev et al. (1978)

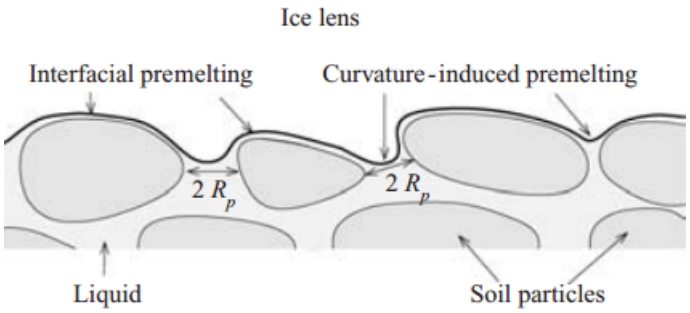

Figure 2.12: A cross-section through the region near the base of a growing ice lens (Wettlaufer and Worster, 2006)

Extending this theory is the notion of premelting of water (Wettlaufer and Worster, 2006). Premelting is a term for unfrozen water. Wettlaufer and Worster (2006) states that there are two mechanisms that allows for unfrozen water below the bulk freezing temperature. The mechanisms are schematically presented in figure 2.12 and are:

1. Interfacial premelting: A process where the equilibrium freezing temperature is reduced due to the interfacial adsorption effects on a solid-liquid interface. The liquid exists as a quasi-liquid.

2. Curvature-induced premelting: The effect is caused by the interactive forces between the water and soil particles, but the surface is concave with respect to the soil grains. This effect is dependent on the curvature denoted as $2R_p$.

Cryosuction, as observed in the adsorbed water, is then a result of the intermolecular forces which causes premelting. The low pressure appears as a drop in free energy, and water is drawn towards the ice front, increasing the size of the water film. As the water film thickens

the intermolecular forces on the water farthest away from the solid decreases until the water is allowed to crystallize.

2.5 Pore Pressure Measurements and Approximations

Effective stress is a result of the amount of the load carried by the soil grains and the pore water. In basic geotechnics, we commonly use the following equation to express the effective stress:

$$\sigma' = \sigma - u \tag{2.18}$$

As the soil freezes however a greater amount of the pores will be solid, and therefore also a greater amount of the stress will be carried by the solid phase. This *solid phase stress* can be expressed by (Ghoreishian Amiri et al., 2016):

$$\sigma^* = \sigma - \theta_{uf} S \tag{2.19}$$

where θ_{uf} is the unfrozen water saturation. This measure of stress combines the stress on the soil grains and the ice. The result is a clear connection between the unfrozen water content, the suction, and the stress state of the soil.

2.5.1 Measurements in a Freezing Cell

This thesis aims to construct a freezing cell dedicated to the measurement of suction. The basic design is presented in chapter 3. For this section, all one needs to know is that the pressure is measured within a soil sample while it is exposed to a freezing environment.

Pore pressure measurements are performed by connecting the pore water to a pressure transducer through a pressure transferring medium. One such medium is a hydraulic fluid, which in mechanical engineering is a medium which transfers power. A hydraulic fluid performs best if the fluid has a low compressibility, i.e. low volumetric reduction due to pressure and thereby acts as a rigid medium. One factor that increases the compressibility of a liquid is dissolved air that is trapped within the liquid. The compressibility of a liquid in its purest state, i.e. no dissolved air, is called the primary compressibility (Kia, 2012). If the fluid is in direct contact with air it may dissolve some of it, which leads to an increase in compressibility, called added secondary compressibility, as seen in equation 2.20. Pressure and temperature control the amount of dissolved water. When the limited amount of air has been dissolved,

all air that is trapped, but not dissolved, exists as air bubbles in the system. These air bubbles behave according to the ideal gas law, and contributes to the added tertiary compressibility, as seen in equation 2.21.

Schwab and Köhler (2003) expressed the compressibility of a pore air-water mixture through equation 2.20, where β is the compressibility of air-water mixture, β_l is the compressibility of water, S_{sat} is the degree of saturation, h_v is Henry's volumetric coefficient of air solubility and P is air pressure. The added tertiary compressibility is given as the inverse of the absolute pressure of the gas.

$$\beta = S\beta_w + \frac{1 - S_{sat} + h_v S_{sat}}{P} \tag{2.20}$$

$$\Delta\beta = -\frac{1}{P} \tag{2.21}$$

Practical Consequences

The alteration of compressibility of the hydraulic fluid is important to be considered. Especially the tertiary compressibility may be critical. *"Even a small volume "air bubble" significantly alters the compressibility of the pore fluid"* (Kia, 2012). It is wise to be aware of processes in which dissolved air may be released as air bubbles. Since the solubility of air decreases with decreasing pressure, see figure 2.13, one may expect that for an experiment as the one performed in this thesis where a negative pore-pressure is instigated, the possibility of air bubbles in the system are great. As the pressure approaches -90 kPa cavitation occurs, and one can observe air bubbles (Kia, 2012).

Magorien (1980) gives some guidelines for creating a system in which the risk of air bubbles can be minimized. Some of these measures are to de-gas the liquid in advance and to limit the amount of flow to the sample. By exerting a high velocity flow into the sample, disturbances in the soil, and the shear readiness of the process, may allow air bubbles to enter the closed system.

Pressure Filter

To separating the hydraulic fluid and the pore water one uses a porous filter. This filter is saturated with the hydraulic fluid. The basic principle is that the moisture in the filter should reach equilibrium with the surrounding pore water (Kia, 2012). The filter also ensures that the transmitted pressure is the pore water pressure, and not an extension of the total pressure.

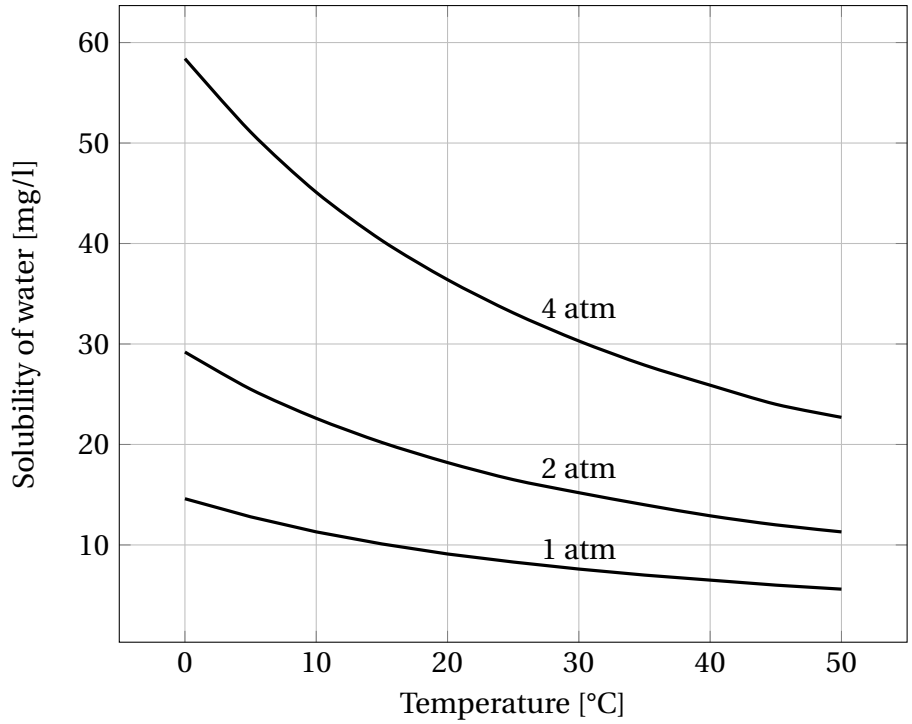

Figure 2.13: Solubility of oxygen in water under different temperatures and pressures. Values from Series (1981)

The filters should also work as a separator for the air bubbles. The filters must allow a relatively free passage of water, whilst keeping the flow of free air to a minimum. A filter with a high resistance to air entry value is a fine filter with a low permeability. Geosense (2014) defines this limit as $\approx 3 \cdot 10^{-8}$ m/s. Air entry value can be estimated by:

$$u_c = \frac{2\sigma_s}{R_s} \tag{2.22}$$

where T_s is the surface tension of the hydraulic fluid, and R_s is the radius of the openings in the filter. It should also be noted that for filters with low air entry, the permeability is low and the rate at which changes in the pressure can be measured decreases.

Measurements

For numerical analyses, we are interested in the local suction that develops in the thin layers of unfrozen water within the frozen fringe. In this thesis however, the measured values are not the local suction, but the total pore pressure at specific heights. It is important to note that, as illustrated in figure 2.11, the water films are on the nano-scale, which makes direct probing and measurements difficult (Wettlaufer and Worster, 2006), and makes it necessary to make regional measurements. The macroscopic pore pressure gradient depends on the unfrozen water content of the soil at different temperatures, as equation 2.19 shows.

To measure the suction in the individual water films one would need direct contact between the film and the pressure sensor. For larger pressure filters the contact is continuous around the filter, and the hydraulic fluid is in equilibrium with the pore water surrounding it. The measured property is an effective pore pressure. The local suction can be estimated by back-calculation of the measured pore pressure. This relation is given by:

$$S = \frac{u_{measured}}{\theta_{uf}} \tag{2.23}$$

2.6 Frost Susceptibility of Soils

Some soils are more susceptible to frost heave than others. Cryosuction will develop in the pores of fine soils rather than coarse soils. Attempts to create a frost susceptibility assessment methodology based on different parameters has been made. One such attempt has been by Konrad (1999). The paper aims to empirically relate the segregation potential and the basic soil index properties. This section will present some of the main contributing factors related to frost susceptibility, but for the entire methodology framework the reader is directed to the article.

2.6.1 Segregation Potential Theory

The frozen fringe is essential to the development of cryosuction. The phenomena can, in some regard, be an issue of impeded drainage within the frozen fringe, which means that the most important factors may be permeability and unfrozen water content. A relationship between the inflow of water to the frozen fringe, and the temperature gradient within the fringe was shown by Konrad and Morgenstern (1980, 1981). They discovered a proportional relationship, connecting the velocity v_u of the pore water entering the frozen fringe, and the temperature gradient ΔT_f. This relationship is expressed by:

$$v_u = \left(\frac{S_i - S_f}{T_s} \overline{K}_f \right) \Delta T_f = \text{SP}\ \Delta T_f \tag{2.24}$$

where SP is the segregation potential and $\overline{K}_f$ is the overall permeability of the frozen fringe. The theory is that the segregation potential could be empirically related to the most important factors affecting a soils susceptibility to cryosuction. A conceptual equation proposing important correlations is proposed as (Konrad, 1999):

$$\text{SP} = f(\text{soil type, porosity, overconsolidation ratio, pore fluid, } S_i, P_e, \text{N, ...}) \tag{2.25}$$

The segregation potential will thus describe the potential of a soil to develop segregating ice lenses, and thereby their frost heave potential. Since cryosuction is the driving force of the water inflow to the segregating ice lens, the segregation potential is a good indicator of a soils ability to develop cryosuction when exposed to a freezing environment.

2.6.2 Influencing Variables

Grain-size Distribution and Fines Content

As mentioned the grain-size distribution is one of the most important indicators of frost susceptibility. The amount of fines of diameter <0.075 mm is especially important. The deciding factor is the ratio within the soil. There is a large difference between soil of sand grains floating in silts and soils where silt is filling the pores of sand. In this regard, a proportionality factor F_V which indicates the amount of fines at porosity n_f required to fill the pore space of a coarser sand structure at a porosity n_c, under the assumption that the density of the solid particles are equal for the coarse and the fine fraction, is made.

$$\%F_V = \frac{n_c(1-n_f)}{1-n_f n_c}100 \tag{2.26}$$

The relative fines content r_f can then be determined as the ratio of fines on the fines content necessary to fill the pore volume. Experiment show that if $r_f > 12\ \%F_V$ then SP>0. One consequence of this is that a soil which is predominately sand needs only 12 $\%F_V$ of a silt before the silt determines the frost susceptibility of the soil. Figure 2.14 shows schematically how the fine fraction of a soil can dictate the freezing pattern. In a soil which is frost susceptible it is proposed to use the mean particle size of the fines fraction, d_{50}(FF), to characterize the soil. Figure 2.15 gives a visual interpretation of the frost susceptibility based on the soil type.

$$r_F = \frac{\%F_F}{\%F_V} \tag{2.27}$$

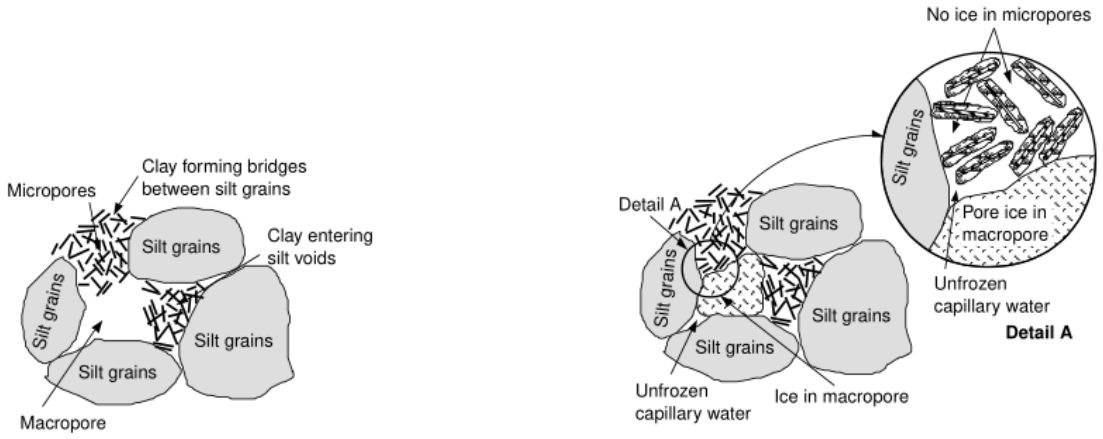

(a) Unfrozen soil

(b) Frozen soil

Figure 2.14: Schematic of phase composition of clayey silts during freezing (Konrad, 1999)

Mineralogy

The mineralogical composition of the soil in question has a great effect on the water mobility in the soil. The unfrozen water is divided amongst the capillary channels in the macro-pores and the adsorbed water in the micro-pores. The absorbed water is greatly dependent on the attraction from the mineral surfaces of the soil particles. The water mobility will vary for different mineral surfaces with different specific surface charge. A strong correlation between SP and specific surface charge has been proven, and thereby also the specific surface area of the fines fraction. If the specific surface area is large, then more water is absorbed and less is capillary water, which decreases water influx and SP. Figure 2.16 shows a relation between SP, d_{50}(FF) and mineralogy.

Density

The dependence upon the density of the soil is related to the void ratio and degree of packing of the soil. This makes intuitively sense as we know that the permeability plays an important role in frost susceptibility. In soils with a large void ratio the pore volume is large relative to the particle volume. This yields a larger volume in which the water can move. Most tests of frost susceptibility are performed on reconstituted soil of water content w above the liquid limit w_L. A relation between the water content and SP has been proposed, and experimental and field values are given in figure 2.17.

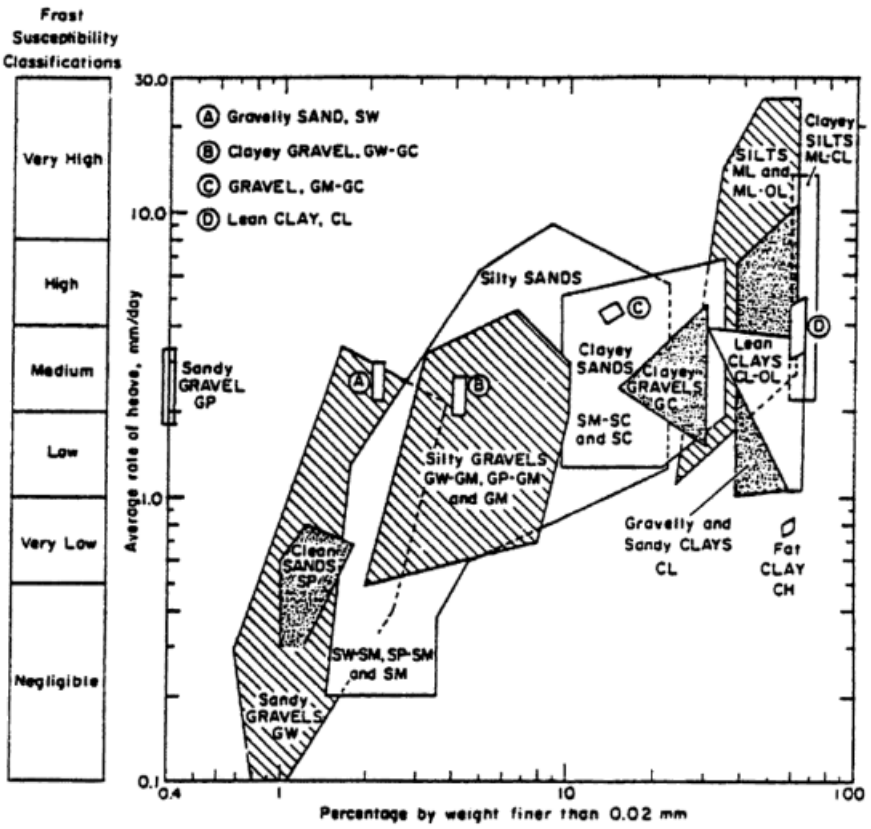

Figure 2.15: Frost susceptibility on the basis of soil type and particle size (Andersland and Ladanyi, 1994)

Influence of overburden Pressure

As one could imagine the segregation potential is also dependent on the overburden pressure on the soil. Two main aspects are worth noting. Increasing overburden pressure induces an increase in stress and decrease in segregation freezing temperature, which yields a reduction in the overall permeability. There is also the fact that an increasing overburden pressure reduces the suction at the base of the ice lens, due to the increase in total stress in the soil. The decreasing suction reduces the hydraulic gradient in the frozen fringe.

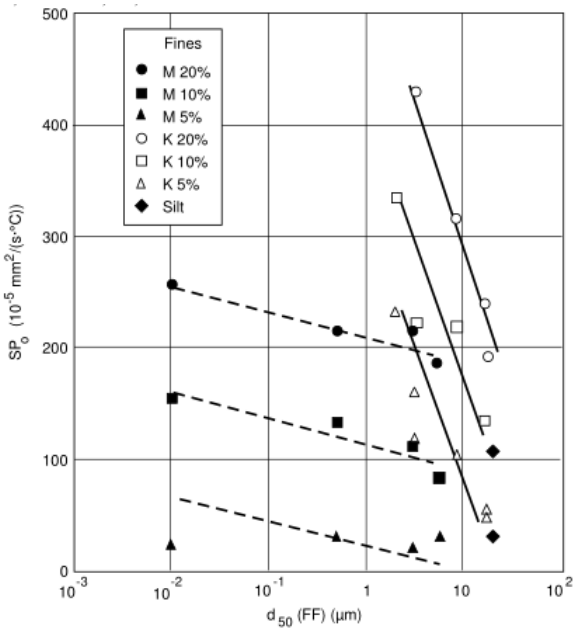

Figure 2.16: SP related to d_{50}(FF) and mineralogy (Konrad, 1999). K stands for kaolinite and M stands for montmorillonite.

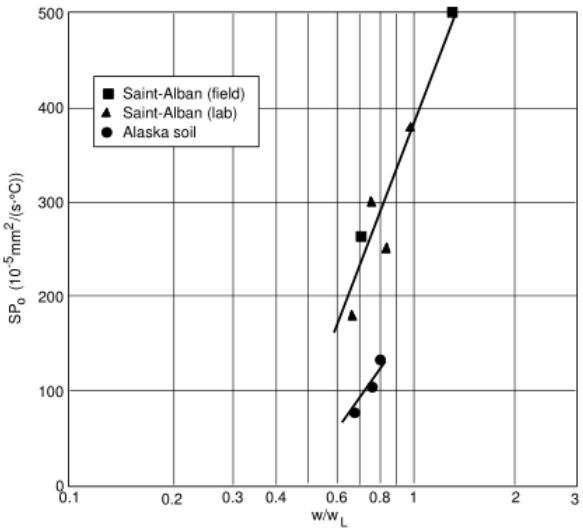

Figure 2.17: Influence of soil fabric on segregation potential (Konrad, 1999). Based on values from Konrad et al. (1995)

Chapter 3

Freezing cell

In this chapter the freezing cell constructed for this thesis is presented in detail. The cell is designed from an idea by Gustav Grimstad, with inspiration from existing freezing cells created for similar purposes, and mainly on Herzog and Boley (2013), Ingersoll and Berg (1981) and Zhang et al. (2014). The freezing cell were constructed in collaboration with the "Geotechnical Laboratory", the "Road and Transportation Laboratory" and "Fellesverkstedet" at the department of Civil and Transport Engineering at NTNU.

3.1 Design and Materials

The basic principle behind the freezing cell is the creation of one-dimensional unsteady heat flow through a cylindrical sample of reconstituted soil, with no access to free water. One-dimensional heat flow requires that no heat loss is present along other than the vertical axis. This is achieved in the cell by using insulation on the sides. The heat flow is instigated by exposing the soil sample to a thermal gradient, imposed by a temperature difference between the top and bottom of the sample. As described in chapter 2, when the freezing front propagates into the sample a negative pore pressure arises in the unfrozen water in the frozen fringe. This negative pore pressure is then measured by four pressure transducers distributed along the vertical axis of the sample. A principal sketch of the freezing cell is shown in figure 3.1

The freezing cell is built out of an insulation cube of dimensions $300x300x300mm^3$. It is assumed that all heat transfer through the insulation can be neglected. A cylindrical hole with diameter 100mm was milled out of the insulation block. In the bottom end of the cylinder an aluminum cap is placed. Beneath this cap there is a bottom piece filled with tubes connected to a cryostat. The cryostat circulates heated fluids of constant temperature

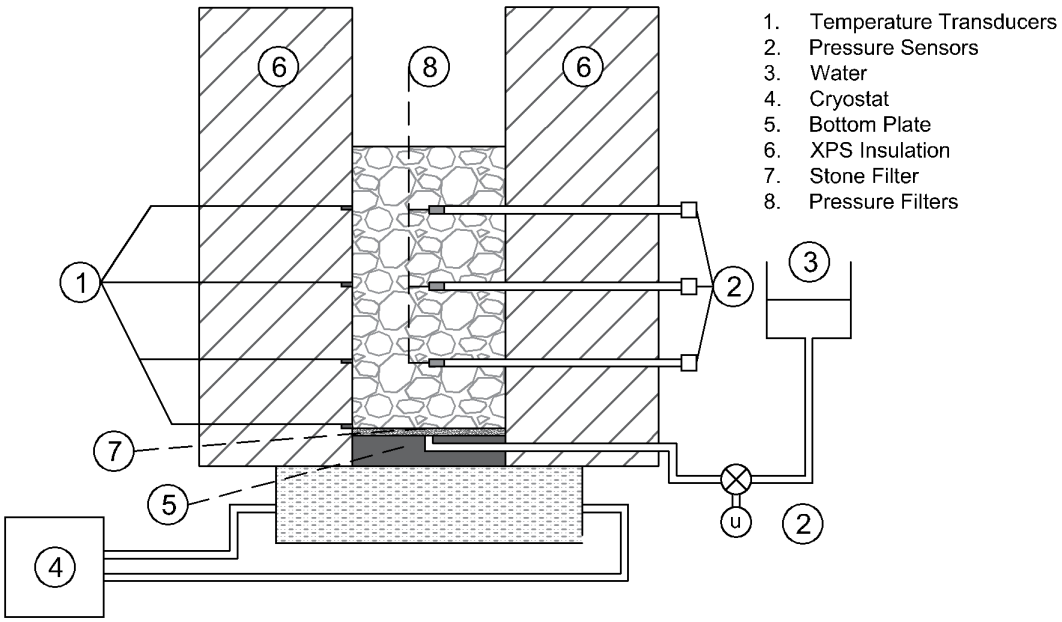

Figure 3.1: Principal sketch of freezing cell

through the bottom element, which in turn heats the aluminum cap. The top of the cylinder is open and exposed to the outside environment. The entire cell is placed inside a freezer room which holds a controlled temperature below 0°*C*.

3.1.1 Parts

In this section the different parts of the cell is presented in detail, with technical specifications and application.

Insulation

The insulation material used in the cube was *Sundolitt XPS 300*. The material has a very low thermal conductivity, with a lambda value of 0.039 W/mK at a thickness of 100 mm. The assumption of no heat loss through the insulation should be quite valid, as the minimum thickness of the cube is 100 mm (see figure 3.2). The insulation has a documented water intake of 1-3 vol.%, and is highly recommended for use in environments exposed to high amounts of moisture. For further technical specifications see appendix F.

The insulation came as plates of 60 mm thickness. These plates had to be cut and glued together to create a 300x300x300 mm^3 cube. The sealant used was an expanding wood glue, see appendix G. Using a low viscosity expanding glue ensures that all surface area is covered, and that all air-bubbles are eliminated. Attempts to glue the cube using a sealant of higher

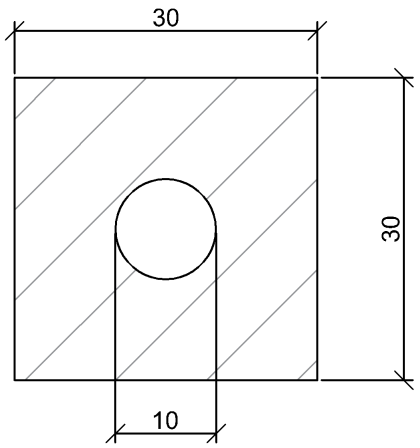

Figure 3.2: Cross-sectional view from the top of the cell with dimensions [cm]

viscosity showed the importance of having a glue that flows out to cover all available surface area. The use of the high viscosity sealant lead to major leaks through the insulation. The low viscosity expanding glue was used both between the insulation plates, and in the holes with tubing for pressure sensors and temperature transducers.

Pressure Sensor

The purpose of the pressure sensors is to measure the suction, or rather the change in pressure, within the pore water around the freezing front, as discussed in chapter 2. It is desirable to have pressure sensors which can measure at different parts of the soil column, as the freezing front propagates through the cylinder. For this aim 3 pressure sensors were distributed along the vertical axis of the cylinder, with 5 cm vertical spacing between each. The distribution is shown in detail in figure 3.3.

The pressure sensors are connected to the soil through a filter of porous stone. These filters are shown in figure 3.4. The porous filters are connected to tubing which is pulled through the insulation block. Theses tubes, as well as the filters, are filled with a mixture of ethylene glycol and water which works as a anti-freeze liquid, see appendix H. The volume ratio used is 60% water and 40% anti-freeze, which results in a freezing-point depression to -23 °C. At the end of the tube a pressure sensor is mounted.

The technical specifications of the pressure sensors used are given in appendix I. The sensors are able to measure both positive and negative pressures. Nominally the range spans to 35 kPa, but the pressure sensors can handle pressures upwards to 140 kPa. Operating temperature range for the sensors are $-40°C$ to $+80°C$. These sensors should be more than suited for the conditions under which we are testing under.

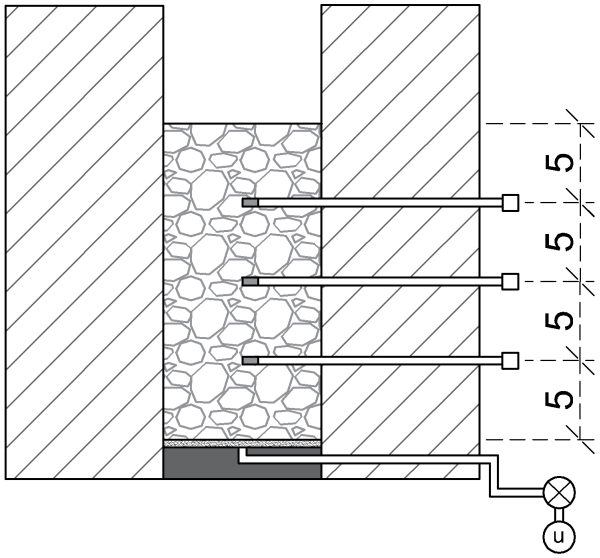

Figure 3.3: Alignment of pressure filters and temperature transducers in the freezing cell

Pressure Filters

The pressure filters, as discussed in section 2.5, must have sufficiently low air entry as to not allow air bubbles to enter the system. The filters used in the freezing cell, showed in figure 3.5, have been shown to have a permeability of $\approx 3 \cdot 10^{-10}$, which according to Geosense (2014) is sufficient for them to be classified as low entry filters. The permeability test is presented in appendix J.

Temperature Transducer

Temperature transducers are placed throughout the freezing cell, and are aligned with the pressure sensors, see figure 3.3, with the addition of one extra transducer. The cell consists of four in total. The transducers used are specified in appendix K. The transducers deliver a power of 1 μA per Kelvin. The current passes through 10 kΩ resistance, which yields 10 mV/K. The data-logger measures voltage only. The temperature transducers must be calibrated before the first test. For accurate measurements the transducers has been tested in the freezing cell with the cell filled up only by the anti-freeze solution, and situated in the freezing chamber. At the steady state the liquid held $\approx$ -3°C. Some difference in temperature with height were detected in the cell, and the sensors were calibrated against the measured temperature at their exact height.

Figure 3.4: Filter stones inside the freezing cell

Figure 3.5: Pressure Filter

Data-Logger

Both the pressure sensors and temperature transducers are connected to a *NI USB-6210* data-logger, which records the pressure and temperature data by measuring the voltage. Specifications on the data-logger is given in appendix L. The setup with the data-logger is given in figure 3.6. The specified temperature range for operating the data-logger is 0°C to 45°C. Since the data-logger is used at -3°C this might yield some sources of error, as the signal may vary.

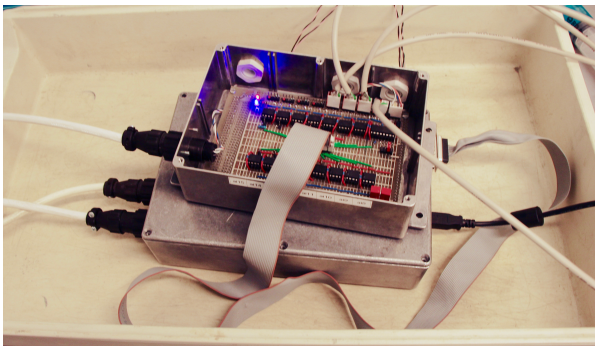

Figure 3.6: Registration device

Cryostat

The cryostat is the device used for heating in this experiment. The cryostat works by tempering a fluid and circulating it through a metal plate. The constant flow of fluid allows the cryostat to have a very low degree of inertia, and adjust temperature fast and keep the temperature relatively constant. The ambient operating range for the cryostat is 5 °C to 40 °C. For these experiments, the ambient temperature is -3 °C. However, tests performed showed good consistency in temperature, and showed the apparatus functioning as intended outside the ambient operating range. The cryostat has a temperature control error of ±0.5°C. Technical specifications for the cryostat is given in appendix M. Figure 3.7 shows the cryostat used in this thesis.

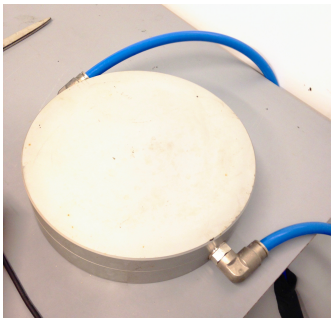

Figure 3.7: Top plate of the cryostat

Aluminum Cap

The aluminum cap is used to keep the soil in the cylinder, saturate the sample and transfer the heat from the cryostat to the soil. The plate has a diameter of 100 mm and a height of 3.4 mm. Inside the plate a continuous hole has been drilled for the plate to be able to lead water. Figure 3.8 and 3.9 shows the plate.

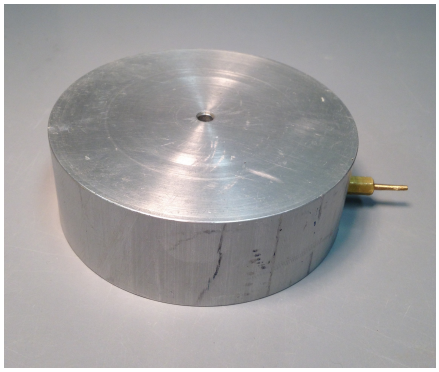

Figure 3.8: Aluminum cap

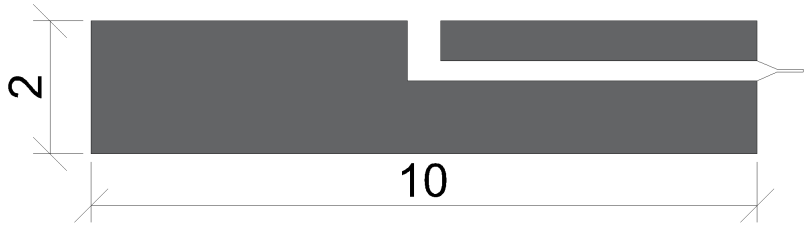

Figure 3.9: Cross-section of cap with dimensions [cm]

Bottom Filter

The bottom filter is placed in the cell to ensure an equal distribution of water whilst saturating the sample. The bottom filter is made of porous metal with thickness of 3 mm, and is saturated in a vacuum chamber in advance of testing. The filter is placed in the bottom of the cylinder, on top of the aluminum plate. The filter separates the bottom tubing from the soil. When the sample is being saturated the water flowing through the filter will disperse over its surface area. This ensures that the parts of the soil that is far away from the tubing is wetted properly. This helps in decreasing the amount of air-bubbles in the saturated soil sample.

Heating Capsule

The tubing that is drawn from the aluminum cap is drawn into a heating capsule. This capsule keeps the water in the tubing from freezing. The capsule consists of a three-folded tubing, aligned with a heating cable which holds a constant +5°C. The capsule has one intake for the pressure sensor, and one for water intake during saturation. A schematic figure, and a picture is given in figure 3.10.

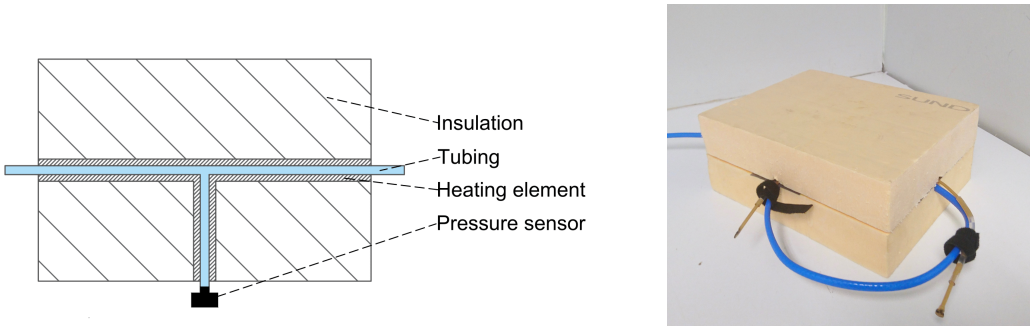

(a) Heating (b) Tubing

Figure 3.10: Insulation piece with heating element to keep the bottom pressure sensor from freezing

Ice Lab

The freezing cell is stationed in an ice lab during testing where temperatures can be controlled with quite high accuracy. The temperature in the room is constant, with a daily variation of $\pm 0.5°C$. The internal temperature and pressure will fluctuate due to the cyclic use of fans in the lab.

3.2 Procedure

In this section the procedure used for testing with the freezing cell is presented.

3.2.1 Preparation of Soil Sample

Before the testing can begin the material to be tested must be prepared. The freezing cell is made for reconstituted samples, and soil should therefore be dried in advance. The wanted density and packing ratio should be determined in advance, and one should make sure that the density can be recreated with a certain degree of accuracy. All relevant soil properties should be determined, such as grain density and specific weight of dry material.

The measured volume of the cylinder with stone filter at the bottom and porous filters for the pressure measurements is $\approx 1530 cm^3$. The volume is approximated up to the maximum soil level used in this thesis, i.e. 20 cm column height. In advance one should put to side an amount of soil that is expected to fill the cylinder volume with the given density.

In the first tests of the freezing cell the soil and water was taken directly from a room-tempered state and placed into the apparatus. This proved inefficient as it added an extra 12 to 14 hours to the testing time. The soil and water should preferably be pre-cooled to the temperature of the heating plate, i.e. $\approx$ +4°C.

3.2.2 Preparation in the Freezing Cell

This section describes the procedure for setting up the experiment. Before the soil can be prepared into the cell all enclosing parts must be prepared. In advance the porous filters must be saturated with their respective liquids, i.e. the pressure filters with anti-freeze liquids and the bottom filter with water. This is done in a vacuum chamber where they are placed until no air bubble are escaping the filters.

When preparing the cell the saturated porous stone filter tips are turned carefully into place. It is recommended to use pliers when installing the filters as not to expose the screw

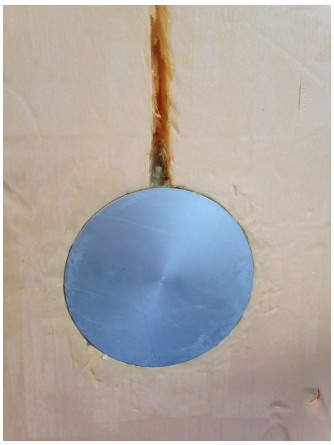

Figure 3.11: Bottom cap placed in the cell

thread, and the sealant, to a excessive pressure. The bottom filter is then carefully inserted into the bottom of the cell. Behind the filter one sheet of filter paper could be placed to separate the bottom filter and the aluminum cap.

The aluminum cap is then inserted into the cylinder. The inside of the cylinder should be lubricated with grease. The grease prevents water transportation between the cylinder wall and the aluminum plate. When inserting the aluminum plate make sure it is aligned with the duct carved out in the bottom of the insulation cell, such that the tubing follows the duct, see figure 3.11. Additional grease should be smeared into the duct, and the duct should be covered by tape.

The dry material is now added to the freezing cell. This is done slowly and carefully to ensure correct density. It is important to have control of how much material is added. The cell is filled up to the given height with soil, and compacted if necessary. Once the soil is properly filled into the cylinder, the saturation of the soil can commence. This is ideally done by inserting water from the bottom at a constant head. For fine-grained materials, a high head pressure is required for this process. It is important to saturate the sample slowly as to not get a critical gradient in the sample which will lift the soil and alter the compaction of the sample. The samples in this thesis were saturated at an approximately constant head difference of 220 mm, and the process lasted about 30 min.

3.2.3 Preparation of Pressure Sensors and Temperature Transducers

Once the cell is filled with soil, and the sample has been prepared, the cell is placed on the cryostat-plate. The tubing from the bottom is placed into the insulation piece designed to keep the water from freezing. At this point the pressure sensors should be connected to the tubing from the freezing cell. Before this is done one must start running the program on the

computer, and set zero pressure to the internal pressure in the ice-lab. The sensor at the bottom should be connected while the tube is open. By allowing the water to flow through the tube before the sensor is connected one ensures that no air bubbles are caught in the system.

The three pressure sensors that shall measure the pressure along the vertical axis must be prepared with an anti-freeze solution. The tubes are filled with the solution by a syringe. Be careful not to add too much fluid with the syringe, such that the anti-freeze liquid flows into the sample. When inserting the tip of the sensor into the tubing make sure that no air is trapped between the tip and the fluid. This could be done by making sure that the tube is overflowing with liquid, and that the tip of the sensor is filled with liquid. The sensor is carefully attached to the tube, and pushed in as long as possible. Visual inspection for air-bubbles is important. The temperature sensors should now also be connected to the registration device.

3.2.4 Testing

The computer should now show reasonable values for both temperature and pressures for all sensors. The pressure should be largest at the bottom of the cell and decrease upwards. If strange results are given control that the tubing is filled with liquid all the way into the sensors. Adjust if needed. Once everything seems good the measurements are started by inserting a saving interval and file name. The complete setup after the test is initiated is shown in figure 3.12. In the figure, *number 1* shows the insulation cell, *number 2* shows the temperature transducers, *number 3* shows the tubing to the pressure sensors, *number 4* shows the data-logger and *number 5* shows the heating capsule connected to the bottom tube.

Computer Program

The interactive computer setup is used to start and stop the measurements, allows for monitoring of the results while the tests is in progress, and is used for calibration of pressure sensors and temperature transducers. The setup is created using *LabView*. Calibration of the sensors and transducers are done directly in the program.

During Testing

The freezing test takes a long time. Depending upon the soil it may take several days to reach a state of thermal equilibrium. While the measurements are being logged it is important to

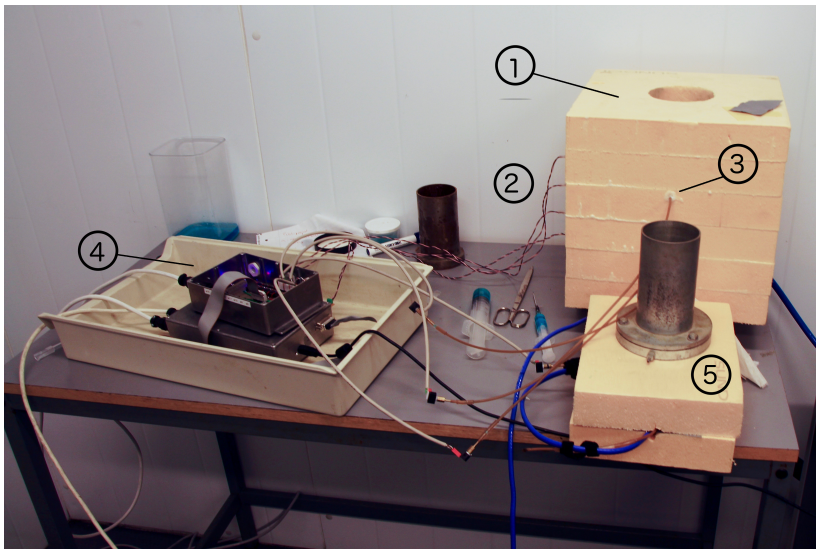

Figure 3.12: Setup during testing

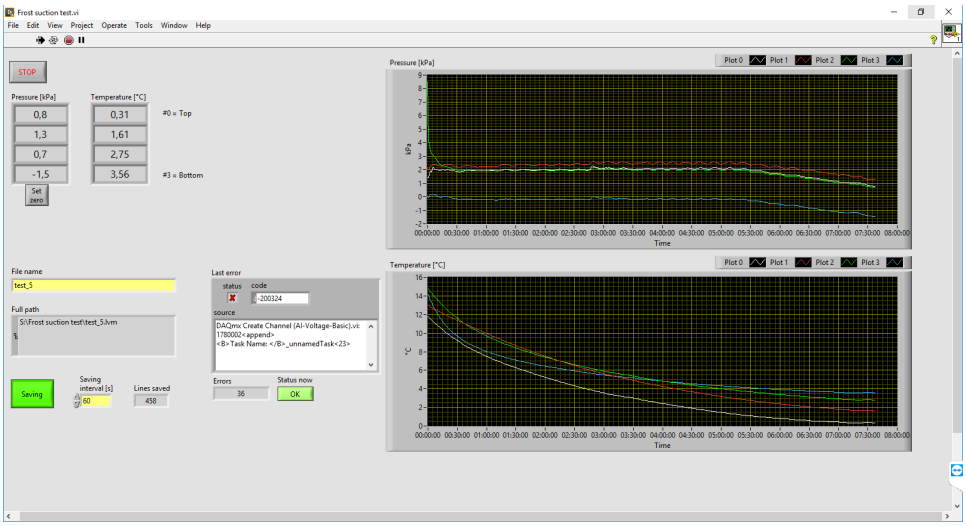

Figure 3.13: Screenshot of the program during testing

monitor the results. Strange behavior in the pressure development can occur, and if one fears that there are air bubbles logged in the system, measure could be taken to get rid of these. It is then important not to alter the internal pressure state of the sample.

Emptying of the Cell

Once the wanted temperature distribution is reached the test can be ended. Firstly, the data-logging should be terminated. The cell should then be released from the data-logger. The cell is then removed from the freezer. Immediately after cancellation the determination of frost penetration should be performed. The easiest way to do this is to remove the aluminum cap and bottom filter and manually measure the distance to the ice lens. The soil is then allowed to thaw, and must be removed from the cell. This can be done with a spoon or by using water

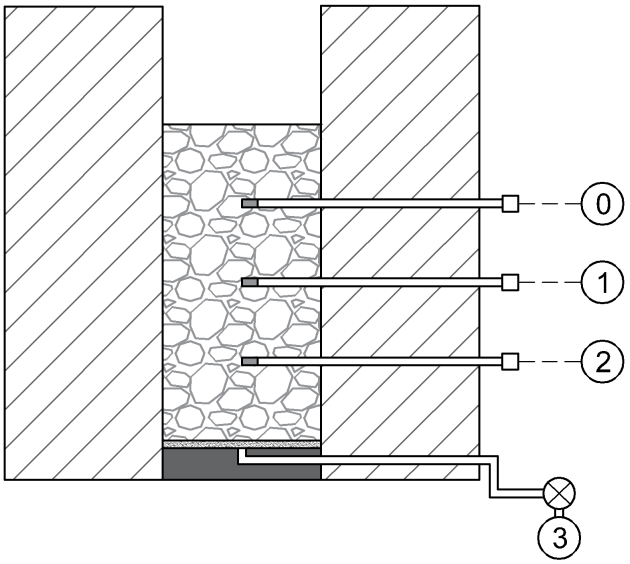

Figure 3.14: Numbering of the temperature transducers and pressure sensors used in the data program

pressure. If a spoon or similar is used one should be careful not to harm the pressure filters. A different way to empty the cell could be to remove the cap, and applying a water pressure from the top down. The soil will pour out through the bottom of the cell. When removing the bottom filter make sure not to damage the duct for the tubing to the cap, as this may lead to leakages in later tests. Once the cell is emptied and clean, the pressure filters should be removed from the cell. All elements should be cleaned.

Chapter 4

Material

The material used for testing in the freezing cell is presented in this chapter. The material is a non-plastic uniform silt from Vassfjellet, Klæbu, Norway. The material was taken in dry condition from storage at the *Geotechnical department* at NTNU. Previous laboratory testing on the silt has been performed by Paniagua (2014) in conjunction with her PhD thesis.

4.1 General Description

A thorough analysis of the composition of the silt has been performed. It was determined that 6% of the material is larger than $74\mu m$, while 91.5% is silt and approximately 2.5% of the material is clay (Paniagua, 2014). It is classified as a silt. Figure 4.1 gives the grain-size distribution of the sample. Mineralogy tests of the sample yielded the results given in table 4.1. Other important properties of the soil are given in table 4.2. Laboratory tests of the silt used has previously been performed by Paniagua (2014). Among these where four constant rate of strain (CRS) oedometer tests.

Mineral	%
Muscovite	35
Quartz	27
Chlorite	18
Feldspar	15
Actinolite	5

Table 4.1: Mineralogy of the silt from Vassfjellet (Paniagua, 2014)

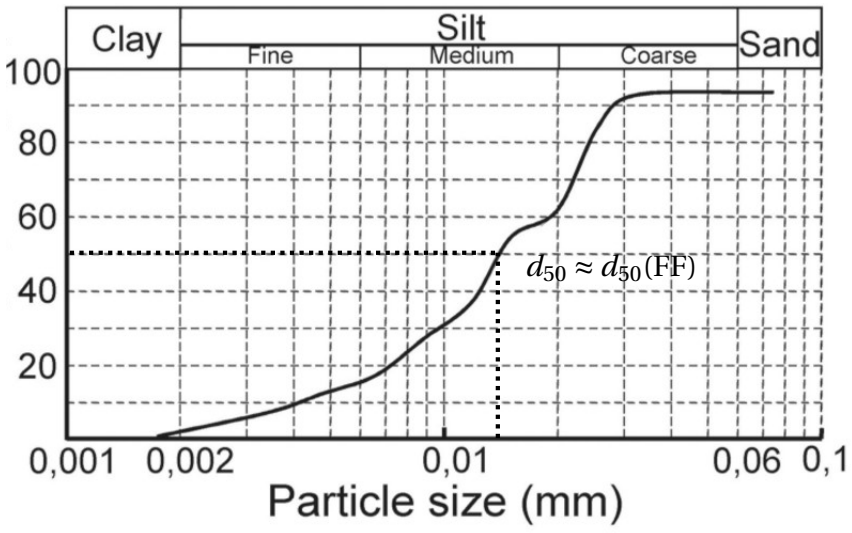

Figure 4.1: Grain-size distribution of the Vassfjellet silt (Paniagua, 2014)

Property	**Value**	**Unit**
e_{max}	1.46	-
e_{min}	0.56	-
$\rho_{d,max}$	1.57	g/cm^3
ρ_s	2.46	g/cm^3

Table 4.2: Key properties determined by Paniagua (2014)

4.2 Density and Packing Ratio

For this thesis, we wish to use loosely packed silt. We also want to be able to control the packing ratio and dry density of the sample before testing. Laboratory tests of packing of a volume comparable to the freezing cell cylinder has been performed to see if possible to recreate a given density. In this test a glass cup of 1.8 liter is used and carefully and slowly filled with the sample material. Once the cup is full the weight is measured. The test was repeated four times. Table 4.3 shows the results from the four tests. It shows good repeatability of the degree of packing with very little variation between the tests. The packing were performed with no compaction.

From the results in table 4.3 several properties can be calculated. An average grain density for silt is estimated by Paniagua (2014) to be ≈ 2.46 g/cm^3. Since the material used is highly homogenous with regard to grain distribution it should be un-problematic to use this

Sample #	1	2	3	4
$W_s\ [kg]$	1.98937	2.00987	2.00037	1.98577

Table 4.3: Test for repeatable dry density and packing ratio

Parameter	Unit	Value
$\overline{W_s}$	$[kg]$	1.996
V	$[l]$	1.8
ρ_s	$[g/cm^3]$	24
V_s	$[cm^3]$	831.8
V_p	$[cm^3]$	968.2
e_0	$[-]$	1.16
n	[%]	0.54

Table 4.4: Density and packing identification.

value. It could be noted that the used value is somewhat lower than the standard value used for Norwegian silts, which is 2.65 g/cm^3 (Sandven et al., 2015; Larsson, 1989). For determination of void ratio, porosity, relative density, pore volume and solid volume standard equations are used (Emdal, 2014). The results are shown in table 4.4. Equation 4.1 gives density of the dry material, equation 4.2 gives the void ratio and equation 4.3 gives porosity.

$$\gamma_d = \frac{W_s g}{V_s} \tag{4.1}$$

$$e_0 = \frac{V_p}{V_s} \tag{4.2}$$

$$n = \frac{V_p}{V} \tag{4.3}$$

The tests showed good repeatability for the loose packing of the soil. It should then be possible to recreate similar densities in the freezing cell.

4.3 Permeability

Permeability has been estimated using results from oedometer tests performed by Paniagua (2014). From oedometer tests one can estimate the permeability through equation 4.4, where c_v is the consolidation coefficient and M is the oedometer modulus(Sandven et al., 2015). Results from oedometer tests are given in appendix E.

$$k = \gamma_w \frac{c_v}{M} \tag{4.4}$$

Using the relation from equation 4.4 one can estimate the permeability and its relation to the void ratio, since the pore volume of the sample decreases as the strain increases. The oedometer modulus and the consolidation coefficient are estimated by linearization of the

curves in the given range, see figure E.1, and calculating the permeability at different void ratios by utilizing the vertical strain. The maximum permeability given from the estimation is $3.88 \cdot 10^{-8}$ m/s for a void ratio of $e = 0.52$. This is within the experience based interval for silts (Emdal, 2014) and seems like a reasonable estimate. The void ratio of the samples used are higher than the loosest state in the oedometer, and the given permeability may be used as a more conservative value than the real case.

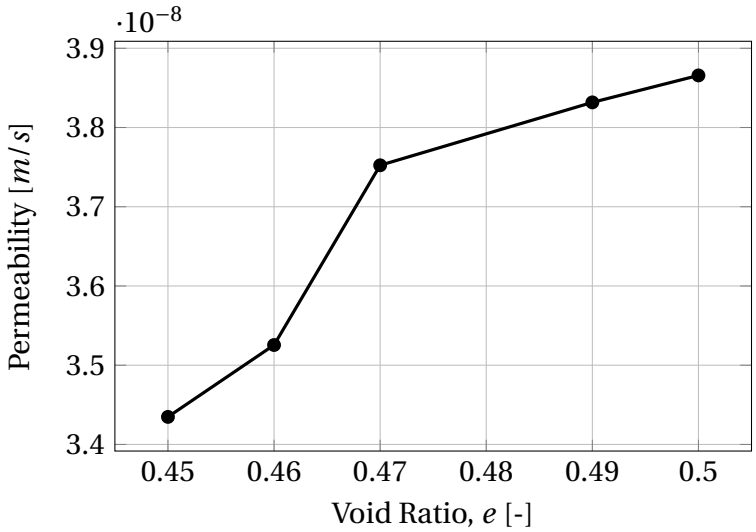

Figure 4.2: Permeability related to void ratio

4.4 Frost Susceptibility

Frost susceptibility of soil is discussed in section 2.6. One of the main influence presented were the grain-size distribution and the fines fraction of the soil. The soil from Vassfjellet has a dominant fines fraction, $F_V = 94\%$, with $d_{50} \approx d_{50}(\text{FF})$, as seen in figure 4.1). Based on this one would expect the silt from Vassfjellet to be very frost susceptible and have a high segregation potential.

One should also take the mineralogy of the soil into account. Table 4.1 gives the fraction of different minerals in the soil. The dominant minerals are, in descending order, muscovite, quartz and chlorite, which combined makes up 80% of the soil particles. These minerals will hence dominate the mineralogical influence on the frost susceptibility. Brandl (2000) has, based on 40 years of comprehensive laboratory testing, comparatively classified the frost susceptibility of different minerals. Quartz is a relatively neutral mineral with regard to frost, susceptibility, whilst both muscovite and chlorite is classified as critical. The soil used should, based on this, be very frost susceptible.

The tests of the freezing cell are to be performed with a large void ratio, preferably e_0>1.0. This ratio is quite high which shows a large pore volume, and therefore a large water volume in the samples. As we know soils with greater void ratio are more frost susceptible than soil with small void ratios. The permeability is estimated to $k \geq 3.88 \cdot 10^{-8}$ m/s for a void ratio larger than $e_0 = 0.52$, which is quite low. Since we operate with a greater void ratio the permeability is greater than the stated value. The permeability may result in quite slow water flow, which may affect the susceptibility.

The conclusion is that the material is fairly frost susceptible, and one should expect successful development of ice lenses and cryosuction.

Chapter 5

Results

In this chapter the results from the testing is presented. Multiple tests of the equipment were made at different times. However, few of them yielded any quantitative results. During the first tests the data-logger did not perform as intended, and values were not stored properly. There also were issues with the calibration of the sensors which gave many different results. Other tests revealed leakages in the cell, and were aborted before completion. The failed tests did however show that the soil did freeze properly, and a definite active and passive zone were detected after exposing the cell to a freezing environment. They also gave good insight into changes that could be made to improve the cell, and eventually the failed tests also led to the construction of a new, more durable cell, as the first cell were more prone to leakages due to the sealant used.

5.1 Results from tests

Three tests has been performed until completion with a usable set of data. The aim was to perform the test under sufficiently equal conditions with regard to soil, temperature and density. The initial state at test initiation is given in table 5.1. All tests were performed on the silt discussed in chapter 4. The packing of the soil was semi-carefully performed, and no vertical compaction were conducted, only light patting on the side of the cube. The sample were saturated with chilled water, and the saturation were performed over approximately thirty minutes, to minimize the pressure gradient. The numbering used for the sensors are the same as presented in figure 3.14. The findings from the test are presented briefly in the following section, in addition to a description of the plots used.

	Unit	Test 1	Test 2	Test 3
Height	cm	20	19	16
$V_{cylinder}$	cm^3	1530	1467.2	1404.3
W_s	g	1786.6	1605.8	1509.9
ρ_s	g/cm^3	2.46	2.46	2.46
V_s	cm^3	726.3	652.8	613.8
V_p	cm^3	803.7	814.4	790.6
W_w	g	802.1	812.8	789.0
e	-	1.11	1.25	1.29
γ	N/m^3	16.60	16.17	16.06

Table 5.1: Initial state of tests

5.1.1 Plots

Pressure and Temperature Plots

The data gathered from the tests are pressure and temperature measurements. Figure 5.1, 5.2 and 5.3 gives the unaltered pressure measurements with time, while figure B.2, C.2 and D.2 gives temperature variation with time.

Altered Pressure

From inspecting the pressure development, it's evident that the pressure calibration at test initiation has not been adequately performed. One should expect a hydrostatic pressure distribution at the initiation of the test, since the soil is saturated in advance, and the freezing has not commenced. If we assume hydrostatic distribution the pressure would be 0.5 kPa at sensor *p0*, and increasing with approximately 0.5 kPa between each sensor. This can be manually enforced on the data. Taking the average value of the pressure at the beginning, or at stable pressure ($\overline{u}$), this can be used as the initial zero level value of the data. The hydrostatic pressure is then enforced. This results in a altered pressure plot which yields much more reasonable results with regards to expected results. The altered pressure is given in figure B.3, C.3 and D.3. The altered pressure has also been smoothed using Loess regression smoothing in *MATLAB*. The altered pressure is given by:

$$u_{alt}(t) = u_{measured}(t) - \overline{u} + u_{hydrostatic} \tag{5.1}$$

Suction

As the aim of this thesis is to measure and quantify the suction that develops under cryogenic conditions a suction graph is necessary. Based on the altered pressure the suction is

calculated as the negative development relative to the enforced hydrostatic pressure. To exclude the normal variation in the pressure measurement as being interpreted as suction all values before the registered initiation of suction is set to zero. The suction is given in figure B.5, C.5 and D.5. Suction at time t is given by:

$$S_{measured}(t) = -u_{alt}(t) + u_{hydrostatic} \tag{5.2}$$

Temperature Distribution

We are also interested in assessing the thermal distribution at termination to see if a steady state has been established. The temperature distribution at termination is taken as the average of the last 20 temperature measurements, and are given in figure B.4, C.4 and D.4. The plot also shows the proposed idealized temperature distribution with basis in the known thermal boundary conditions, where the temperature varies from -3°C at the top and +4°C at the bottom. It is clear by investigating the distribution that the soil does not hold a temperature of +4°C at the bottom. The idealized bottom temperature is adjusted to be equal to the measured average temperature at sensor *t3*, since there is little variation in temperature at this sensor.

5.1.2 Test 1

The first successful test of the freezing cell was performed over 109 hours, and were terminated as the temperature distribution approached thermal steady state. During the preparation of the sample, after the saturation of the sample, some of the pore volume collapsed, and the sample height decreased with ≈ 8 mm.

The sudden increase in pressure that appeared at about 0.4 days into the testing appeared as a result of meddling with the equipment. Sensor *p0* showed some strange variations due to a loosely attached sensor. The sensor was then disconnected and the tubing were refilled with anti-freeze liquid. As the sensor were plugged in all sensors showed a spike in pressure, which were sustained until the pressure decrease started.

Visual Inspection

A visual inspection of the soil sample was performed after the termination of the test. The aim of the inspection was to see if the sample had frozen properly, and any other aspects of interest. At the top of the cylinder a well-developed ice cap of approximately 5 mm thickness were observed which indicated a groundwater level above the soil level.

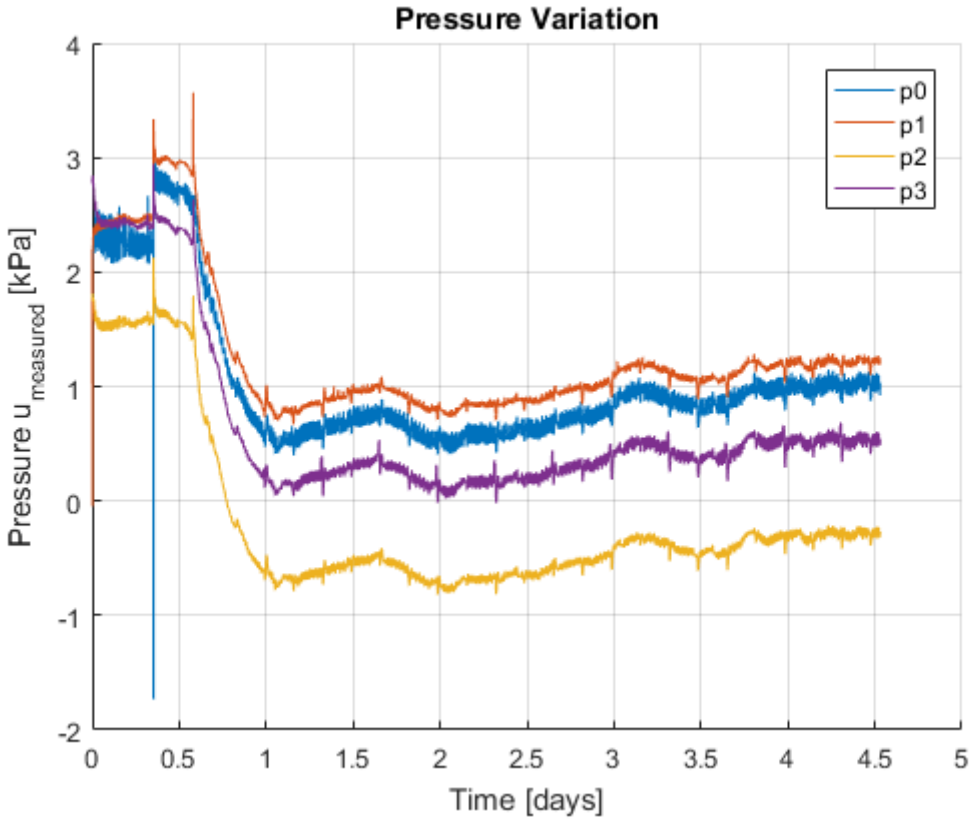

Figure 5.1: Pressure measurement from test 1

The bottom cap was then removed from the cell, whilst the cell lay in a horizontal direction. The soil was removed from the warm end. The latest ice lens were determined to be approximately 15 cm from the bottom of the cell, i.e. at 8.7 cm depth from the top. Around the pressure filters there was a zone where the soil were unfrozen even above the ice lens, which indicates that the soil around the pressure filters might not freeze properly. By interpolating between the temperature sensors, the temperature at the ice lens, i.e. the segregation freezing temperature, were determined to be T_s = -0.66°C. The ice lens is given in figure B.4 along with the temperature distribution at termination of the test.

5.1.3 Test 2

Test 2 of the freezing cell was performed over 98.4 hours. The volume of the cylinder was reduced by ≈ 50 cm^3 due to the introduction of filter paper under the bottom filter, to avoid getting grease onto the filter. During testing, sensor *p2* lost contact which yielded it to give strange results, see figure C.1. By visual inspection it was concluded that the tubing to the sensor had been emptied, perhaps as a result of the suction in the sample.

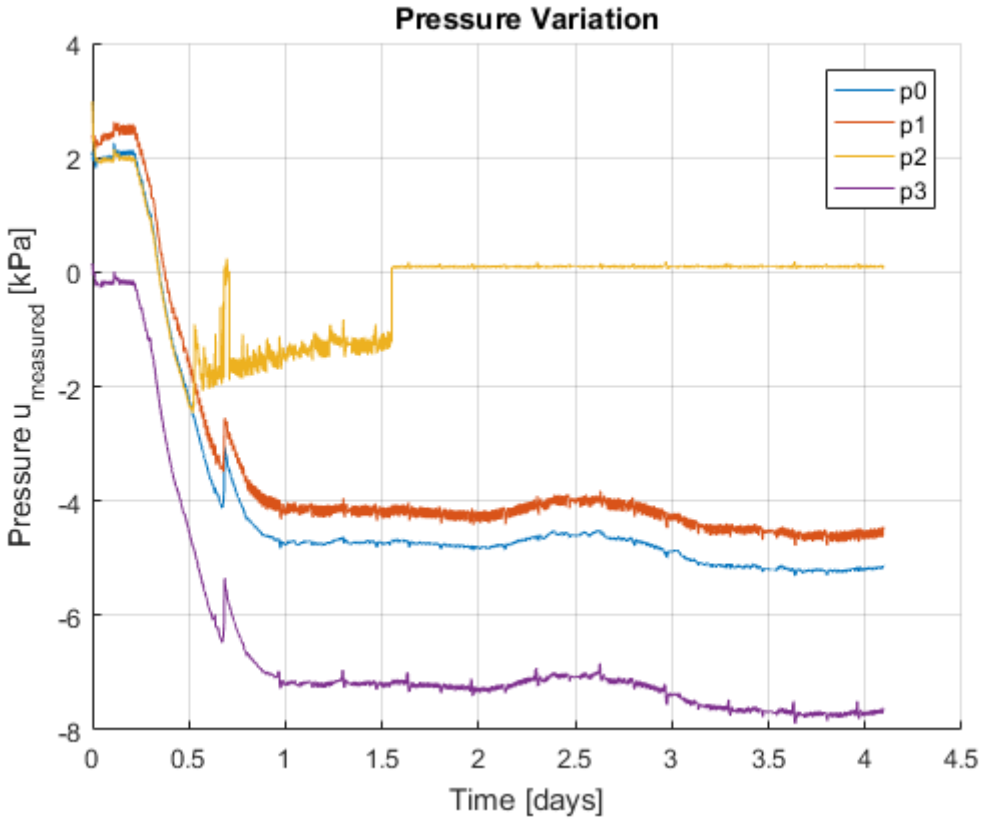

Figure 5.2: Pressure measurement from test 2

Visual Inspection

After the experiment was terminated a visual inspection of the soil were performed. The freezing front were determined to be approximately 6.8 cm from the top of the cell. As with the sample from test 1 the soil surrounding the pressure filters were unfrozen, even above the freezing front. By investigation of figure C.4 the temperature at the ice lens were determined to be T_s = -0.55°C.

5.1.4 Test 3

Test 2 of the freezing cell was performed over 51 hours. The cylinder was only filled to approximately 16.5 cm height. The difference in height is due to lack of material at hand at preparation of sample. The test was prematurely terminated due to system malfunction with regards to the data logger, as it lost contact with the computer. The pressure development had not yet peaked at termination. However, it looks to be very close to the peak, but it's not definitely determined. During the test sensor *p0* had an abrupt change that was due to the filter being completely separated from the unfrozen water by the ice lens.

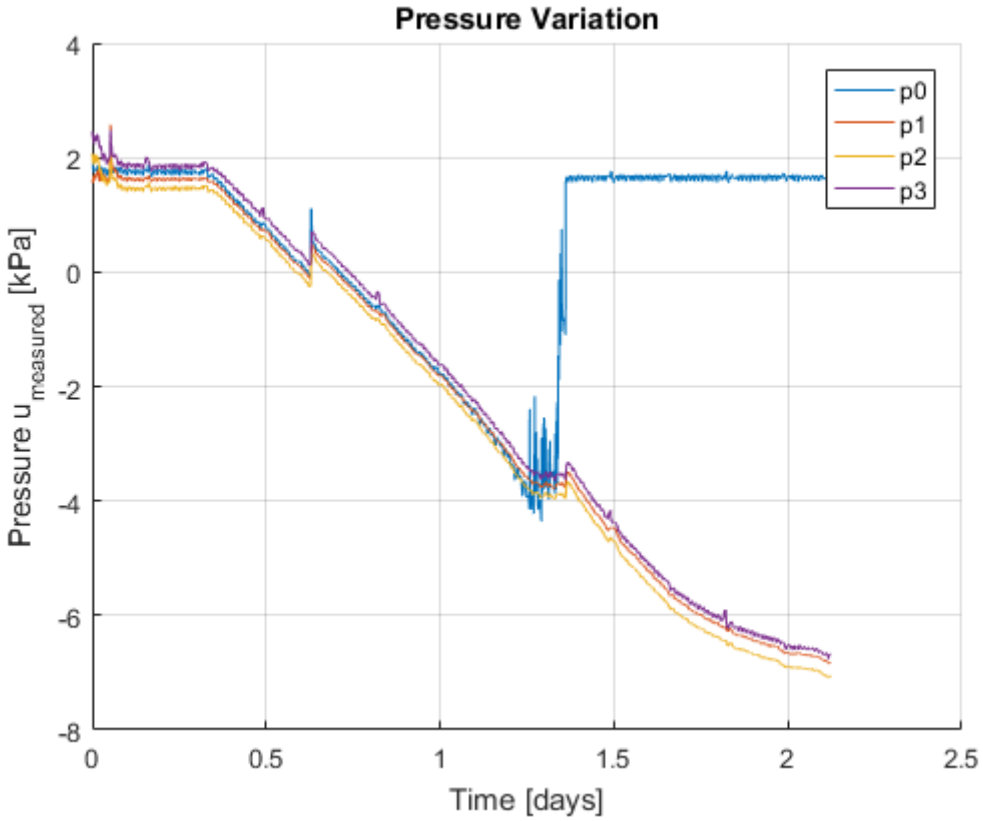

Figure 5.3: Pressure measurement from test 3

Visual Inspection

After the experiment was terminated a visual inspection of the soil were performed. The freezing front were determined to be approximately 4 cm from the top of the cell. As opposed to the sample from test 1 the soil surrounding the pressure filters were seemingly completely frozen. The ice lens was determined to be stationed approximately 4 cm below the top. By investigation of figure D.4 the temperature at the ice lens were determined to be T_s = -0.50°C.

Chapter 6

Discussion

In this chapter the results from the testing of the freezing cell is discussed and evaluated, and possible influencing factors are identified.

6.1 Evaluation of Results

The results from the tests, as presented in chapter 5 and appendix B, C and D, shows a clear tendency towards the reduction of pore pressure with decreasing temperature, which is the wanted trend for the pressure. Dependency of pore pressure between the sensors are evident, and the variation in pressure is approximately identical for all sensors at all time. This indicates good water communication in the soil columns, i.e. the water at the bottom of the column is in continuous communication with the water at the other sensors.

6.1.1 Temperature Variations

Looking at the temperature variations from figure 6.1 the measured temperature curves seems reasonable. All measurements quickly align to the expected distribution with lowest temperature at *t0* and highest temperature at *t3*, and then slowly approaches a state of thermal equilibrium.

Since the bottom and top temperature is controlled the temperature distribution should be easily predicted. However, the temperature at the bottom is, as seen in figure B.4, C.4 and D.4, lower than the expected +4°C. This indicates that some of the heat is lost at the bottom. It should also be noted that the temperature transducer at the bottom isn't placed onto the aluminum cap, but approximately one centimeter above, due to the bottom filter. A temperature gradient through the soil and bottom filter will be present. There will also be a gradient between the top of the bottom plate and the heating plate. The important factor isn't the

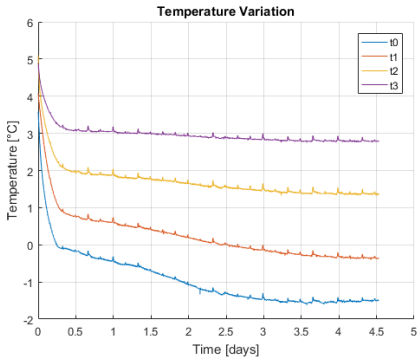

(a) Test 1

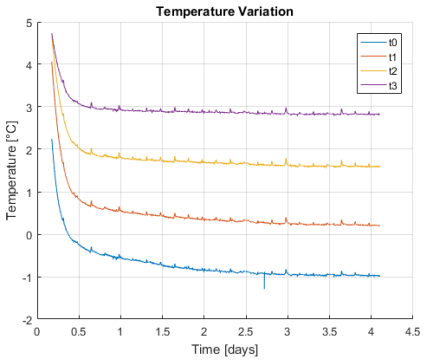

(b) Test 1

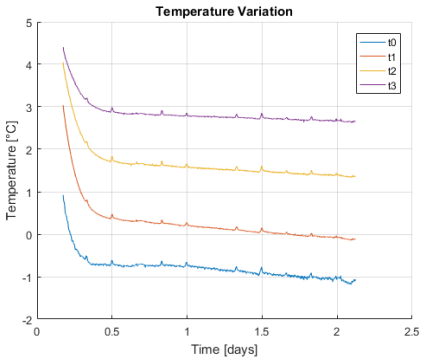

(c) Test 1

Figure 6.1: Temperature measurements from tests

absolute temperature, but the variation in temperature. It is evident that the temperature at the bottom is stable, with little variation and reduction after the initial stabilization.

The temperature distribution at the end of each test indicates that test 1 is run until thermal steady state is reached. Test 2 almost reaches steady state and test 3 is terminated long before steady state.

The forementioned variation of $\pm 0.5°C$ in temperature in the ice lab seems to have no effect on the freezing of the sample. It seems the system has too great an inertia to be effected by such a small variation in temperature. The same goes for the variation in the cryostat. It should also be noted that the temperature decrease indicates that there is little to no heat loss through the insulation, and the assumption of no heat loss is valid.

6.1.2 Suction

For numerical analyses we are interested in the local suction that develops in the thin layers of unfrozen water within the frozen fringe. In this experiment however the measured values are not the local suction, but the total pore pressure, or macroscopic suction. To evaluate the cryosuction in the micro-pores an adjustment for the unfrozen water content must be

made. By equation 2.23 we can estimate the suction in the water films at given unfrozen water content by assuming a water content for the given segregation freezing temperature.

No determination of unfrozen water content has been performed in this thesis, and no characteristic values are given for the material used. Any assumptions with regard to the unfrozen water content at the observed segregation freezing temperatures should be experienced based. However, in lack of characteristic behavioural properties with regards to unfrozen water content in Vassfjellet silt, we use characteristic values determined for other silts. Characteristically it is found that frozen silts have a lower unfrozen water content than clays. We make a very rough estimation of the unfrozen water content. Investigating the results found by Patterson and Smith (1981), see figure 6.2, an estimate of $\theta_{uf} \approx 10-15\%$ can be used for the segregation freezing temperatures determined in test 1, 2 and 3.

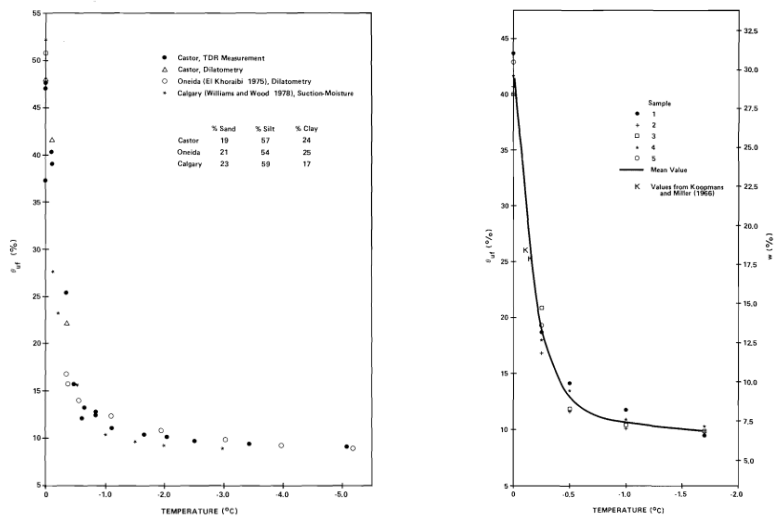

(a) Various silt loams (b) Manchester silt

Figure 6.2: Comparison of freezing characteristic data for various silt loams (Patterson and Smith, 1981)

Clausius-Clapeyron, equation 2.17, gives the basis for the estimation of the suction at the base of the ice lens as $S = -\rho_i l \ln \frac{T}{T_0}$. Using $\rho_i = 0.9167$ g/cm^3, $l = 33355$ Ncm/g and $T_0 = 273.16$ K the theoretical suction at the ice lens is established. The results from the theoretical and measured suction is given in table 6.1. A large discrepancy is given between the measured and theoretical values of suction. Even the best measurement from test 3 is much smaller than the predicted theoretical suction. It should be noted that the measured suction is calculated based on an assumptive unfrozen water content, and that the stress state in the cell isn't properly accounted for, as will be further investigated later.

[1]Assuming 10% unfrozen water content

	Test 1	Test 2	Test 3
T_S	-0.66 °C	-0.55 °C	-0.50 °C
Measured S [1]	25 kPa	75 kPa	85 kPa
Calculated S	738 kPa	617 kPa	560 kPa

Table 6.1: Measured and calculated suction at the ice lens

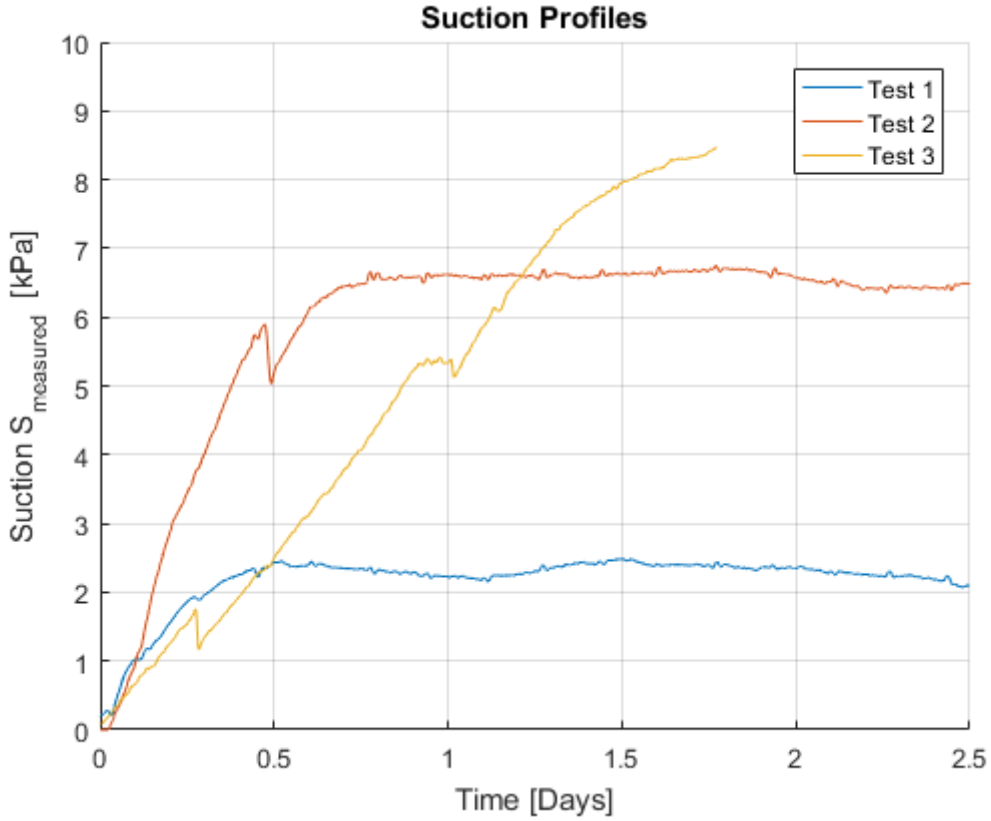

Figure 6.3: Comparative Suction plot for tests based on measurements from sensor *p1*. The profiles are adjusted such that time equals zero when suction initiates.

Comparing the results from test 1 and 2 to the result from test 3 it is interesting to note that the rate in which the suction is developing differs. In test 1 and 2 a peak suction is reached after 0.5 to 0.7 days. In test 3 however the maximum suction appears to be reached after 1.8 days, which is substantially longer, as indicated in figure 6.3. This difference in rate at which suction develops seems strange and counter-intuitive with respect to expected results. A shorter sample, as in test 3, should not take longer to develop suction than a taller sample, according to the constitutive models. The thermal gradient through sample 3 is 43.75 k/m while for test 1 and 2 it is 35 K/m. A greater thermal gradient increases the rate of frost penetration, and thereby the rate of suction development should increase. The results from our testing yields the opposite. It is important to note that with such small sample size as in this thesis, only three samples, we don't get the possibility to inspect if this would be a

reoccurring trend, or just an anomaly.

A sudden change in pressure is measured by all the sensors in test 2 and 3 during suction development. The origin of this change is unknown, but the effect seems insignificant. The pressure development seems to carry on in the same path as before the change. The sudden change might be attributed to change in internal pressure in the lab.

Background Noise

The pressure measured in the freezing cell seems to follow a periodic scattering pattern. To have an idea of the magnitude of this variation a measurement has been performed by leaving the pressure sensors unstressed and recording the impact. For this case the pressure sensors should ideally register zero kPa at all times. Figure 6.4 shows the result from this test. The standard variation for sensor *p2* is about ±0.04 kPa which is not significant relative to the measured values from test 1, 2 and 3. The variation in sensor *p3* were not measured due to bad wiring. The variation in pressure could most likely be attributed to the fans in the ice lab.

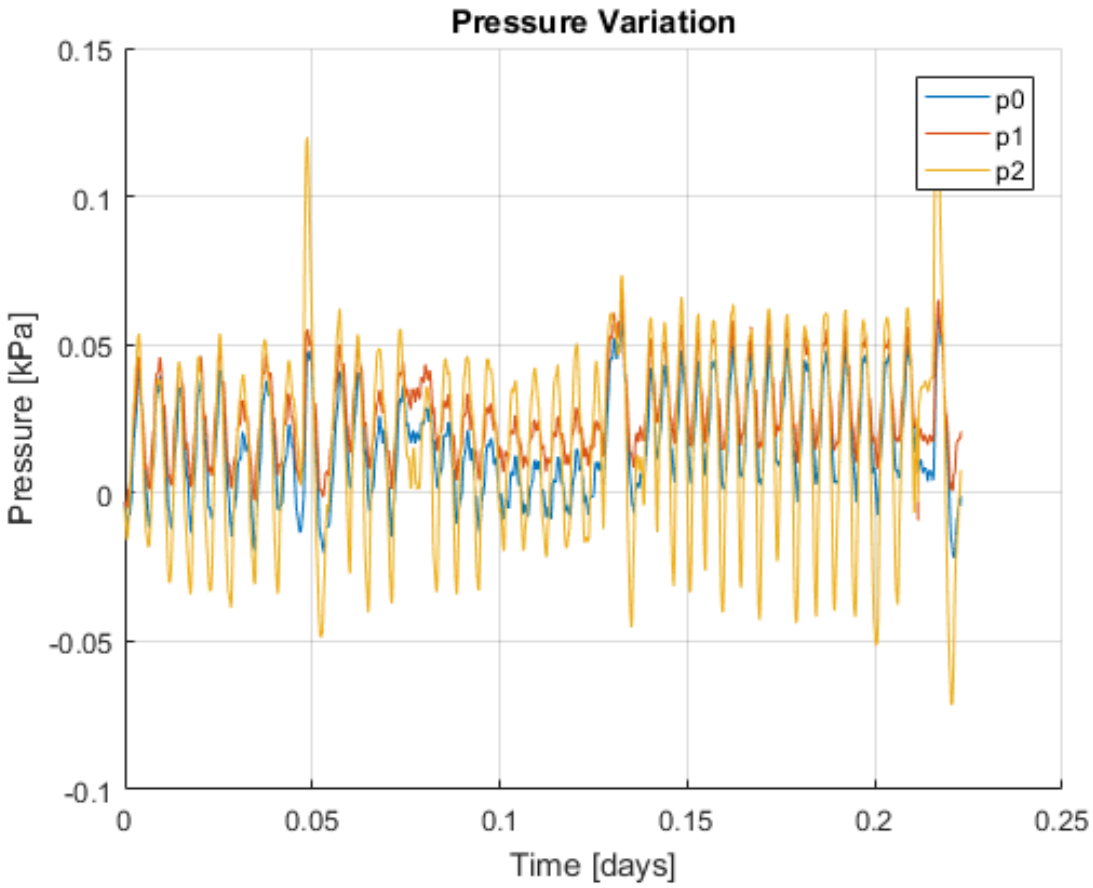

Figure 6.4: Measured variation in pressure when no intentional pressure is applied

Pressure State

The freezing cell is designed to measure the change in pore pressure within a freezing soil column. The assumption is that the measured pressure, and the measured change of this pressure, is related to a change in the macroscopic pore-pressure, related to the local pore-pressure through unfrozen water content and area. This relation is given equation 6.1, based on equation 2.23. This assumption is only valid as long as the freezing of the soil doesn't induce additional total pressure, as indicated in equation 6.2. An increase in total pressure makes it harder to measure the change in pore pressure, without simultaneously capturing the additional total pressure, especially since the test is run undrained and saturated and therefore no volumetric decrease is allowed. Since the total pressure is increasing and the pressure is decreasing, the effects dilute each other. This theory is also supported by the theory presented in section 2.6, where a clear dependency between overburden pressure and decrease in frost susceptibility were presented.

$$\Delta u_{measured} = \Delta S \cdot \Theta_{uf} \tag{6.1}$$

$$\Delta \sigma = \Delta \sigma' + \Delta u_{measured} \neq 0 \tag{6.2}$$

During frost heave the soil tries to expand in the direction of the heat loss. On the interface between the soil and the inner walls side friction will restrict the vertical movement, and thereby induce an increase in total pressures. When the soil sample is saturated a thin layer of water could cover the top of the soil. As the water freezes this ice lens will act as a cap on the soil. The friction between the ice cap and the inner walls will induce a downwards pressure on the soil, see figure 6.5.

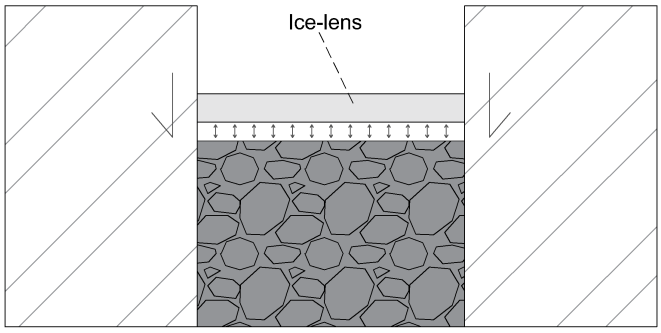

Figure 6.5: Pressure induced due to side friction and ice cap

At the bottom of the cell the bottom plate needs to be able to move relatively unrestricted. If the soil movement upwards is restricted, then it must be able to lift the cell to allow for vertical expansion. If the bottom plate is fastened too hard the same case of friction occurs

at the bottom, see figure 6.6. In the tests performed the aluminum cap where firmly attached at the bottom due to the tight fit in the cell.

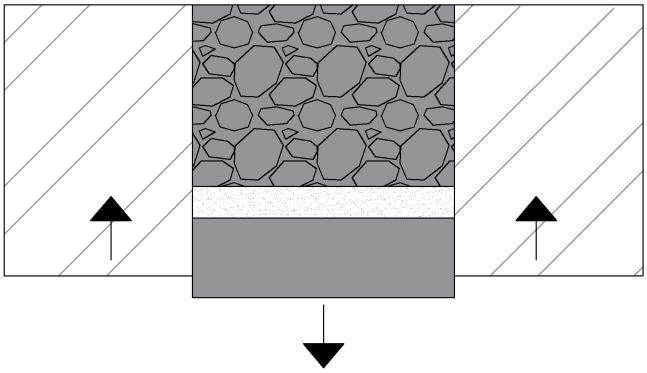

Figure 6.6: Pressure induced due to restricted heave of the cell

The accumulated effect of the side friction on the soil, the ice-cap and bottom plate is an increased total pressures. It is hard to separate the total pressure from the pore pressure decrease. Presently no values of the side friction due to interaction between the soil and the insulation is available.

A definite measurement of the side friction and total pressure change has not been made. However, one *failed* test were performed where the ground water table where located approximately 2 centimetres above the soil level. In this test a very clear ice cap developed on the top of the sample during freezing. This cap had a large effect on the measured pressure. It was clear that as the pore water began freezing, it were not allowed to expand, which resulted in a sharp increase in pressure, as seen in figure 6.7, instead of the expected decrease. The test were prematurely terminated due to this ice cap.

Since the test is performed in a closed cell without access to water the expansion in the cell at this point is mainly due to the volumetric expansion when water crystallizes. At the point of termination the added pressure were approximately 2 kPa, and sensor *0* registered a temperature of ≈ 0°C, which indicates that . The further development of the stress state is unknown, but it is evident that the ice cap had a large contribution on the measured water pressure.

Altering the Freezing Pattern

To prevent the pressure sensors from freezing the tubes connected are filled with anti-freeze liquid, or more specifically ethylene glycol. This liquid is a water mixture. When the porous filters saturated with anti-freeze liquid comes in contact with the saturated soil the water and anti-freeze liquid may interchange in position, i.e. some anti-freeze liquid may enter the

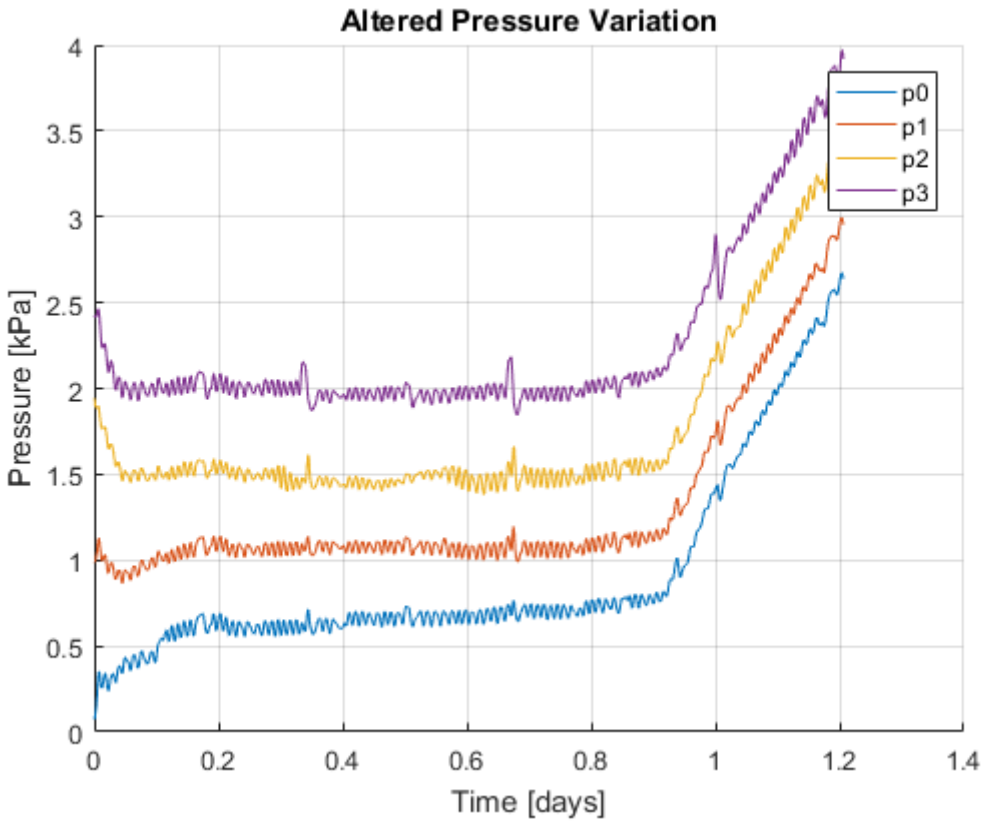

Figure 6.7: Pressure variation at test with thick ice cap

pore volume of the soil, and some water may infiltrate the pressure filters. This interchange could possibly alter the freezing pattern in the surrounding pores and therefore may alter the conditions under which we measure the pore pressure.

Table H.1 given in appendix H shows some characteristic properties of water and ethylene glycol. Ethylene glycol is heavier, and also has a higher viscosity than pure water. The mixture will then also have higher density and viscosity than the pore water in the soil. In the tests a mixture of 60-vol% water and 40-vol% ethylene glycol was used. The higher viscosity of the anti-freeze liquid will make it less prone to flow from the filter, and to some degree hinder the interchange of the pore-water and the solution, but not entirely.

In test 1 it was identified a zone of unfrozen slurry around filter *p0*. This indicates that the pore water around the filter had not crystallized. This is a strong indicator that an interchange between the water and the anti-freeze solution is occurring. This also mean that the pore-water will be continuous even behind the ice lenses. A such reduction in the cross-sectional area of the ice lens reduces the total amount of the sample in which there are developing cryosuction. A substantial amount of the water that would normally freeze, will not freeze due to the interchange of fluids. When calculating the suction we assume that the ice lens is continuous throughout a cross-sectional plane. If this area is reduced, then the area

in which suction occurs is reduced. The effect of this is a reduction of the suction in the sample. This could explain, to some degree, why the measured suction is as low as it is.

6.1.3 Continuity of Water Phase

Continuity of the water phase is essential for the transmission of pressure. As the freezing front propagates through the soil sample the unfrozen water content will decrease. The measured suction in the sample is dependent upon continuity of the water phase, and will not give correct measurements if the pore water in connection with the pressure sensor is cut off from the rest of the unfrozen water. The required continuity in the soil sample seems to be fulfilled throughout the tests. The clear dependency between the pressure sensors indicate good communication.

Even though the sample is saturated slowly over ≈ 30 minutes, the vertical upward water flow still yields current forces above the critical gradient, which means that the soil particles acts as if weightless during saturation (Emdal, 2014). The gradient is calculated by equation 6.4.

$$i = \frac{dh}{L} = \frac{220cm}{20cm} = 11 \tag{6.3}$$

$$i_c = \frac{\gamma'}{\gamma_w} = \frac{16.43 - 10}{10} \approx 7 \tag{6.4}$$

The critical flows alters the compaction and distribution of the soil and could result in accumulated pore volumes. The flow is critical since $i > i_c$. This is a general consideration and is unquantified by visual inspections or similar. As discussed in section 2.5, a critical gradient and disturbances in the soil may allow for more air to enter the system, which may disturbe the pressure measurements.

Chapter 7

Conclusions and Recommendations for Further Work

7.1 Conclusions

A freezing cell has been constructed for measurements of pressure change in a saturated soil column exposed to one-dimensional unsteady heat flow. The freezing cell consists of four pressure sensors and temperature transducers. The cell were tested in an ice lab holding -3°C, and were heated from the bottom by a cryostat holding +4°C. Multiple tests were performed with the cell, in which three yielded complete results. All test showed good continuity in the water phase through the sample, as a clear communication of pressure were present.

The soil used for testing were taken from Vassfjellet, and is classified as a silt. The soil consisted of 6% material larger than $74\mu m$, 91.5% silt and approximately 2.5% clay. The soil were deemed to be medium to very frost susceptible by inspecting mineralogy, grain-size distribution, void ratio and overburden pressure.

The measured pressure change from test 1-3 were the macroscopic pressure, and correlates to the suction in the thin water films adsorbed by ice and soil particles through the unfrozen water content. The largest measured suction was 8.5 kPa, in test 3. Adjusted for unfrozen water content, with an estimated unfrozen water content of 10%, this equals approximately 85 kPa of cryosuction. The theoretically estimated suction is 560 kPa, which yields a large gap between calculated and measured suction. It is noted that the measured suction of 8.5 kPa equals a pressure reduction of almost 1 meter water column height, which in engineering terms is very significant, even though it is lower than the expected value.

The measured pore pressure is diluted by a total pressure change, which is induced by

side friction on the interface between soil and cell walls. The side friction restricts the soils ability to heave. On some of the tests an ice cap were also detected, which also will restrict heaving. The temperature distribution from the tests shows the establishment towards a steady state temperature distribution. The variation in temperature in the soil indicates that little heat is lost through the insulation, and thereby that the assumption of negligible heat loss is valid.

There is no question that the sample size is too small to accurately assess the freezing cell. An estimation of the suction is better done if more tests are performed, which can be compared. However, the general trend in the results from the tests that has been performed are promising, in regards to measuring a suction in the freezing soil.

7.2 Further Work

7.2.1 Further Testing

For this thesis the sample size of performed tests of the freezing cell is quite small. Only 3 tests has been performed due to restrictions in time, and with very little variation between them. No variation in temperature gradient or soil has been used, and although a drop in pore pressure has been detected, the absolute pore pressure change has not been sufficiently determined. Measures to reduce the side friction in the cell should also be looked into. For further work it could be interesting to investigate how the cell works with:

- Different soils and void ratios
- Different temperature gradients
- Free access to water from the bottom. This will allow for ice lenses to develop through the column

As discussed the interchangeability of the anti-freeze liquid may pose an issue. One solution to this problem may be to use a hydrophobic liquid as hydraulic fluid, such as a mineral oil. This would mean that the liquids would be less prone to mix, whilst the pressure would still be adequately transferred from the water to the mineral oil. When investigating different mineral oils there is also many possibilities to find liquids with less air entrainment, lower compressibility and higher viscosity.

Additional tests could be performed post-testing. For example would it be interesting to measure the water content at different depths at termination. This could easily be done by

going in from the bottom of the cell and extracting material, and could be done in conjunction with the visual inspection of the ice lens.

7.2.2 Equipment

As discussed the instrumentation used to measure the pressure were used at sub-optimal temperatures, and thereby not ideal for use in a freezing environment. The ambient temperature interval for the data-logger is exceeded. This should in most cases not be a problem, but the effect is unknown. Many issues connected to weak signals were experienced, but these can also be contributed to the use of excessively long cables, which might cause the signal to be weak.

7.2.3 Numerical Simulations

As discussed above the measured suction was much less than expected, and this may be attributed to side friction within the cell, and restricted movement in the vertical direction. Further work should include numerical simulations of the freezing cell with side friction as a component in the simulations. This could clarify the relation between total pressure increase and pore pressure reduction. The simulations should be performed in PLAXIS with the *Frozen and Unfrozen Soil Model*, where results from the lab can be backtracked to create a simulation giving similar results. The simulations could be performed by establishing a model consisting of a 2D cross-section of the soil sample, and applying thermal boundary conditions to the column, with no overburden stress, and defining the interface behaviour. The basic concept would allow for no heat loss through the sides, and a constant temperature at top and bottom of the sample.

Bibliography

Andersland, O. and Anderson, D. (1978). *Geotechnical engineering for cold regions*. McGraw-Hill.

Andersland, O. B. and Ladanyi, B. (1994). *Frozen ground engineering*. John Wiley & Sons, second edition.

Beskow, G. (1935). *Tjälbildningen och tjällyftningen: med särskild hänsyn till vägar och järnvägar*. Statens Väginstitut.

Brady, J. (1990). *General chemistry: principles and structure*. Wiley.

Brandl, H. (2000). Freezing–thawing behaviour of soils and unbound road layers. In *Proceedings of the 1st Central Asian Geotechnical Symposium, Astana, Kazakhstan*, pages 25–28.

Casagrande, A. (1932). A new theory of frost heaving: discussion. *Proceedings of US highway research board*, 11(Pt I):168–172.

Clausius, R. (1867). *The mechanical theory of heat: with its applications to the steam-engine and to the physical properties of bodies*. J. van Voorst.

Edlefsen, N., Anderson, A., et al. (1943). Thermodynamics of soil moisture. *California Agriculture*, 15(2):31–298.

Emdal, A. (2014). *Introduksjon til Geoteknikk*. Geotechnical Division: Norwegian University of Science and Technology.

Farouki, O. T. (1986). Thermal properties of soils. *Trans Tech Pub*.

Fredlund, D., Gan, J., and Rahardjo, H. (1991). Measuring negative pore-water pressures in a freezing environment. *The Emergence of Unsaturated Soil Mechanics*, page 70.

Geosense (2014). *Application Guide - Piezometers*. https://www.geosense.co.uk/media/BlockAttributeValueFile/141/file/3PiezometersApplicationGuideV1.0.pdf.

Ghoreishian Amiri, S., Grimstad, G., Kadivar, M., and Nordal, S. (2016). Constitutive model for rate-independent behavior of saturated frozen soils. *Canadian Geotechnical Journal*, 53(10):1646–1657.

Herzog, F. and Boley, C. (2013). Mechanisms during formation of ice lenses and suction in freezing soils. *Actes du colloque*, 1:322–325.

Hohmann, M. (1997). Soil freezing—the concept of soil water potential. state of the art. *Cold Regions Science and Technology*, 25(2):101–110.

Ingersoll, J. and Berg, R. (1981). Simulating frost action by using an instrumented soil column. *Transportation Research Record*, (809):34–42.

Kia, M. (2012). *Measuring Pore-water Pressures in Partially Frozen Soils*. PhD thesis, University of Alberta.

Konrad, J.-M. (1999). Frost susceptibility related to soil index properties. *Canadian Geotechnical Journal*, 36(3):403–417.

Konrad, J.-M. and Morgenstern, N. (1980). A mechanistic theory of ice lens formation in fine-grained soils. *Canadian Geotechnical Journal*, 17(4):473–486.

Konrad, J.-M. and Morgenstern, N. R. (1981). The segregation potential of a freezing soil. *Canadian Geotechnical Journal*, 18(4):482–491.

Konrad, J.-M., Roy, M., Rochelle, P. L., Leroueil, S., and Bergeron, G. (1995). Field observations of frost action in intact and weathered champlain sea clay. *Canadian geotechnical journal*, 32(4):689–700.

Kudryavtsev, A., Dostovalov, B., and Garagulya, L. (1978). Radiation-heat balance of the soil surface as a factor in the formation and dynamics of seasonally frozen soils and permafrost. In *Permafrost: Second International Conference, July 13-28, 1973: USSR Contribution*, page 18. National Academies.

Larsson, R. (1989). *Jords egenskaper*. Statens geotekniska institut.

LibreTexts (2017). *Density and Percent Compositions*. https://chem.libretexts.org/Core/Analytical_Chemistry/Quantifying_Nature/Density_and_Percent_Compositions.

Low, P. and Lovell, C. W. (1959). The factor of moisture in frost action: Informational report. *Joint Highway Research Project, Indiana Department of Transportation and Purdue University, West Lafayette, Indiana, 1959*.

Ma, T., Wei, C., Xia, X., Zhou, J., and Chen, P. (2015). Soil freezing and soil water retention characteristics: Connection and solute effects. *Journal of Performance of Constructed Facilities*, pages D4015001–1 to D4015001–8.

Magorien, V. (1980). Keeping air out of hydraulic systems. *Machine Design*, 52(18):71–76.

Morishige, K. and Kawano, K. (1999). Freezing and melting of water in a single cylindrical pore: The pore-size dependence of freezing and melting behavior. *The Journal of chemical physics*, 110(10):4867–4872.

Paniagua, P. (2014). *Model testing of cone penetration in silt with numerical simulations*. PhD thesis, Ph. D. thesis, Norwegian University of Science and Technology, Trondheim, Norway.

Patterson, D. and Smith, M. (1981). The measurement of unfrozen water content by time domain reflectometry: Results from laboratory tests. *Canadian Geotechnical Journal*, 18(1):131–144.

Sandven, R., Senneset, K., Emdal, A., Nordal, S., Janbu, N., Grande, L., and Kornbrekke, H. (2015). *Geotechnics: Field and Laboratory Investigations*. Geotechnical Division: Norwegian University of Science and Technology.

Schwab, R. and Köhler, H. (2003). Behaviour of near-saturated soils under cyclic wave loading. In *International Symposium on Deformation Characteristics of Geomaterials*.

Series, S. D. (1981). *Solubility Data Series. Volume 7: Oxygen and Ozone, ed. R. Battino*. Pergamon Press, Oxford.

Taber, S. (1929). Frost heaving. *The Journal of Geology*, 37(5):428–461.

Taber, S. (1930). The mechanics of frost heaving. *The Journal of Geology*, 38(4):303–317.

Thomas, H. R., Cleall, P. J., Li, Y., Harris, C., and Kern-Luetschg, M. (2009). Modelling of cryogenic processes in permafrost and seasonally frozen soils. *Geotechnique*, 59(3):173–184.

Van Wijk, W. R. et al. (1963). Physics of plant environment. *Physics of plant environment*.

Wettlaufer, J. and Worster, M. G. (2006). Premelting dynamics. *Annu. Rev. Fluid Mech.*, 38:427–452.

Williams, P. J. (1964). Unfrozen water content of frozen soils and soil moisture suction. *Geotechnique*, 14(3):231–246.

Zhang, L., Ma, W., Yang, C., and Yuan, C. (2014). Investigation of the pore water pressures of coarse-grained sandy soil during open-system step-freezing and thawing tests. *Engineering Geology*, 181:233–248.

Appendix A

Properties of Water and Ice

Temp ($°C$)	**Density** (kg/m^3)	**Specific Heat** ($kJ/kg°C$)	**Thermal Conductivity** (W/mK)	**Latent Heat of Evaporation** (kJ/kg)
-10	997.94	4.268	-	2523
-5	999.18	-	-	-
0	999.87	4.2150	0.567	2499
4	100.00	-	-	-
5	999.99	4.1995	0.574	2487
10	999.73	4.1894	0.596	2476
15	999.13	4.1832	0.595	2464
20	998.23	4.1790	0.603	2452
25	997.08	4.1769	0.611	2440
30	995.68	4.1756	0.620	2428
35	994.06	4.1752	0.628	2417
40	992.25	4.1756	0.632	2405
45	990.24	4.1765	0.605	2393
50	988.07	4.1777	0.645	2381

Table A.1: Physical properties of liquid water (Van Wijk et al., 1963)

Temp ($°C$)	**Density** (kg/m^3)	**Specific Heat** ($kJ/kg°C$)	**Thermal Conductivity** (W/mK)	**Latent Heat of Sublimation** (kJ/kg)	**Latent Heat of Evaporation** (kJ/kg)
-20	920	1.958	2.433	2836	289
-10	919	2.029	2.319	2835	312
0	917	2.105	2.240	2833	333

Table A.2: Physical properties of ice (Van Wijk et al., 1963)

Appendix B

Results Test 1

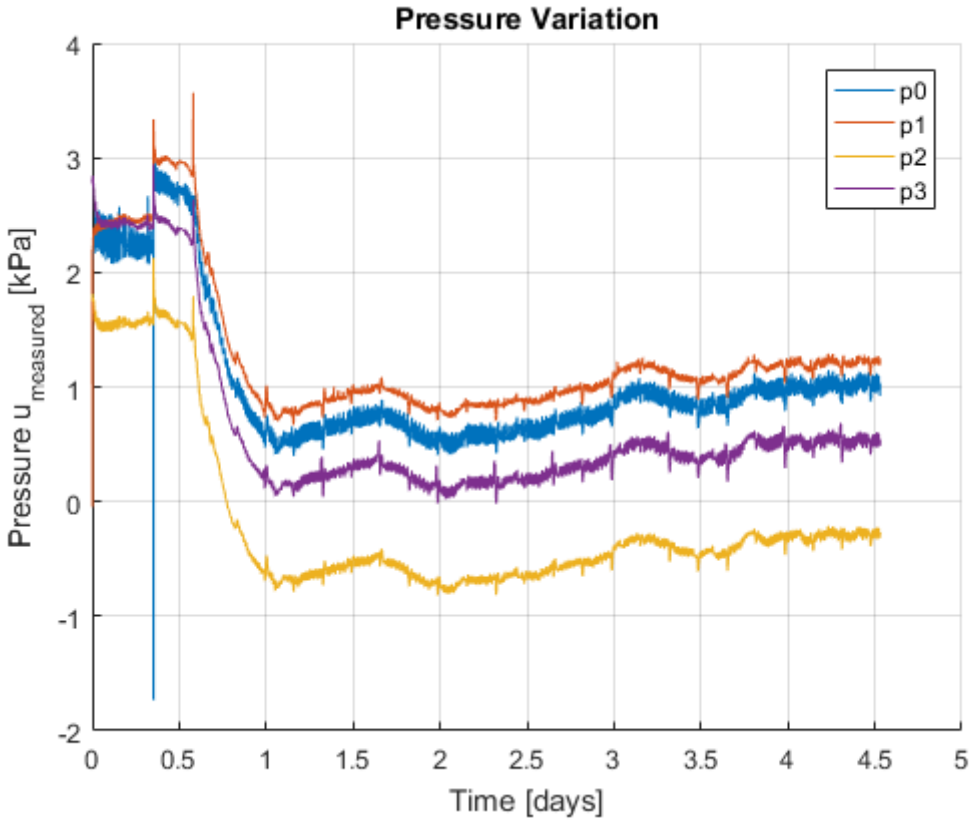

Figure B.1: Measured pressure test 1

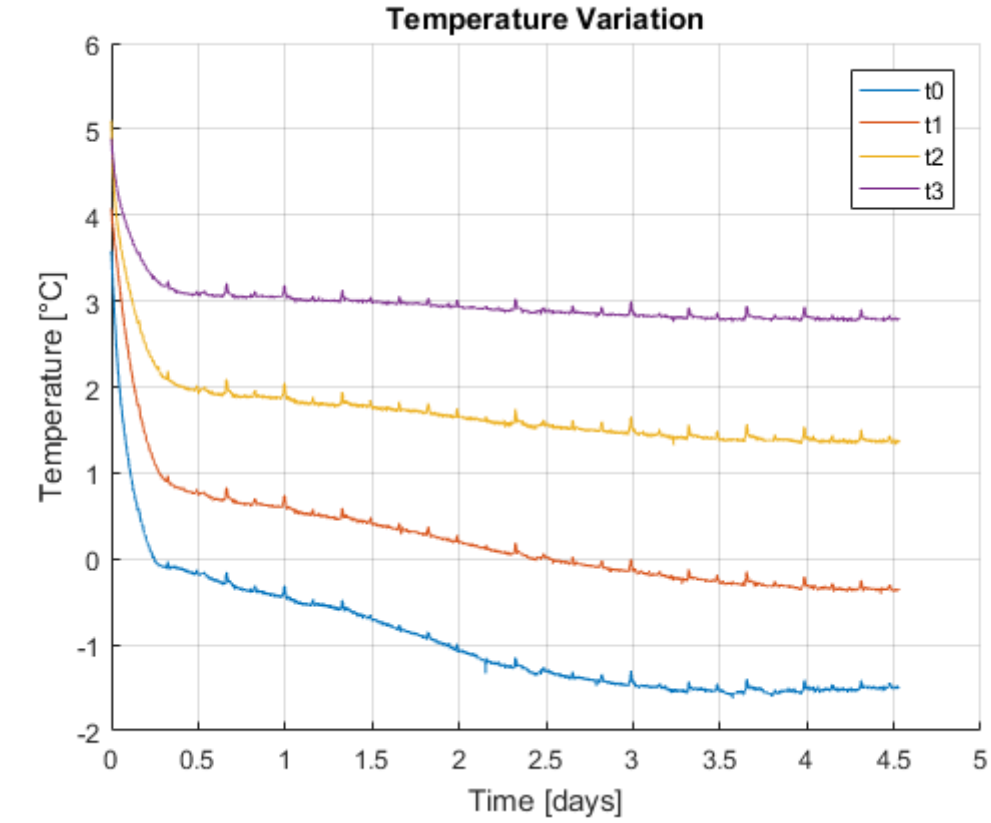

Figure B.2: Measured temperature test 1

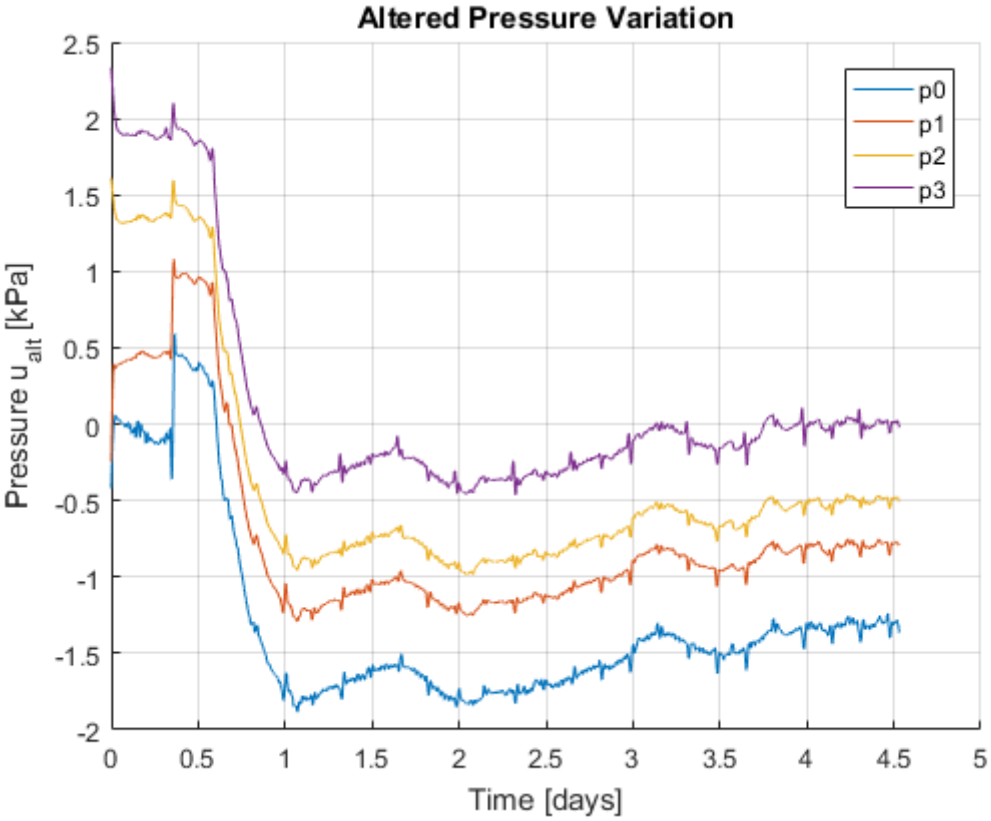

Figure B.3: Altered pressure test 1

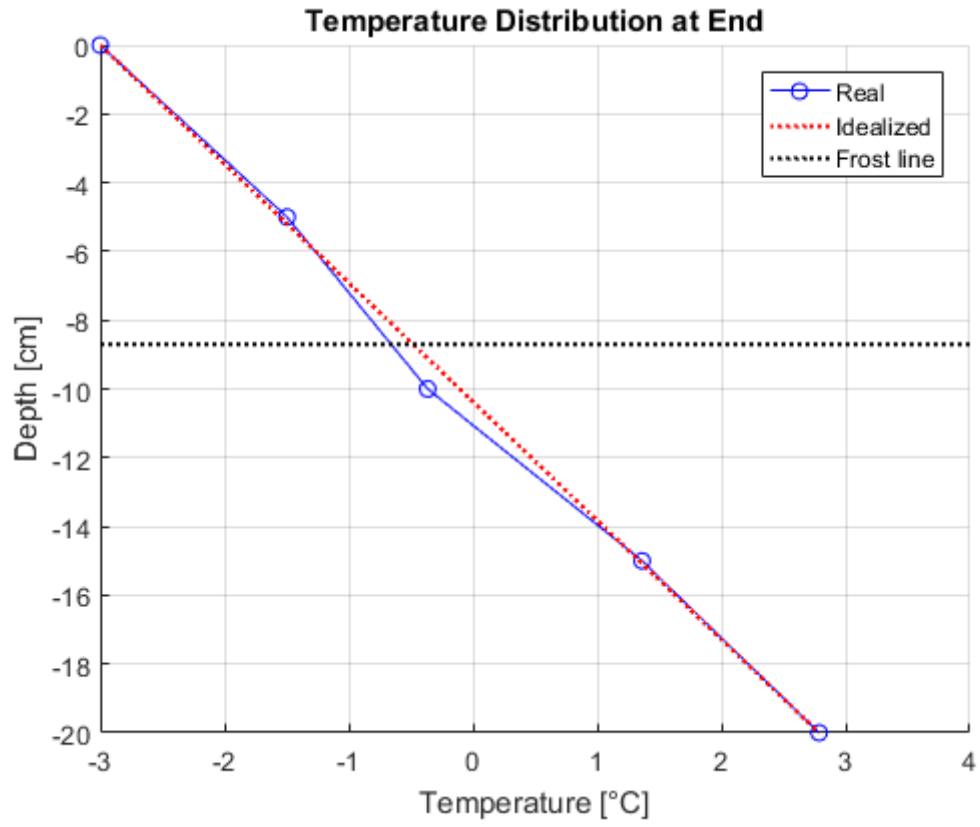

Figure B.4: Temperature distribution at termination for test 1

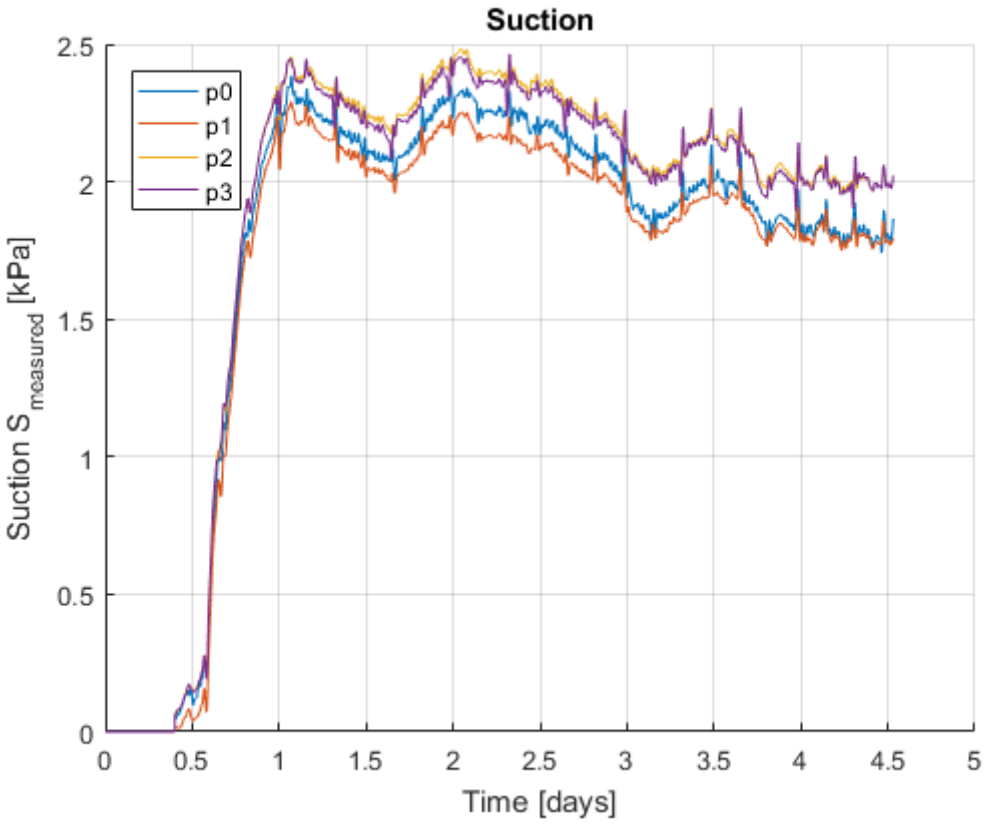

Figure B.5: Measured suction test 1

Appendix C

Results Test 2

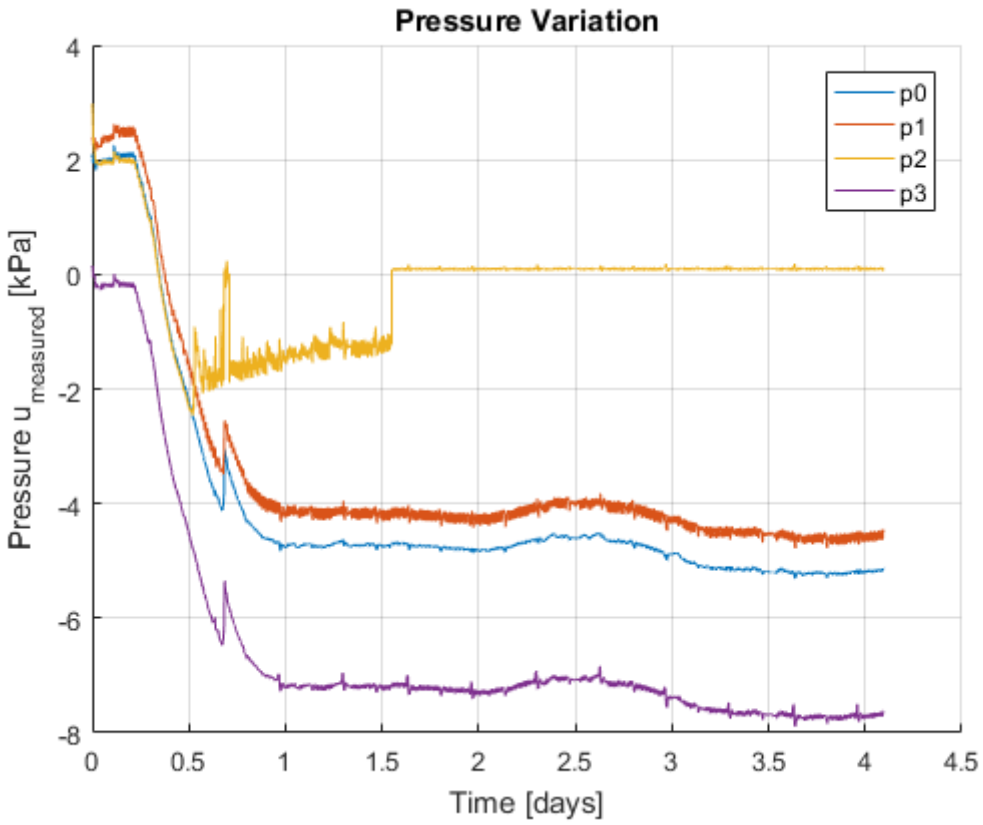

Figure C.1: Measured pressure test 2

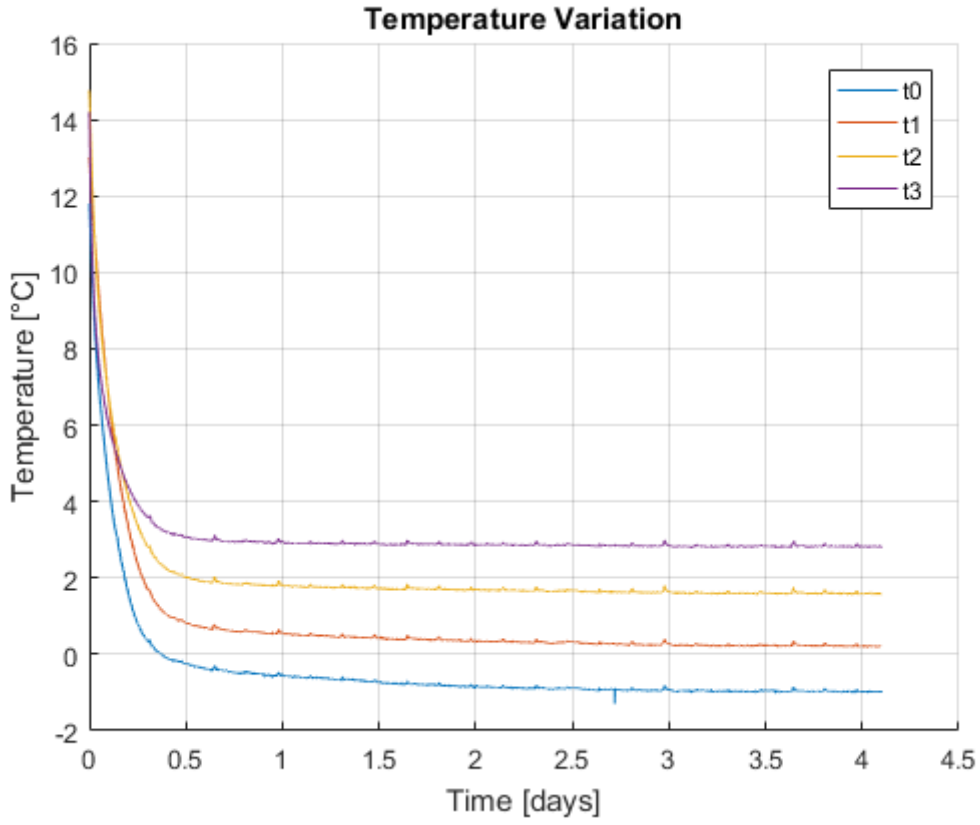

Figure C.2: Measured temperature test 2

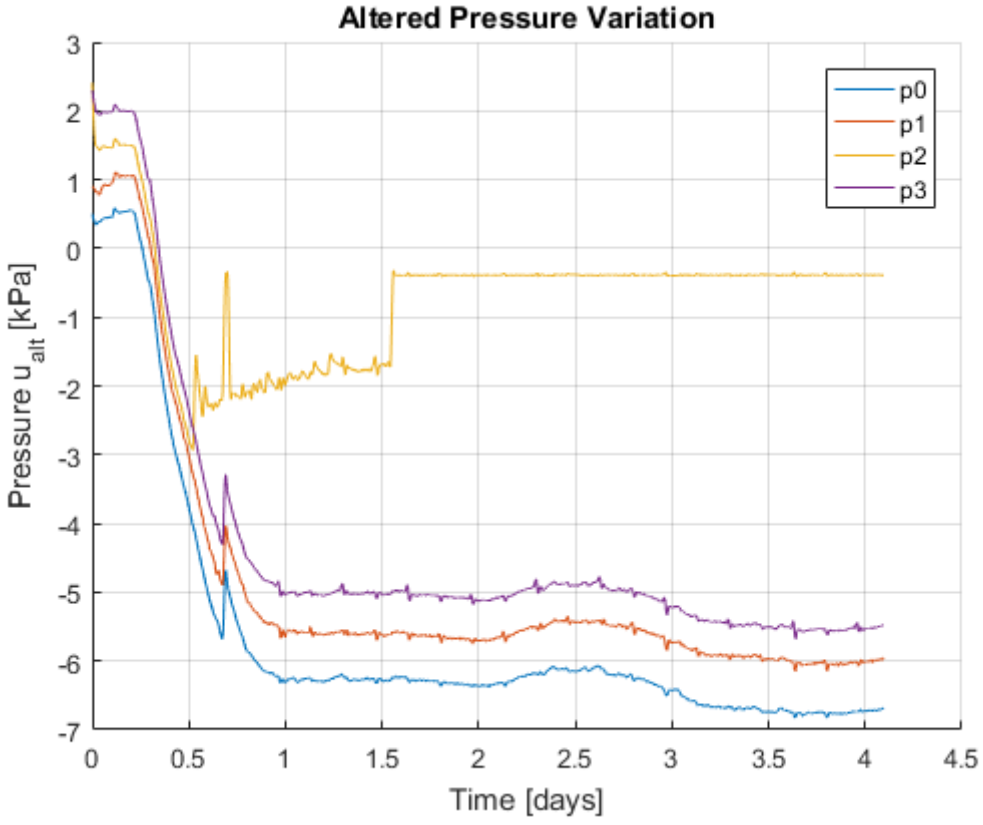

Figure C.3: Altered pressure test 2

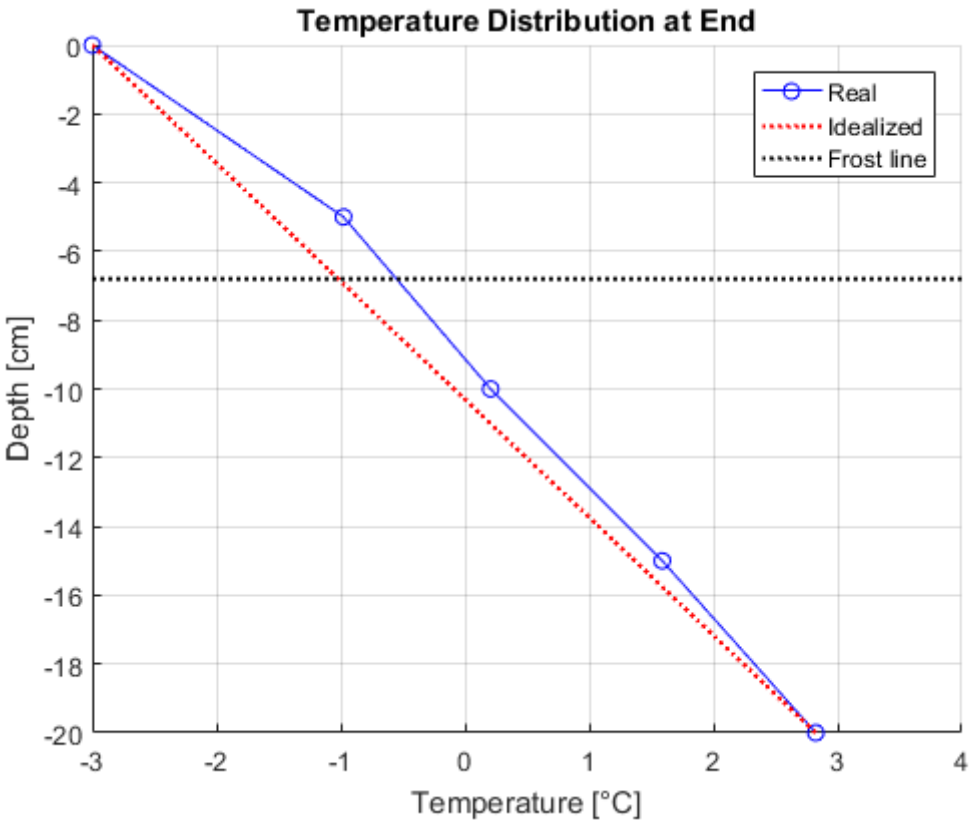

Figure C.4: Temperature distribution at termination for test 2

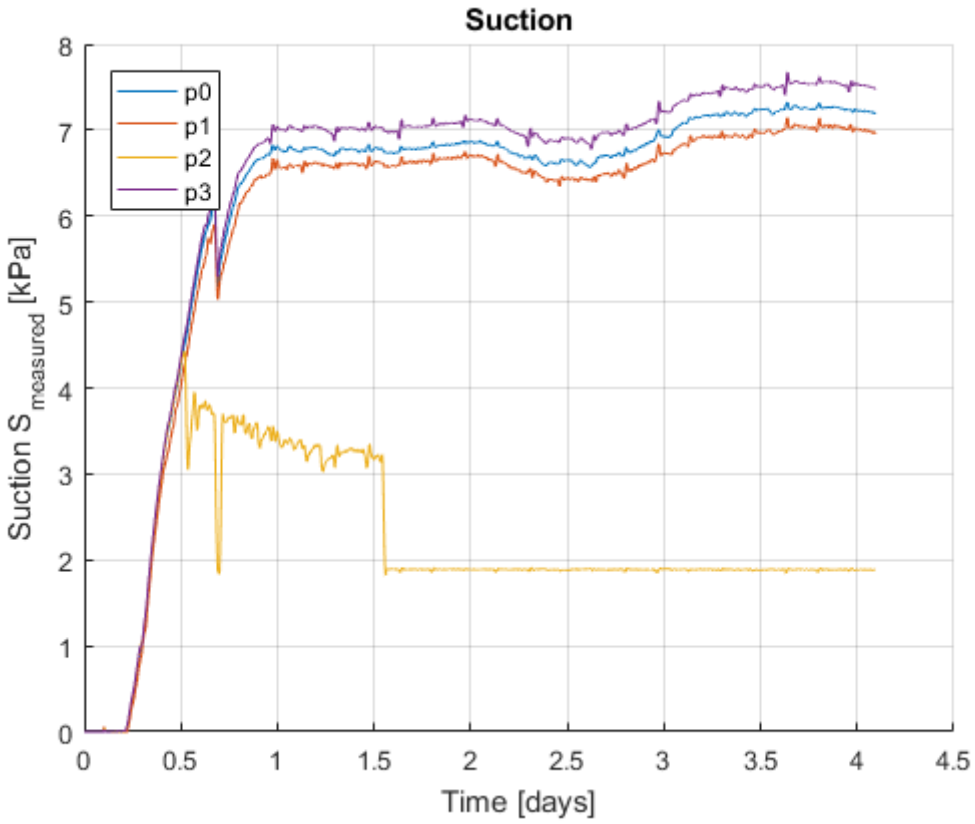

Figure C.5: Measured suction test 2

Appendix D

Results Test 3

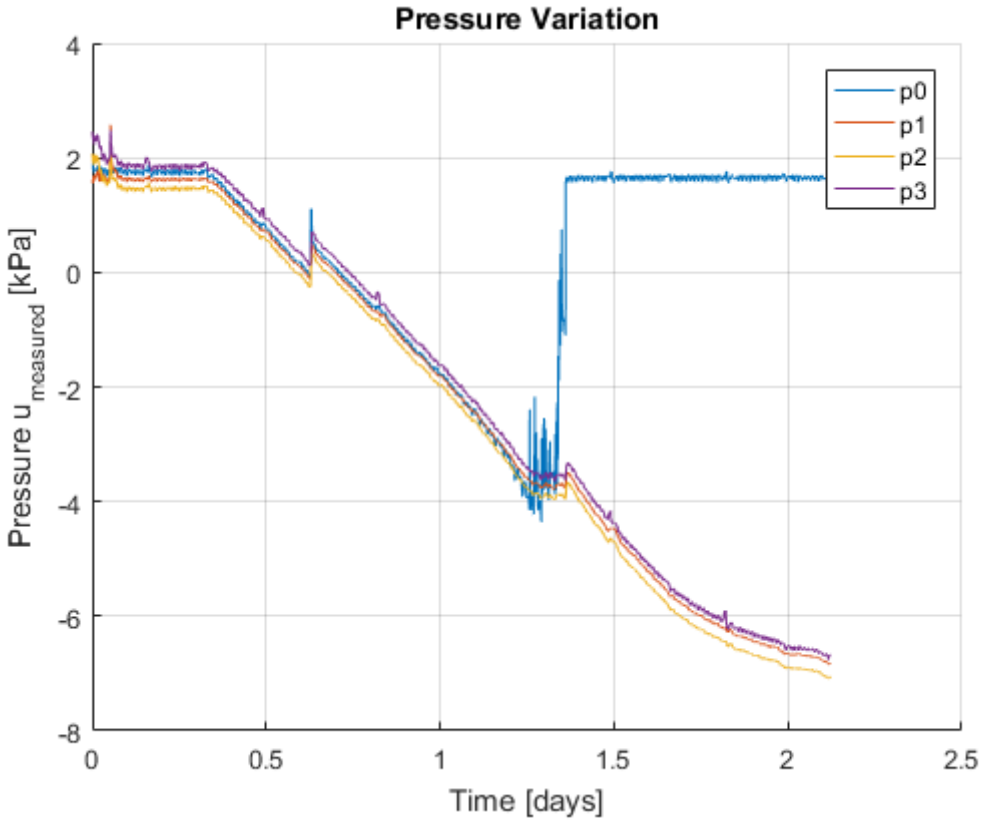

Figure D.1: Measured pressure test 3

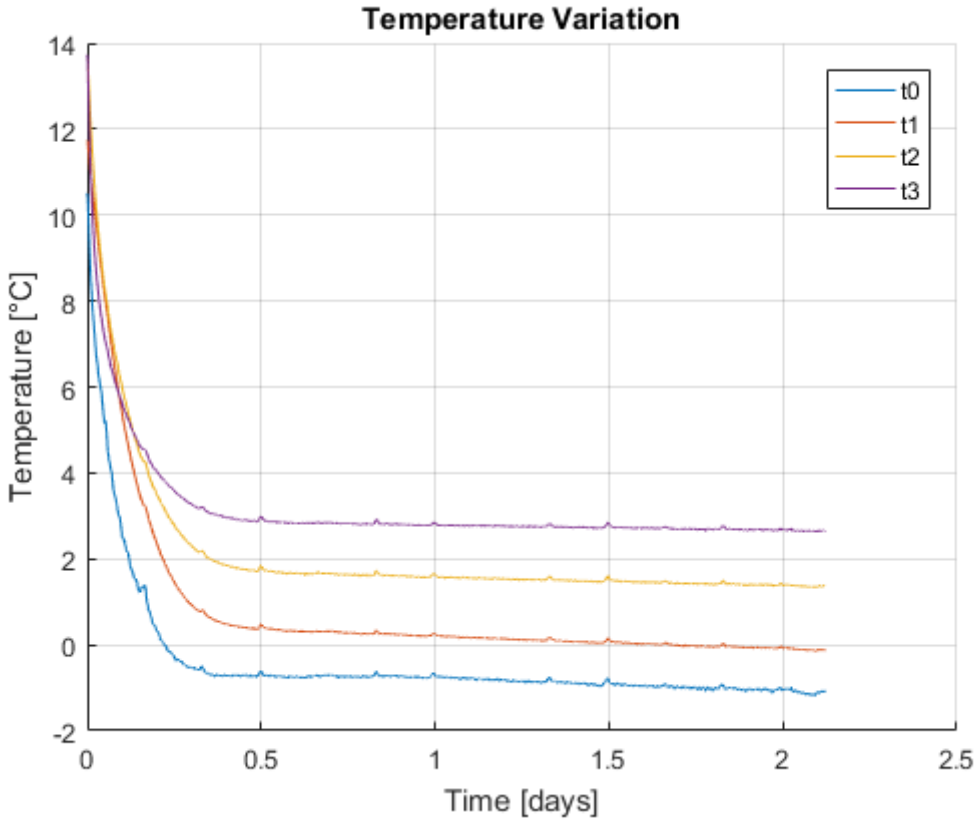

Figure D.2: Measured temperature test 3

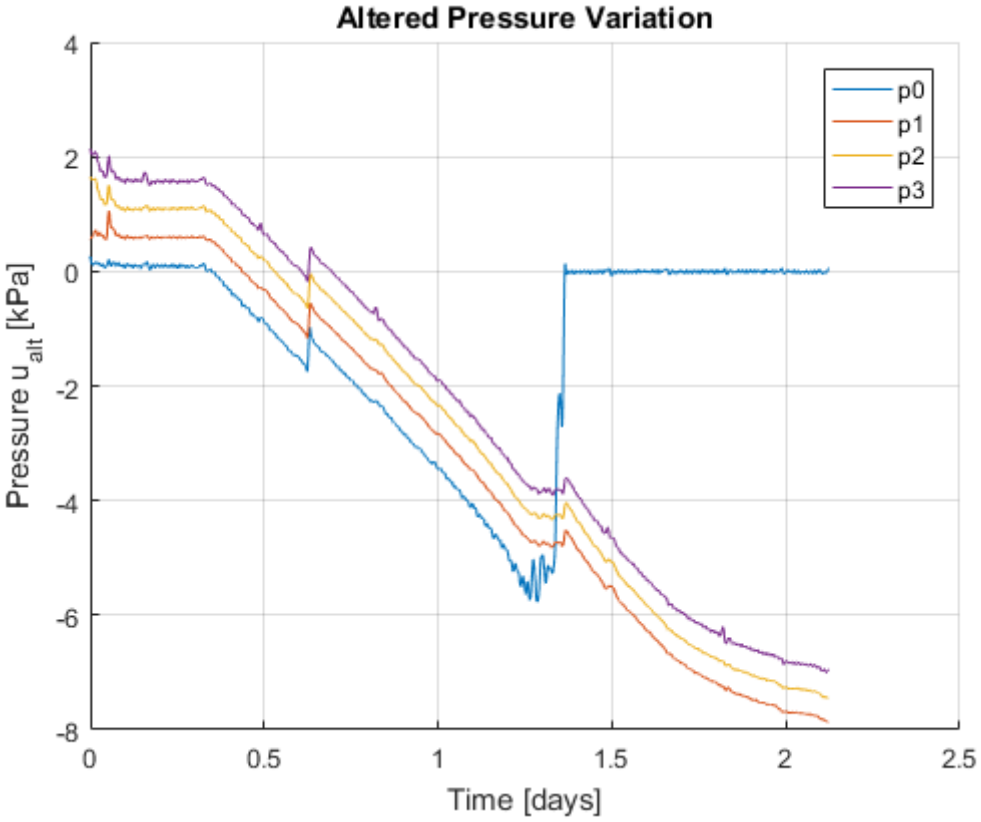

Figure D.3: Altered pressure test 3

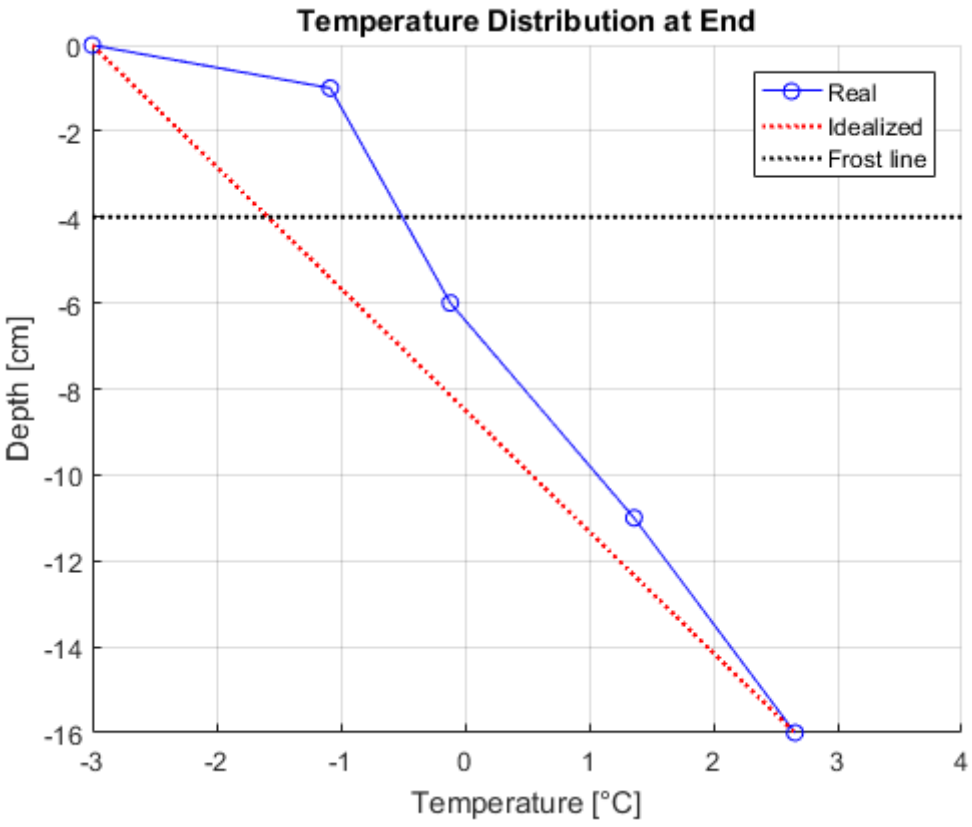

Figure D.4: Temperature distribution at termination for test 3

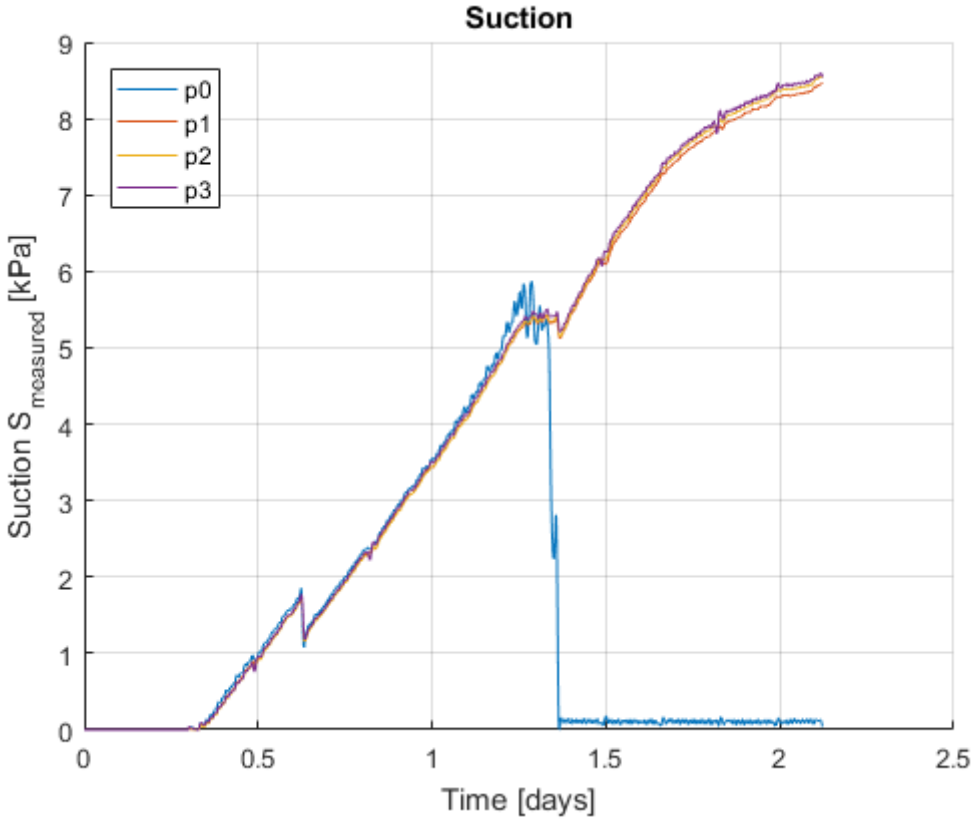

Figure D.5: Measured suction test 3

Appendix E

Oedometer Test - Vassfjellet Silt

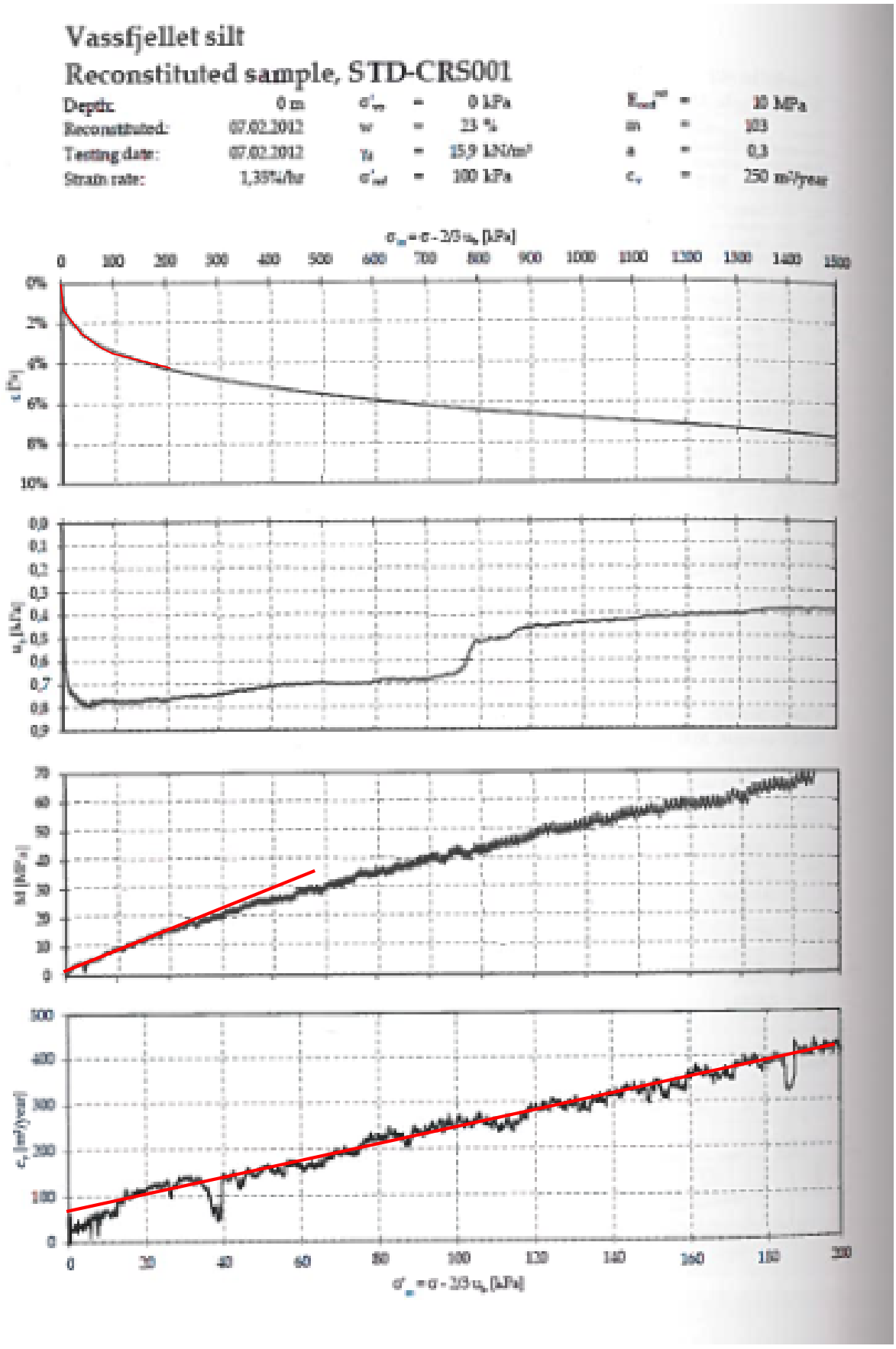

Figure E.1: Linearization of oedometer curves for estimation of permeability

Appendix F

Technical Specifications - Insulation

TEKNISK DATABLAD

Byggkatalogen
juni 12

Brødr. Sunde as | **Isolasjon og byggfolie** | **1030**

Sundolitt XPS isolasjonsplate, XPS300

NOBB modulnr. 23394463

1.5.6 TEK-23394463

1. PRODUKTBESKRIVELSE, ANVENDELSESOMRÅDE

Beskrivelse
Sundolitt XPS300 er en plate i ekstrudert polystyren (XPS) og leveres i flere tykkelser.

Sundolitt XPS300 benyttes som isolasjon i fuktutsatte områder som grøfter, kulverter, omvendte tak samt telesikring av bygninger.. Platene har lav vekt og er lette å håndtere.

Sundolitt XPS300 har en trykkfasthetsklasse på 300 kPa iht EN 826 v/10% def. (korttid)

Sundolitt XPS300 har følgende lambdaverdi:

30-40mm	0,033 W/mK
50mm	0,034 W/mK
60-70mm	0,036 W/mK
80mm	0,037 W/mK
100mm	0,039 W/mK

Anvendelsesområde

Sundolitt XPS300 benyttes som isolering og telesikring på områder som er utsatt for store belastninger, f.eks. veier, industrigulv og fundament i fabrikker og rullebaner

2. TEKNISKE DATA

Faste målangivelser:

Enhet:	**Verdi:**
Tykkelser:	30, 40, 50, 60, 80, 100 mm
Bredde:	585 mm
Lengde:	1185 mm 2385 mm
Trykkfasthetkl.:	300 kPa
Trykkfasthet2%:	140 kPa
Vannopptak:	1-3 vol. %
Lambdaverdi:	0,033 W/mK – 0,039 W/mK
Kant:	Falset (SL)
	Rett (BE)

Farger:
Orange

Brødr. Sunde as | Isolasjon og byggfolie | 1030

Sundolitt XPS isolasjonsplate, XPS300

NOBB modulnr. 23394463

TEK-23394463

3. SAMSVARSERKLÆRINGER OG PRODUKTMERKING

Produktgodkjenninger utstedt av sertifiserte kontrollorganer:
Ingen.

Frivillige kontrollordninger, bransjenorm, sertifikater etc.:
Brødr. Sunde AS er medlem av Isolasjonsprodusentenes forening.

CE-merke:

XPS300 har CE merking.

4. TRANSPORT OG LAGRING

Utvis forsiktighet under håndtering, da platene lett kan brekke.

5. MONTERING/UTFØRELSE

NS 3420-kode for utførelse:

Sundolitt XPS isolasjonsplate monteres iht. S12, isolasjon av cellematerialer.

S12:1, spesifikasjonsmatrise for cellematerialer.

Referanse til NBI byggdetaljer:

513.121, frostsikring av byggegrunn og fundamenter.

525.307, tak for biltrafikk og parkering. Del 1 og 2.

573.344, varmeisolasjonsmaterialer. Typer og egenskaper.

Øvrige henvisninger:
Sages med håndsag eller sirkelsag. Platene legges forbandt på et avrettet underlag.
Er det behov for å lime platene, kan Casco S40 fugelim eller Casco Multifix benyttes.

Brødr. Sunde as | Isolasjon og byggfolie | 1030

Sundolitt XPS isolasjonsplate, XPS300

NOBB modulnr. 23394463

TEK-23394463

6. AVFALLSBEHANDLING OG EMBALLASJE

Avfallsbehandling:
Sundolitt XPS kan resirkuleres til nye produkter eller til energiproduksjon. Alternativt deponering som vanlig restavfall. Produktet inneholder ikke miljøfarlig avfall.

Avfallstype iht. NS-9431:
Annet: XPS.

Type emballasje:
Plast.

7. SIKKERHETSTILTAK VED BEARBEIDING, MONTERING OG LAGRING

Ingen særskilte sikkerhetstiltak ved bearbeiding, montering og lagring er påkrevd.

Spesielle sikkerhetstiltak:
Det er ikke påkrevd med verneutstyr. Eventuelt støv i øynene fra kapping av platene skylles med vann.

Se også eget HMS-datablad for Sundolitt XPS isolasjonsplate fra Brødr. Sunde as.

8. ANSVARLIG FIRMA

Produsent	Brødr. Sunde as
Organisasjonsnr.:	NO 916416784 MVA
Adresse	PB. 8115, Spjelkavik
Postnr og poststed	6022 Ålesund
Telefon	06494
Faks	70 14 34 10
E-post	norway@sundolitt.com

Appendix G

Technical Specifications - Sealant

Erstatter: Ny

Dato: 09.01.2012

Cascol Polyurethane 1809

Et sterkt og fuktbestandig 1-komponent fuktherdende polyuretan trelim. Limer tre mot tre mot andre materialer som f.eks. metall og hard plast. Gir en tilnærmet fargeløs limfuge. Limet skummer og krever et høyt presstrykk. Ikke til bærende konstruksjoner.

- Vannbestandig D4 kvalitet
- Lys limfuge
- Limer tre med høy fuktighet
- Kort presstid Limer ned til + 5°C

TEKNISK DATA

Produkttype:	Diphenylmethane- diisocyante
Emballasje:	100, 300 og 750 ml
Farge:	Lys gul
Løsemiddel:	Ingen
Tørrstoff:	100 %
Konsistens:	Tyktflytende
Densitet:	1230 kg/m^3
Viskositet:	Ca. 2400 mPas ved +25°C
Ventetid:	Åpen ventetid: maks 10-15 min. Lukket ventetid: min.5 min. - maks 25 min.
Herdetid:	Full styrke etter ca. 24 timer
Fuktinnhold i materialer:	Maks 20 % - anbefalt mellom 8-12 %. Ved liming av tre til utendørs bruk - maks 15 %.
Arbeidstemperatur:	Min. +5 °C - + 90°C - best ved + 15°C-+25°C
Temp.bestandighet:	-20 °C - +100° C
Fuktbestandighet:	EN 204, klasse D4
Flammepunkt:	>150°C
Brannfare:	Ingen
Forbruk:	100-300 g/m^2 avhengig av materialsammensetning
Oppbevaring:	Minst 12 mndr. i uåpnet emballasje ved + 5- + 30°C. Lukk Flasken umiddelbart etter limpåføring, da produktet lett absorberer fuktigheten fra luften, og dermed påvirker lagrings-tiden.

BRUKSANVISNING

Trefukt: Cascol Polyuretan D4 limer tre med et fuktinnhold på maks 20 %. Generelt bør fuktigheten i treverk ved liming inne, ligge mellom 8 og 12 %. Ved liming av treverk til utendørs bruk, maks 15 %. I vinterhalvåret kan man med fordel spraye litt vann på emnene for å få en hurtigere herding. Trykkimpregnert tre skal lagres i ett å for at treet og kjemikaliene som er benyttet i trykkimpregneringen skal få tørket.

FORBEHANDLING

Underlaget skal være rent, tørt og fritt for løse partikler. Treverk skal være nybearbeidet, slipt/høvlet og ha god passform. Plast og metall skal slipes og avfettes med for eksempel aceton.

PÅFØRING

Påføres direkte fra limflasken, med fin tannet sparkel eller med rull/pensel.

MONTERING

Etter påføring av lim legges flatene sammen umiddelbart, og holdes sammen med lett presstrykk. Etter en ventetid på 5 min. – maks 25 min. – settes flatene i endelig press. Da limet skummer opp under herding, er det viktig med et kraftig og tett presstrykk.

PRESSTID

Da limet herder ved fuktpåvirkning, vil høy RF forkorte presstiden og lav RF forlenge presstiden. Ved 50 % RF og +23°C, vil presstiden være ca. 4 timer.

OVERFLATEBEHANDLING

Limfugen tåler normal overflatebehandling etter 1 døgn.

RENGJØRING

Generelt bør god renslighet overholdes. Limet inneholder isocyanat og hudkontakt bør unngås. Beskyttelseshansker og briller bør benyttes. Ved hudkontakt vask med såpe og vann, evt. et håndrensemiddel. Verktøy rengjøres med aceton før herding Herdet lim fjernes mekanisk.

HELSE OG MILJØ

Oppbevares utilgjengelig for barn. Unngå innånding av damp. Unngå kontakt med hud og øyne. Ved kontakt med øynene, skyll straks med store mengder vann og kontakt lege. Bruk egnede verneklær og hansker. Ved uhell eller illebefinnende, kontakt lege (vis etiketten om mulig). Ved svelging, kontakt lege omgående og vis denne etikett eller emballasje. Ved innånding/svelging: Flytt den skadelidende til frisk luft, og hold personen i ro. Inneholder isocyanat. Personer som allerede er følsomme for diisocyanat, kan utvikle allergiske reaksjoner ved bruk av dette produktet.

Personer som lider av astma, eksem eller hudproblemer, bør unngå kontakt, inkludert kontakt med dette produktet. Produktet bør ikke brukes under forhold med dårlig ventilasjon, med mindre beskyttende maske med et egnet gassfilter (dvs. type A1 iht. standard EN14387) benyttes.

Ytterligere informasjon: Se Sikkerhetsdatablad

FDV

Ikke aktuelt, gjelder kun overflateprodukter.

Sertifisert iht.:

SIKA NORGE AS
Postadresse:
Postboks 71
2026 SKJETTEN
Tlf.: +47 67 06 10 90
Web: www.casco.no

Appendix H

Technical specifications - Anti Freeze

This appendix presents the technical specifications of the anti-freeze liquid used in the freezing cell. The solution was mixed with a water to anti-freeze ratio of 60.vol% to 40.vol%. The densities and viscosities of the respective liquids are given in table H.1. The total density of the solution can be estimated as given in equation H.1 (LibreTexts, 2017).

$$d = \frac{d_1 \cdot v_1 + d_2 \cdot v_2}{v_1 + v_2} = \frac{998.23 \cdot 60\% + 1126 \cdot 40\%}{100\%} = 1049.3 \text{kg/m}^3 \tag{H.1}$$

	Water	Ethyleneglycol
Density [kg/m^3]	998.23	1126
Viscosity [mm^2/s]	1.004	2.0 - 2.5

Table H.1: Characteristics of ethylene glycol and water at 20 °C

STATOIL ANTI FREEZE

Special

APPLICATIONS

Statoil Anti Freeze is recommended for protecting all water-cooled engines, both diesel and petrol from the effects of freezing temperatures. This product is compatible with steel, aluminium and other alloys.

Mix at least 30 % Statoil Anti Freeze in water for sufficient protection against corrosion and normal winter temperatures (down to -15 °C). For maximum protection against extreme low temperatures mix at 60 % in water. Coolant in the crankcase can cause serious damage. Have leaking gaskets repaired and use separate gauges and funnels when handling Anti Freeze.

Have the Anti Freeze content checked regularly and change once a year for diesel engines and once every two years for petrol engines.

The above is for guidance only. Always follow the engine manufacturer's own recommendations.

ADVANTAGES

Statoil Anti Freeze is also an effective summer coolant and a separate fluid is not needed for different seasons.

CHARACTERISTICS

Statoil Anti Freeze is an amine, phosphate and nitrate free ethyleneglycol formulation with effective additives to prevent corrosion, foaming and oxidation. This product is an anti freeze fluid with a high boiling point. This means minimal evaporation at high engine temperatures.

Water freezes at 0 °C. Statoil Anti Freeze solidifies at about -13 °C. When mixed with water a synergistic effect is obtained, resulting in an even lower freezing point.

Anti Freeze concentrate or dilutions spilled on paintwork must be rinsed off immediately otherwise damage to the surface may result.

ENVIRONMENT

Ethyleneglycol is readily biodegradable, with low toxicity towards water organisms and no bioaccumulation in the aqueous environment. Normal handling and small discharges are of no harm to the environment. Larger discharges or repeated smaller discharges can however have a negative impact.

TYPICAL INSPECTIONS

CHARACTERISTICS	METHODS	UNITS	
Colour	Visual	-	Blue-green
Density at 20 °C	ASTM D 4052	kg/m³	1126
Viscosity at 20 °C	ASTM D 445	mm²/s	20-25
Flashpoint COC	ASTM D 92	°C	>120
Boiling Point	-	°C	>150
pH - concentrate	-	-	5.5-7.0
Water content - concentrate	-	wt-%	<5

HANDLING AND STORAGE

Harmful if swallowed. INGESTION MAY CAUSE DEATH OR KIDNEY DAMAGE.
If swallowed, seek medical advice immediately and show the container or label.
Remove contaminated clothing as soon as possible.
Wash the skin with water and soap.
Avoid inhalation of vapours.
Keep out of the reach of children.

Statoil Lubricants, 118 88 Stockholm.

Customer service tel 08-429 68 50, fax 08-429 68 51, email: smobest@statoil.com

2000-10-25

Appendix I

Technical Specifications - Pressure Sensor

Pressure Sensors

26PC Series

Gage and Differential/Unamplified-Compensated

Temperature Compensated Sensors

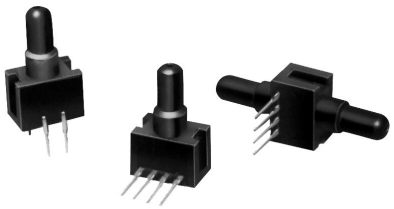

FEATURES

- Lowest priced sensor with temperature compensation and calibration
- Variety of gage pressure port configurations - easily and quickly modified for your special needs
- Operable after exposure to frozen conditions
- Choice of termination for gage sensors
- Calibrated Null and Span
- Temperature compensated for Span over 0 to 50°C
- Provides interchangeability
- Can be used to measure vacuum or positive pressure
- Ideal for wet/wet differential applications

Unamplified

26PC SERIES PERFORMANCE CHARACTERISTICS at 10.0 ±0.01 VDC Excitation, 25°C

	Min.	Typ.	Max.	Units
Excitation	---	10	16	VDC
Repeatability & Hysteresis	---	±0.20	---	%Span
Response Time	---	---	1.0	msec
Input Resistance	5.5 K	7.5 K	11.5 K	ohms
Output Resistance	1.5 K	2.5 K	3.0 K	ohms
Stability over One Year	---	±0.5	---	%Span
Weight	---	2	---	grams

Total error calculation, see page 105.

ENVIRONMENTAL SPECIFICATIONS

Operating Temperature	−40° to 85°C (−40° to +185°F)
Storage Temperature	−55° to +100°C (−67° to +212°F)
Compensated Temperature	0° to +50°C (32° to +122°F)
Shock	Qualification tested to 150 g
Vibration	MIL-STD-202. Method 213 (150g halfsine, 11 msec)
Media (P1 & P2)	Limited only to those media which will not attack polyetherimide, silicon, fluorosilicone, silicone, EPDM, and neoprene seals.

26PC SERIES ORDER GUIDE

Catalog Listing	Pressure Range (psi)	Linearity (% span)		Null Shift (mV)		Null Offset (mV)			Span Shift (% span)		Span (mV)			Sensitivity mV/psi	Over-pressure psi
		Typ.	Max	Typ.	Max	Min.	Typ.	Max.	Typ.	Max.	Min.	Typ.	Max.	Typ.	Max.
26PCA TYPE	1	0.25	0.5	±0.5	±1.0	−1.5	0	+1.5	±1.0	±2.0	14.7	16.7	18.7	16.7	20
26PCB TYPE	5	0.4	0.5	±0.5	±1.0	−1.5	0	+1.5	±1.0	±1.5	47	50	53	10.0	20
26PCC TYPE	15	0.25	0.5	±0.5	±1.0	−1.5	0	+1.5	±0.75	±1.5	97	100	103	6.67	45
26PCD TYPE	30	0.1	0.2	±0.75	±1.5	−1.5	0	+1.5	±0.75	±1.5	97	100	103	3.33	60
26PCF TYPE	100	0.1	0.2	±1.0	±2.0	−2.0	0	+2.0	±0.5	±1.5	95	100	105	1.0	200
26PCJ TYPE	38*	0.1	0.5	±0.7	±1.5	−1.5	0	+1.5	±1.0	±1.5	37.5	39.5	41.5	2.63	60
26PCK TYPE	38*	0.1	0.5	±0.7	±1.5	−1.5	0	+1.5	±1.0	±1.5	37.5	39.5	41.5	2.63	60

*Accuracy specifications calculated at 15 psi.

Pressure Sensors

26PC Series

Gage and Differential/Unamplified-Compensated

SENSOR SELECTION GUIDE

2 Product Family	6 Circuit Type	PC Pressure Transducer	B Pressure Range	F* Type of Seal	A Type of Port	2 Termination Style	G Pressure Measurement
2 20PC family	**6** Compensated Calibrated		**A** 1 psi **B** 5 psi **C** 15 psi **D** 30 psi **F** 100 psi **J** 38 psi **K** 38 psi (passivated**)	**E** EPDM **F** Fluorosilicone **N** Neoprene **S** Silicone	**A** Straight **B** Barbed **C** Luer **D** Modular **H** M5 Thread **I** 90° Port **J** Needle **K** Reverse 90° Port **L** 1/4-28 UNF w/Cable Lock **M** 1/4 - 28 UNF w/o Cable Lock **S** Manifold	**1** 1 x 4 (.400″) **2** 2 x 2 **6** 1 x 4 (.600″)	**G** Gage **D** Differential

Example: 26PCBFA2G
Compensated and calibrated 5 psi sensor with fluorosilicone seal, straight port, 2 x 2 terminals, and Gage pressure measurement.
*Other media seal materials may be available.
**P2 side of die coated for environmental and dielectric protection.

See Accessories Guide, page 27.

Not all combinations are established. Contact 800 number before final design.

ACCESSORIES SELECTION GUIDE

Catalog Listing	Description	Drawing
PC-10182	Steel lockring (included with Port Style A, 1 x 4 terminals only) 22, 24, 26PC only	Figure 1
PC-15111	Cable retaining clip for large port Flow-Through sensor only	Figure 4
PC-15110	Single hole plastic bracket	Figure 3
PC-15015	Mounting bracket	Figure 6
PC-15132	Plastic Mounting bracket	Figure 5
20PCWHRC	Flow-Through wire harness and retaining clip	Figure 2
26PCBKT	Mounting bracket for large port Flow-Through sensor only	Figure 7
PC-15202	Mounting bracket for Luer Port	Figure 8
PC-15204	Mounting bracket for Straight Port	Figure 9

Figure 1 PC-10182
Steel Lockring

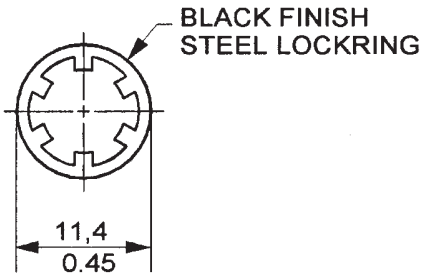

Figure 2 20PCWHRC
Wire Harness and Retaining Clip

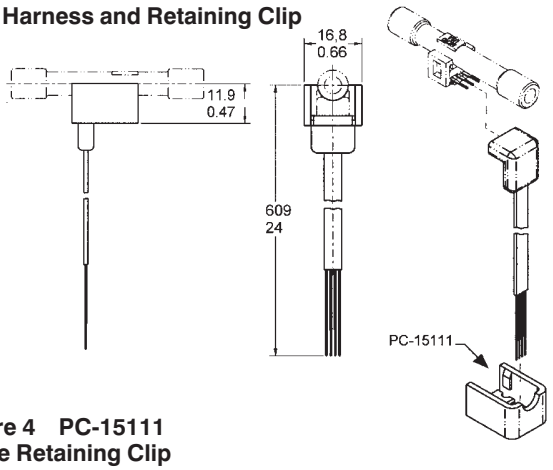

Figure 3 PC-15110
Single Hole Plastic Bracket

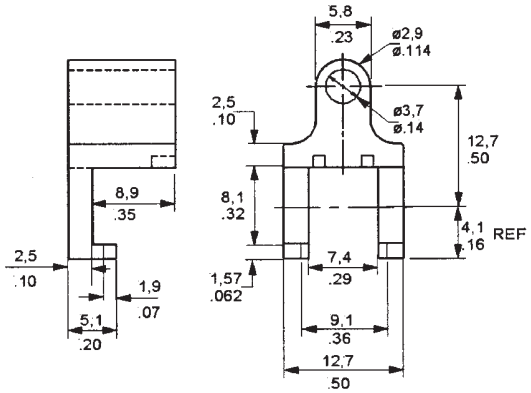

Figure 4 PC-15111
Cable Retaining Clip

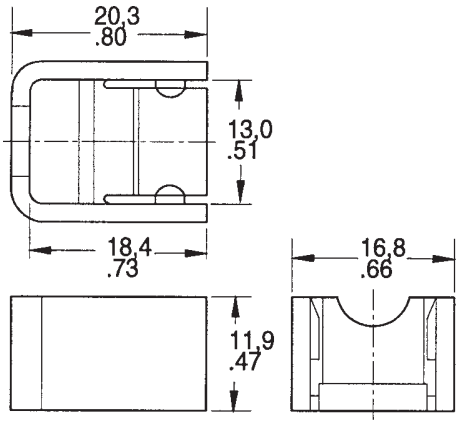

Figure 5 PC-15132
Plastic Mounting Bracket

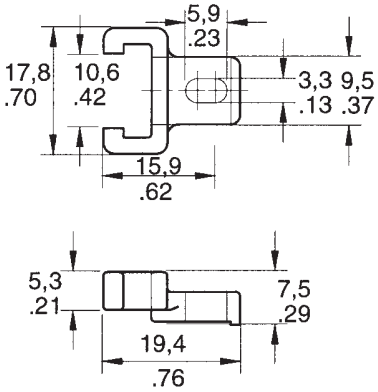

Figure 6 PC-15015
Mounting Bracket

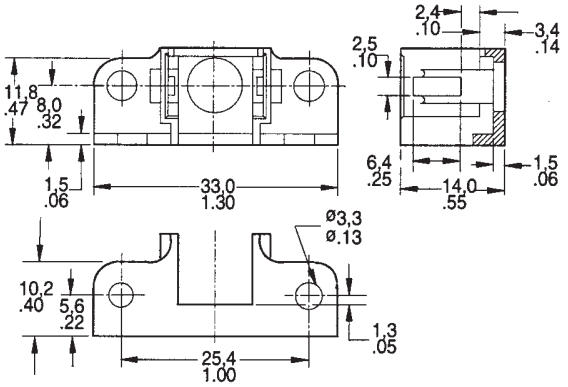

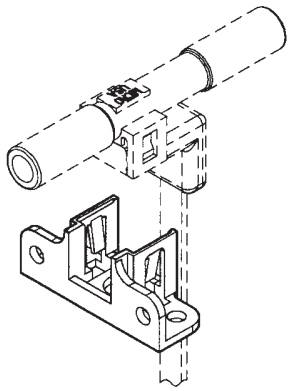

Figure 7 26PCBKT
For use with N, P Large Ports

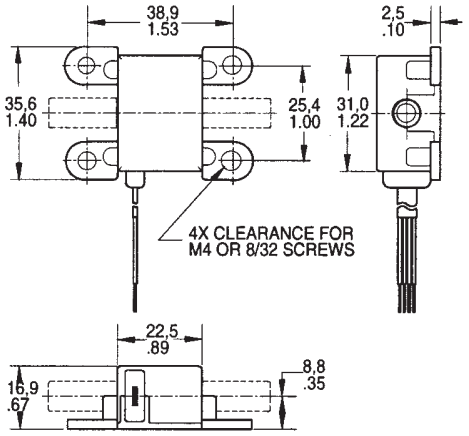

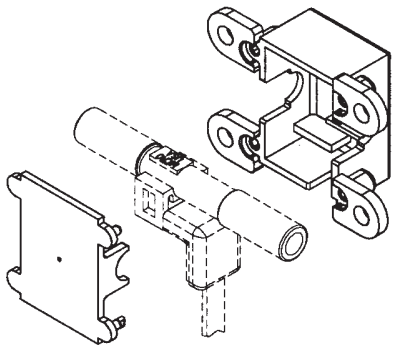

Figure 8 PC-15202
For use with C Luer Port

Figure 9 PC-15204
For use with A Straight Port

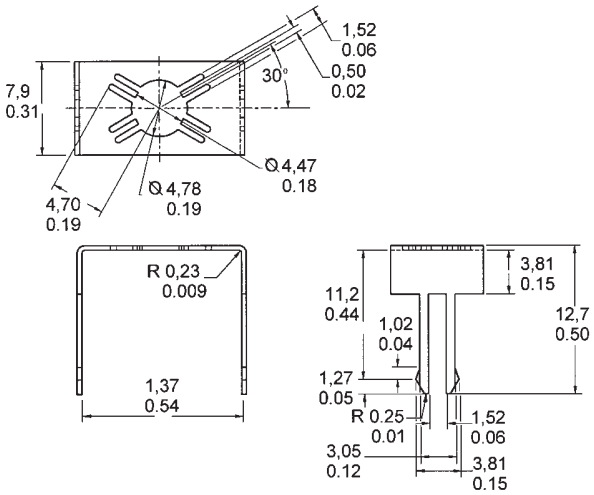

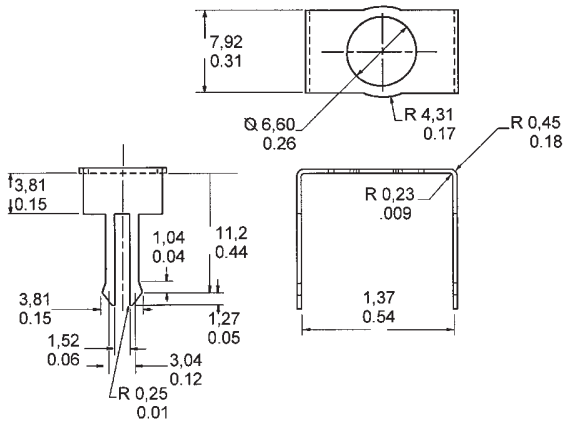

Note: PC-15202 and PC-15204 are Printed Circuit Board mountable and solderable; designed to be used in a .063 thick PC Board with a recommended mounting hole size of .125 ±.005 in.

Gage and Differential/Unamplified

MOUNTING DIMENSIONS (for reference only)

GAGE SENSOR
Pressure is applied to port P2.
Port P1 vents to ambient pressure.

"1 x 4" Termination (Style 1), Port Style A, Straight
Pin 1 is notched, and is shown at the right of the package.
Pin 2 is next to pin 1, etc.

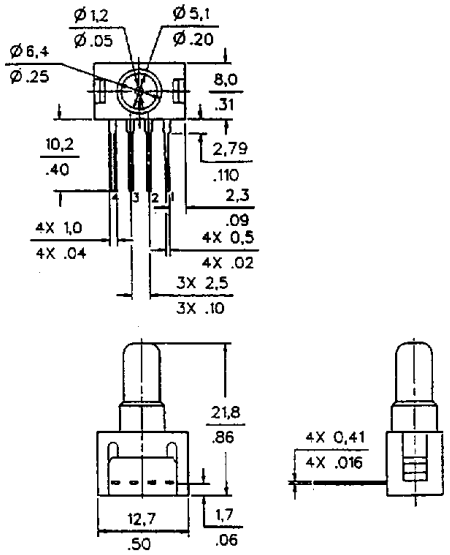

DIFFERENTIAL SENSOR
Straight Port, 1 x 4 termination (Style 2) ONLY
Port P1 is near terminals.

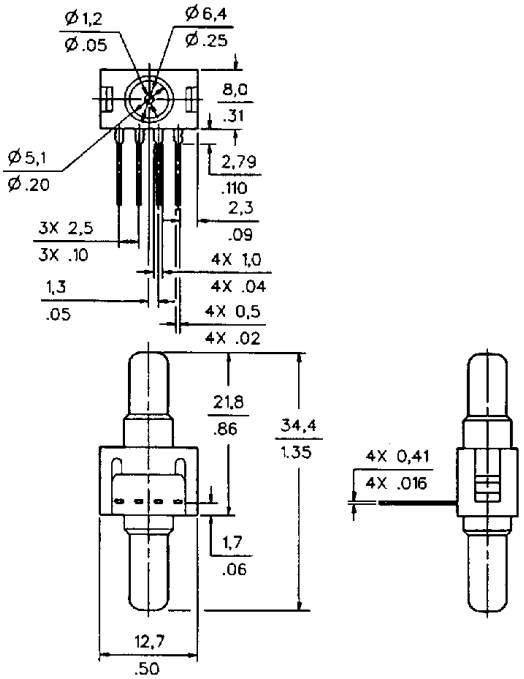

"2 x 2" Termination (Style 2), Port Style A, Straight
Pin 1 is notched, and is shown at lower right corner.
Pins 2, 3 and 4 are clockwise.

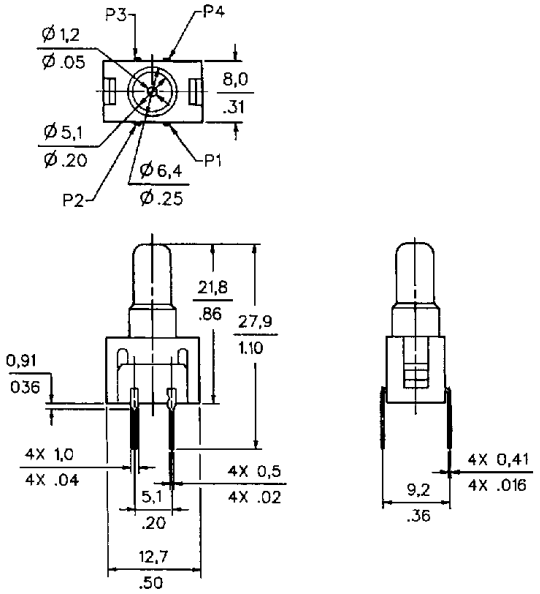

ACCESSORIES
Lockring (included with A port)
PC10182

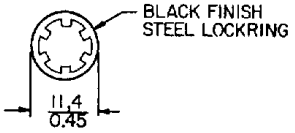

Single hole Plastic Bracket (purchase separately)
PC10949

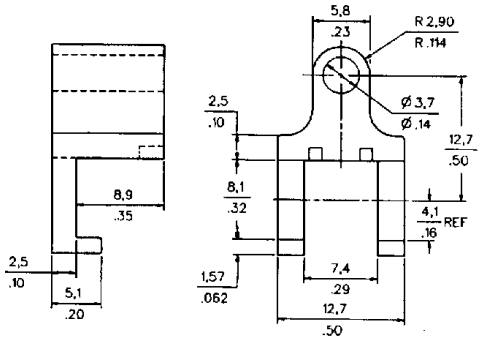

Dual Port Plastic Bracket (purchase separately)
PC15015

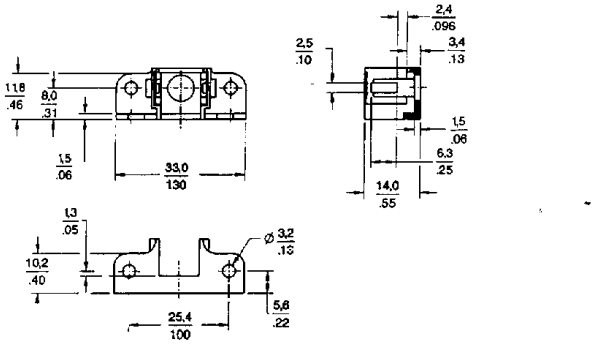

OTHER GAGE SENSOR PORT STYLES
(2 x 2 or 1 x 4 Termination)

B Barbed

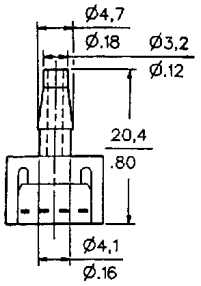

C Luer

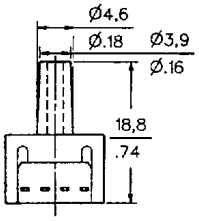

D Modular

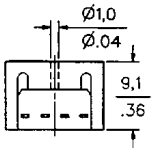

H M5 Thread

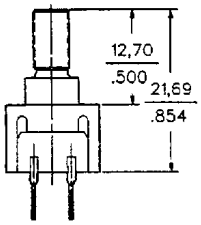

O-Ring
Size 007
O-Ring Counterbore

.040" deep ±.005 × .30 ±.003"

I 90°

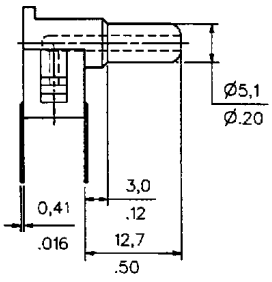

J Needle

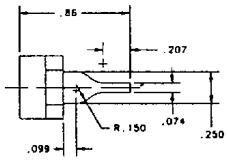

M ¼–28 UNF Thread

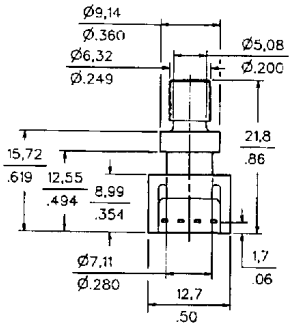

O-Ring
Size 009
O-Ring Counterbore

.040" deep ±.002 × .360" ±.003"

20PC SERIES CIRCUIT - NOTES

1. Circled numbers refer to Sensor Terminals (interface pins).
2. V_0 increases with pressure change.
3. $V_0 = V_2 - V_4$
4. Pin 1 designated with a notch.

Pin Designation

Pin 1	V_S (+)
Pin 2	Output (+)
Pin 3	Ground (–)
Pin 4	Output (–)

EXCITATION

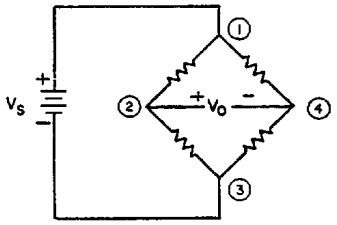

20PC Construction

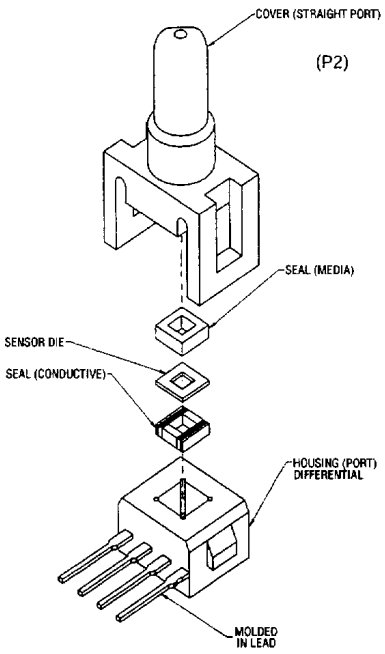

Unamplified

Appendix J

Permeability of Pressure Filters

The pressure filters used in this thesis was in advance unspecified with regard to permeability and air entry. A simple determination of the permeability has been performed in the laboratory. A saturated filter was placed under constant pressure head, applied by a water column, for a given amount of time. The water that passed through the filter during the time interval was recorded. The permeability was then approximated using known relations between water flow and pressure gradient. The pressure gradient i is given by the total height difference and the thickness of the filter, see equation J.1. The thickness and area of the filter were approximately determined.

$$i = \frac{dh}{L} \tag{J.1}$$

$$q = \frac{Q}{t} \tag{J.2}$$

$$k = \frac{q}{i \cdot A} \tag{J.3}$$

	Value	**Unit**
m_w	4.39	g
dh	127	cm
L	0.3	cm
i	423.3	-
Q	4.39	cm^3
t	70800	s
q	$6.2 \cdot 10^{-5}$	cm^3/s
A	10	cm^2
k	$\mathbf{1.5 \cdot 10^{-10}}$	**m/s**

Table J.1: Permeability calculations for pressure filter

Appendix K

Technical Specifications - Temperature Transducer

Low Cost, Precision IC Temperature Transducer

AD592

FEATURES
High Precalibrated Accuracy: 0.5°C max @ +25°C
Excellent Linearity: 0.15°C max (0°C to +70°C)
Wide Operating Temperature Range: –25°C to +105°C
Single Supply Operation: +4 V to +30 V
Excellent Repeatability and Stability
High Level Output: 1 μA/K
Two Terminal Monolithic IC: Temperature In/ Current Out
Minimal Self-Heating Errors

CONNECTION DIAGRAM

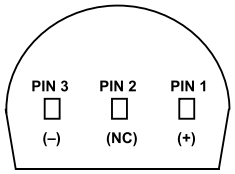

* PIN 2 CAN BE EITHER ATTACHED OR UNCONNECTED
BOTTOM VIEW

PRODUCT DESCRIPTION

The AD592 is a two terminal monolithic integrated circuit temperature transducer that provides an output current proportional to absolute temperature. For a wide range of supply voltages the transducer acts as a high impedance temperature dependent current source of 1 μA/K. Improved design and laser wafer trimming of the IC's thin film resistors allows the AD592 to achieve absolute accuracy levels and nonlinearity errors previously unattainable at a comparable price.

The AD592 can be employed in applications between –25°C and +105°C where conventional temperature sensors (i.e., thermistor, RTD, thermocouple, diode) are currently being used. The inherent low cost of a monolithic integrated circuit in a plastic package, combined with a low total parts count in any given application, make the AD592 the most cost effective temperature transducer currently available. Expensive linearization circuitry, precision voltage references, bridge components, resistance measuring circuitry and cold junction compensation are not required with the AD592.

Typical application areas include: appliance temperature sensing, automotive temperature measurement and control, HVAC (heating/ventilating/air conditioning) system monitoring, industrial temperature control, thermocouple cold junction compensation, board-level electronics temperature diagnostics, temperature readout options in instrumentation, and temperature correction circuitry for precision electronics. Particularly useful in remote sensing applications, the AD592 is immune to voltage drops and voltage noise over long lines due to its high impedance current output. AD592s can easily be multiplexed; the signal current can be switched by a CMOS multiplexer or the supply voltage can be enabled with a tri-state logic gate.

The AD592 is available in three performance grades: the AD592AN, AD592BN and AD592CN. All devices are packaged in a plastic TO-92 case rated from –45°C to +125°C. Performance is specified from –25°C to +105°C. AD592 chips are also available, contact the factory for details.

PRODUCT HIGHLIGHTS

1. With a single supply (4 V to 30 V) the AD592 offers 0.5°C temperature measurement accuracy.
2. A wide operating temperature range (–25°C to +105°C) and highly linear output make the AD592 an ideal substitute for older, more limited sensor technologies (i.e., thermistors, RTDs, diodes, thermocouples).
3. The AD592 is electrically rugged; supply irregularities and variations or reverse voltages up to 20 V will not damage the device.
4. Because the AD592 is a temperature dependent current source, it is immune to voltage noise pickup and IR drops in the signal leads when used remotely.
5. The high output impedance of the AD592 provides greater than 0.5°C/V rejection of supply voltage drift and ripple.
6. Laser wafer trimming and temperature testing insures that AD592 units are easily interchangeable.
7. Initial system accuracy will not degrade significantly over time. The AD592 has proven long term performance and repeatability advantages inherent in integrated circuit design and construction.

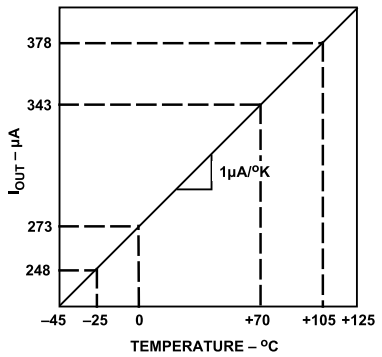

REV. A

One Technology Way, P.O. Box 9106, Norwood, MA 02062-9106, U.S.A.
Tel: 617/329-4700 **Fax: 617/326-8703**

AD592–SPECIFICATIONS (typical @ T_A = +25°C, V_S = +5 V, unless otherwise noted)

Model	AD592AN Min	AD592AN Typ	AD592AN Max	AD592BN Min	AD592BN Typ	AD592BN Max	AD592CN Min	AD592CN Typ	AD592CN Max	Units
ACCURACY										
Calibration Error @ +25°C[1]		1.5	**2.5**		0.7	**1.0**		0.3	**0.5**	°C
T_A = 0°C to +70°C										
Error over Temperature		1.8	3.0		0.8	1.5		0.4	0.8	°C
Nonlinearity[2]		0.15	0.35		0.1	0.25		0.05	0.15	°C
T_A = –25°C to +105°C										
Error over Temperature[3]		2.0	**3.5**		0.9	**2.0**		0.5	**1.0**	°C
Nonlinearity[2]		0.25	0.5		0.2	0.4		0.1	0.35	°C
OUTPUT CHARACTERISTICS										
Nominal Current Output @ +25°C (298.2K)		298.2			298.2			298.2		µA
Temperature Coefficient		1			1			1		µA/°C
Repeatability[4]			0.1			0.1			0.1	°C
Long Term Stability[5]			0.1			0.1			0.1	°C/month
ABSOLUTE MAXIMUM RATINGS										
Operating Temperature	–25		+105	–25		+105	–25		+105	°C
Package Temperature[6]	–45		+125	–45		+125	–45		+125	°C
Forward Voltage (+ to –)			**44**			**44**			**44**	V
Reverse Voltage (– to +)			**20**			**20**			**20**	V
Lead Temperature (Soldering 10 sec)			300			300			300	°C
POWER SUPPLY										
Operating Voltage Range	4		30	4		30	4		30	V
Power Supply Rejection										
+4 V < V_S < +5 V			**0.5**			**0.5**			**0.5**	°C/V
+5 V < V_S < +15 V			**0.2**			**0.2**			**0.2**	°C/V
+15 V < V_S < +30 V			**0.1**			**0.1**			**0.1**	°C/V

NOTES
[1]An external calibration trim can be used to zero the error @ +25°C.
[2]Defined as the maximum deviation from a mathematically best fit line.
[3]Parameter tested on all production units at +105°C only. C grade at –25°C also.
[4]Maximum deviation between +25°C readings after a temperature cycle between –45°C and +125°C. Errors of this type are noncumulative.
[5]Operation @ +125°C, error over time is noncumulative.
[6]Although performance is not specified beyond the operating temperature range, temperature excursions within the package temperature range will not damage the device.
Specifications subject to change without notice.
Specifications shown in boldface are tested on all production units at final electrical test. Results from those tests are used to calculate outgoing quality levels. All min and max specifications are guaranteed, although only those shown in boldface are tested on all production units.

METALIZATION DIAGRAM

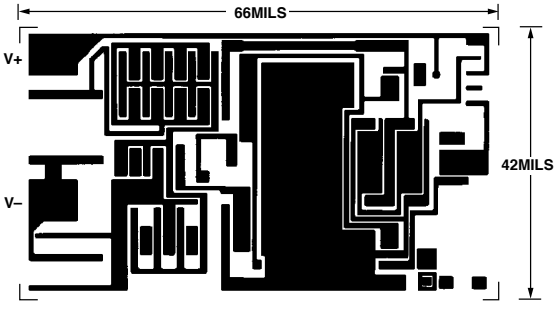

TEMPERATURE SCALE CONVERSION EQUATIONS

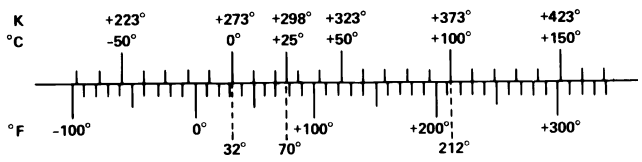

$$°C = \frac{5}{9}(°F - 32) \qquad K = °C + 273.15$$

$$°F = \frac{9}{5}°C + 32 \qquad °R = °F + 459.7$$

ORDERING GUIDE

Model	Max Cal Error @ +25°C	Max Error –25°C to +105°C	Max Nonlinearity –25°C to +105°C	Package Option
AD592CN	0.5°C	1.0°C	0.35°C	TO-92
AD592BN	1.0°C	2.0°C	0.4°C	TO-92
AD592AN	2.5°C	3.5°C	0.5°C	TO-92

Typical @ V_S = +5 V

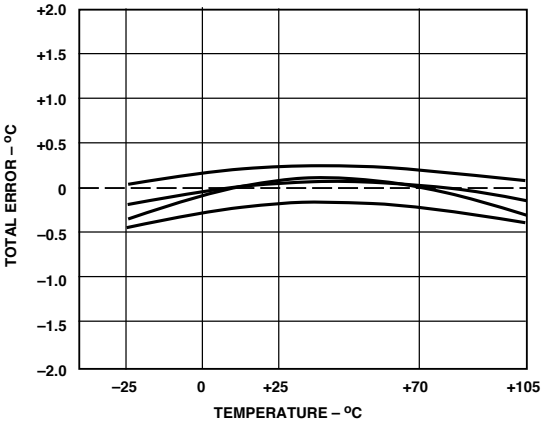

AD592CN Accuracy Over Temperature

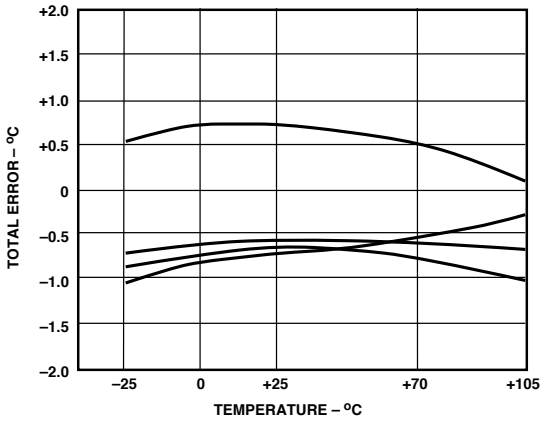

AD592BN Accuracy Over Temperature

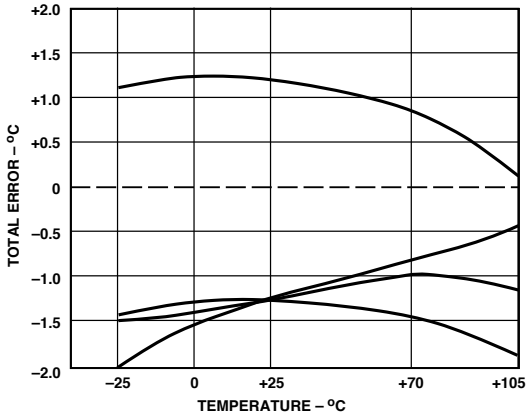

AD592AN Accuracy Over Temperature

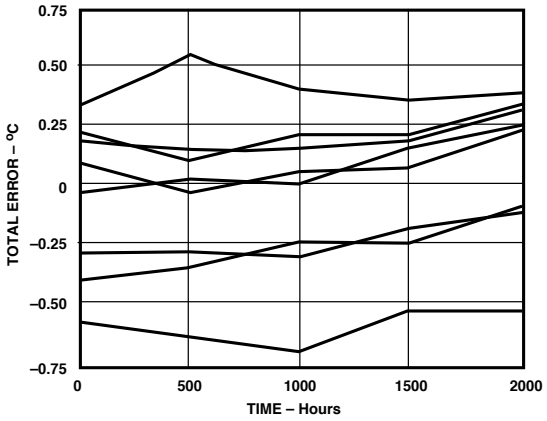

Long-Term Stability @ +85°C and 85% Relative Humidity

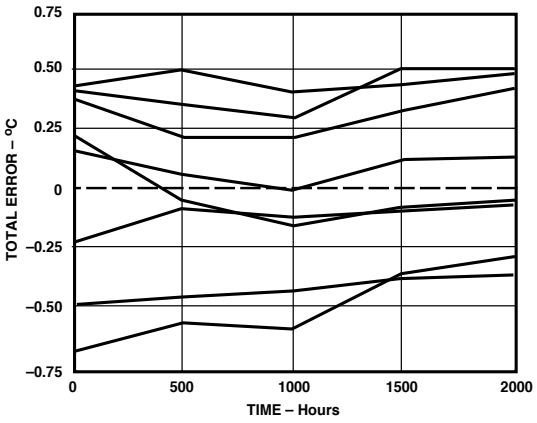

Long-Term Stability @ +125°C

THEORY OF OPERATION

The AD592 uses a fundamental property of silicon transistors to realize its temperature proportional output. If two identical transistors are operated at a constant ratio of collector current densities, r, then the difference in base-emitter voltages will be (kT/q)(ln r). Since both k, Boltzman's constant and q, the charge of an electron are constant, the resulting voltage is directly Proportional To Absolute Temperature (PTAT). In the AD592 this difference voltage is converted to a PTAT current by low temperature coefficient thin film resistors. This PTAT current is then used to force the total output current to be proportional to degrees Kelvin. The result is a current source with an output equal to a scale factor times the temperature (K) of the sensor. A typical V-I plot of the circuit at +25°C and the temperature extremes is shown in Figure 1.

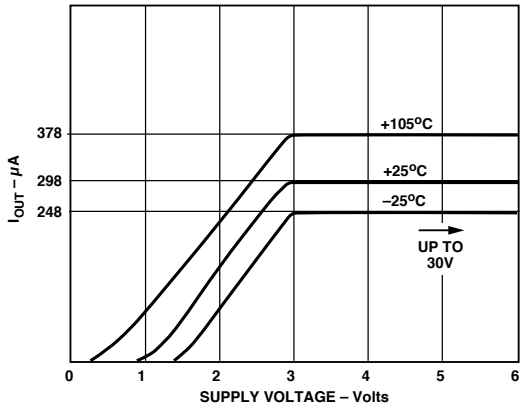

Figure 1. V-I Characteristics

Factory trimming of the scale factor to 1 μA/K is accomplished at the wafer level by adjusting the AD592's temperature reading so it corresponds to the actual temperature. During laser trimming the IC is at a temperature within a few degrees of 25°C and is powered by a 5 V supply. The device is then packaged and automatically temperature tested to specification.

FACTORS AFFECTING AD592 SYSTEM PRECISION

The accuracy limits given on the Specifications page for the AD592 make it easy to apply in a variety of diverse applications. To calculate a total error budget in a given system it is important to correctly interpret the accuracy specifications, nonlinearity errors, the response of the circuit to supply voltage variations and the effect of the surrounding thermal environment. As with other electronic designs external component selection will have a major effect on accuracy.

CALIBRATION ERROR, ABSOLUTE ACCURACY AND NONLINEARITY SPECIFICATIONS

Three primary limits of error are given for the AD592 such that the correct grade for any given application can easily be chosen for the overall level of accuracy required. They are the calibration accuracy at +25°C, and the error over temperature from 0°C to +70°C and –25°C to +105°C. These specifications correspond to the actual error the user would see if the current output of an AD592 were converted to a voltage with a precision resistor. Note that the maximum error at room temperature, over the commercial IC temperature range, or an extended range including the boiling point of water, can be directly read from the specifications table. All three error limits are a combination of initial error, scale factor variation and nonlinearity deviation from the ideal 1 μA/K output. Figure 2 graphically depicts the guaranteed limits of accuracy for an AD592CN.

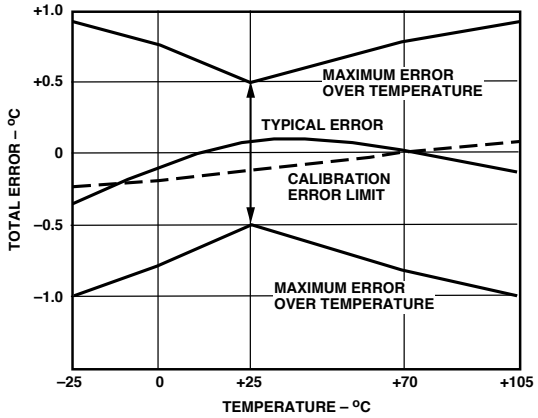

Figure 2. Error Specifications (AD592CN)

The AD592 has a highly linear output in comparison to older technology sensors (i.e., thermistors, RTDs and thermocouples), thus a nonlinearity error specification is separated from the absolute accuracy given over temperature. As a maximum deviation from a best-fit straight line this specification represents the only error which cannot be trimmed out. Figure 3 is a plot of typical AD592CN nonlinearity over the full rated temperature range.

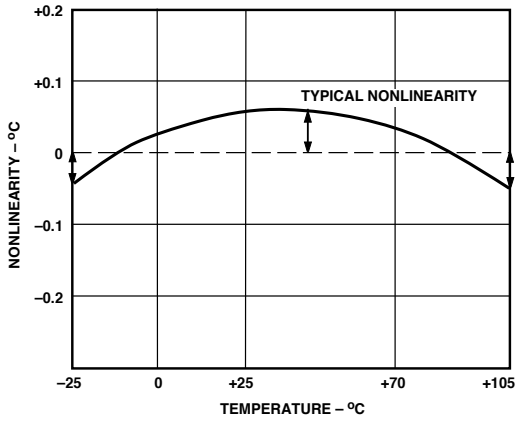

Figure 3. Nonlinearity Error (AD592CN)

TRIMMING FOR HIGHER ACCURACY

Calibration error at 25°C can be removed with a single temperature trim. Figure 4 shows how to adjust the AD592's scale factor in the basic voltage output circuit.

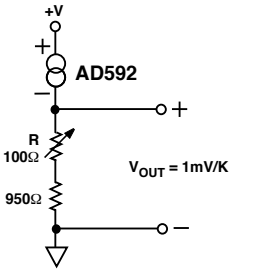

Figure 4. Basic Voltage Output (Single Temperature Trim)

To trim the circuit the temperature must be measured by a reference sensor and the value of R should be adjusted so the output (V_{OUT}) corresponds to 1 mV/K. Note that the trim procedure should be implemented as close as possible to the temperature highest accuracy is desired for. In most applications if a single temperature trim is desired it can be implemented where the AD592 current-to-output voltage conversion takes place (e.g., output resistor, offset to an op amp). Figure 5 illustrates the effect on total error when using this technique.

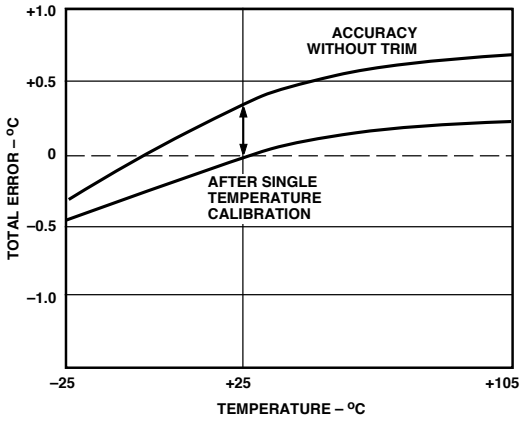

Figure 5. Effect of Scale Factor Trim on Accuracy

If greater accuracy is desired, initial calibration and scale factor errors can be removed by using the AD592 in the circuit of Figure 6.

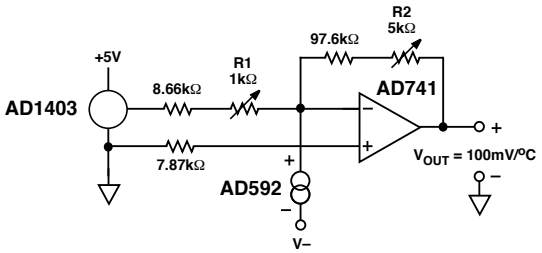

Figure 6. Two Temperature Trim Circuit

With the transducer at 0°C adjustment of R1 for a 0 V output nulls the initial calibration error and shifts the output from K to °C. Tweaking the gain of the circuit at an elevated temperature by adjusting R2 trims out scale factor error. The only error remaining over the temperature range being trimmed for is nonlinearity. A typical plot of two trim accuracy is given in Figure 7.

SUPPLY VOLTAGE AND THERMAL ENVIRONMENT EFFECTS

The power supply rejection characteristics of the AD592 minimizes errors due to voltage irregularity, ripple and noise. If a supply is used other than 5 V (used in factory trimming), the power supply error can be removed with a single temperature trim. The PTAT nature of the AD592 will remain unchanged. The general insensitivity of the output allows the use of lower cost unregulated supplies and means that a series resistance of several hundred ohms (e.g., CMOS multiplexer, meter coil resistance) will not degrade the overall performance.

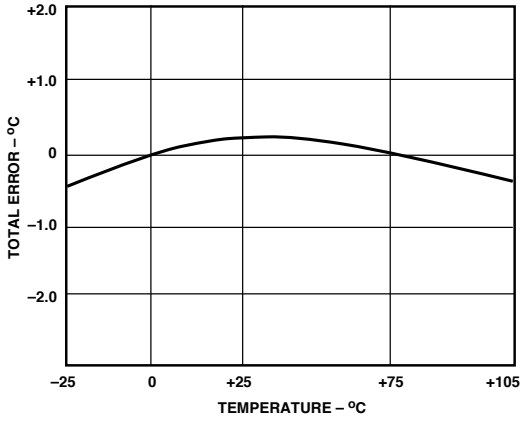

Figure 7. Typical Two Trim Accuracy

The thermal environment in which the AD592 is used determines two performance traits: the effect of self-heating on accuracy and the response time of the sensor to rapid changes in temperature. In the first case, a rise in the IC junction temperature above the ambient temperature is a function of two variables; the power consumption level of the circuit and the thermal resistance between the chip and the ambient environment (θ_{JA}). Self-heating error in °C can be derived by multiplying the power dissipation by θ_{JA}. Because errors of this type can vary widely for surroundings with different heat sinking capacities it is necessary to specify θ_{JA} under several conditions. Table I shows how the magnitude of self-heating error varies relative to the environment. In typical free air applications at +25°C with a 5 V supply the magnitude of the error is 0.2°C or less. A common clip-on heat sink will reduce the error by 25% or more in critical high temperature, large supply voltage situations.

Table I. Thermal Characteristics

Medium	θ_{JA} (°C/watt)	τ (sec)*
Still Air		
Without Heat Sink	175	60
With Heat Sink	130	55
Moving Air		
Without Heat Sink	60	12
With Heat Sink	40	10
Fluorinert Liquid	35	5
Aluminum Block**	30	2.4

NOTES

*τ is an average of five time constants (99.3% of final value). In cases where the thermal response is not a simple exponential function, the actual thermal response may be better than indicated.

**With thermal grease.

Response of the AD592 output to abrupt changes in ambient temperature can be modeled by a single time constant τ exponential function. Figure 8 shows typical response time plots for several media of interest.

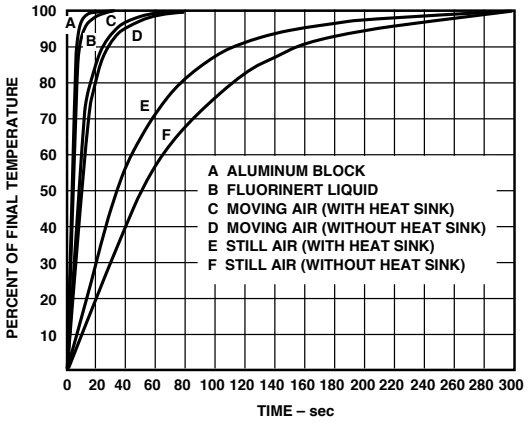

Figure 8. Thermal Response Curves

The time constant, τ, is dependent on θ_{JA} and the thermal capacities of the chip and the package. Table I lists the effective τ (time to reach 63.2% of the final value) for several different media. Copper printed circuit board connections where neglected in the analysis, however, they will sink or conduct heat directly through the AD592's solder dipped Kovar leads. When faster response is required a thermally conductive grease or glue between the AD592 and the surface temperature being measured should be used. In free air applications a clip-on heat sink will decrease output stabilization time by 10-20%.

MOUNTING CONSIDERATIONS

If the AD592 is thermally attached and properly protected, it can be used in any temperature measuring situation where the maximum range of temperatures encountered is between –25°C and +105°C. Because plastic IC packaging technology is employed, excessive mechanical stress must be safeguarded against when fastening the device with a clamp or screw-on heat tab. Thermally conductive epoxy or glue is recommended under typical mounting conditions. In wet or corrosive environments, any electrically isolated metal or ceramic well can be used to shield the AD592. Condensation at cold temperatures can cause leakage current related errors and should be avoided by sealing the device in nonconductive epoxy paint or dips.

APPLICATIONS

Connecting several AD592 devices in parallel adds the currents through them and produces a reading proportional to the average temperature. Series AD592s will indicate the lowest temperature because the coldest device limits the series current flowing through the sensors. Both of these circuits are depicted in Figure 9.

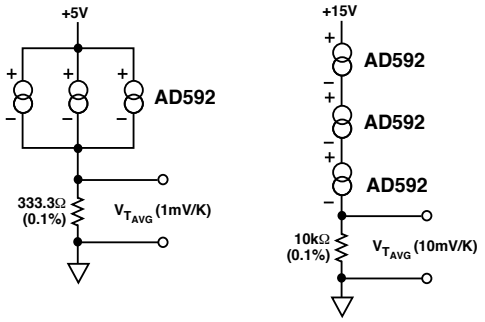

Figure 9. Average and Minimum Temperature Connections

The circuit of Figure 10 demonstrates a method in which a voltage output can be derived in a differential temperature measurement.

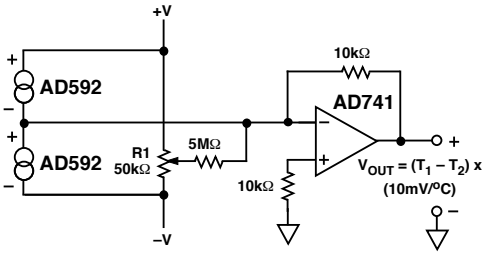

Figure 10. Differential Measurements

R1 can be used to trim out the inherent offset between the two devices. By increasing the gain resistor (10 kΩ) temperature measurements can be made with higher resolution. If the magnitude of V+ and V– is not the same, the difference in power consumption between the two devices can cause a differential self-heating error.

Cold junction compensation (CJC) used in thermocouple signal conditioning can be implemented using an AD592 in the circuit configuration of Figure 11. Expensive simulated ice baths or hard to trim, inaccurate bridge circuits are no longer required.

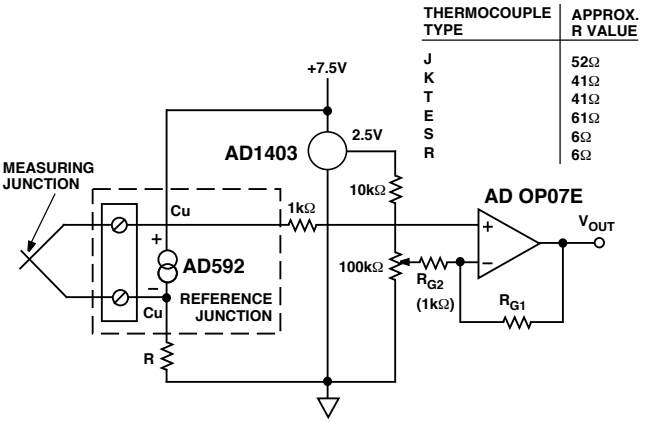

Figure 11. Thermocouple Cold Junction Compensation

The circuit shown can be optimized for any ambient temperature range or thermocouple type by simply selecting the correct value for the scaling resistor – R. The AD592 output (1 μA/K) times R should approximate the line best fit to the thermocouple curve (slope in V/°C) over the most likely ambient temperature range. Additionally, the output sensitivity can be chosen by selecting the resistors R_{G1} and R_{G2} for the desired noninverting gain. The offset adjustment shown simply references the AD592 to °C. Note that the TC's of the reference and the resistors are the primary contributors to error. Temperature rejection of 40 to 1 can be easily achieved using the above technique.

Although the AD592 offers a noise immune current output, it is not compatible with process control/industrial automation current loop standards. Figure 12 is an example of a temperature to 4–20 mA transmitter for use with 40 V, 1 kΩ systems.

In this circuit the 1 μA/K output of the AD592 is amplified to 1 mA/°C and offset so that 4 mA is equivalent to 17°C and 20 mA is equivalent to 33°C. Rt is trimmed for proper reading at an intermediate reference temperature. With a suitable choice of resistors, any temperature range within the operating limits of the AD592 may be chosen.

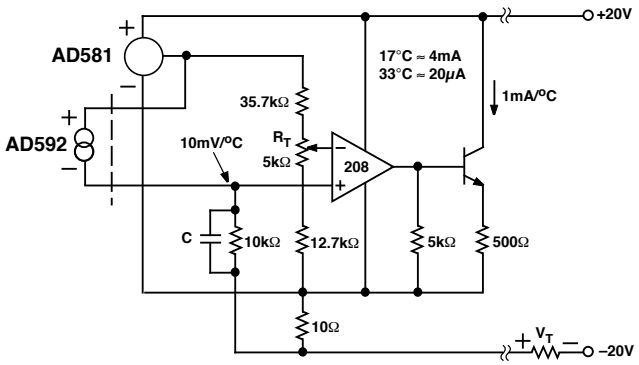

Figure 12. Temperature to 4–20 mA Current Transmitter

Reading temperature with an AD592 in a microprocessor based system can be implemented with the circuit shown in Figure 13.

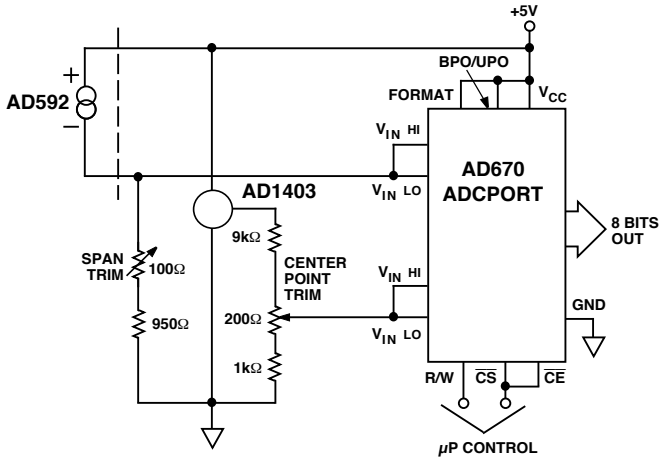

Figure 13. Temperature to Digital Output

By using a differential input A/D converter and choosing the current to voltage conversion resistor correctly, any range of temperatures (up to the 130°C span the AD592 is rated for) centered at any point can be measured using a minimal number of components. In this configuration the system will resolve up to 1°C.

A variable temperature controlling thermostat can easily be built using the AD592 in the circuit of Figure 14.

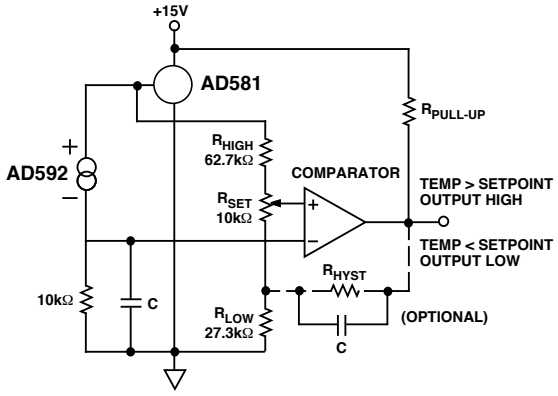

Figure 14. Variable Temperature Thermostat

R_{HIGH} and R_{LOW} determine the limits of temperature controlled by the potentiometer R_{SET}. The circuit shown operates over the full temperature range (–25°C to +105°C) the AD592 is rated for. The reference maintains a constant set point voltage and insures that approximately 7 V appears across the sensor. If it is necessary to guardband for extraneous noise hysteresis can be added by tying a resistor from the output to the ungrounded end of R_{LOW}.

Multiple remote temperatures can be measured using several AD592s with a CMOS multiplexer or a series of 5 V logic gates because of the device's current-mode output and supply-voltage compliance range. The on-resistance of a FET switch or output impedance of a gate will not affect the accuracy, as long as 4 V is maintained across the transducer. MUXs and logic driving circuits should be chosen to minimize leakage current related errors. Figure 15 illustrates a locally controlled MUX switching the signal current from several remote AD592s. CMOS or TTL gates can also be used to switch the AD592 supply voltages, with the multiplexed signal being transmitted over a single twisted pair to the load.

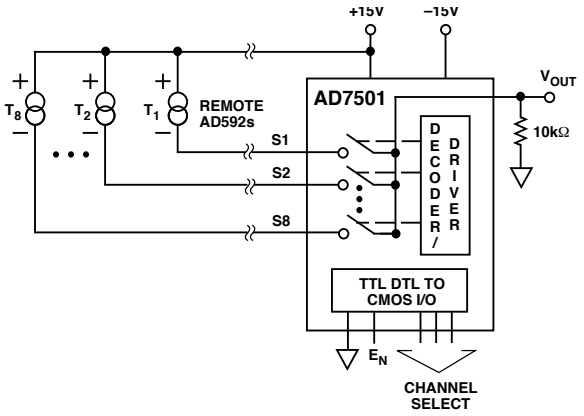

Figure 15. Remote Temperature Multiplexing

To minimize the number of MUXs required when a large number of AD592s are being used, the circuit can be configured in a matrix. That is, a decoder can be used to switch the supply voltage to a column of AD592s while a MUX is used to control which row of sensors are being measured. The maximum number of AD592s which can be used is the product of the number of channels of the decoder and MUX.

An example circuit controlling 80 AD592s is shown in Figure 16. A 7-bit digital word is all that is required to select one of the sensors. The enable input of the multiplexer turns all the sensors off for minimum dissipation while idling.

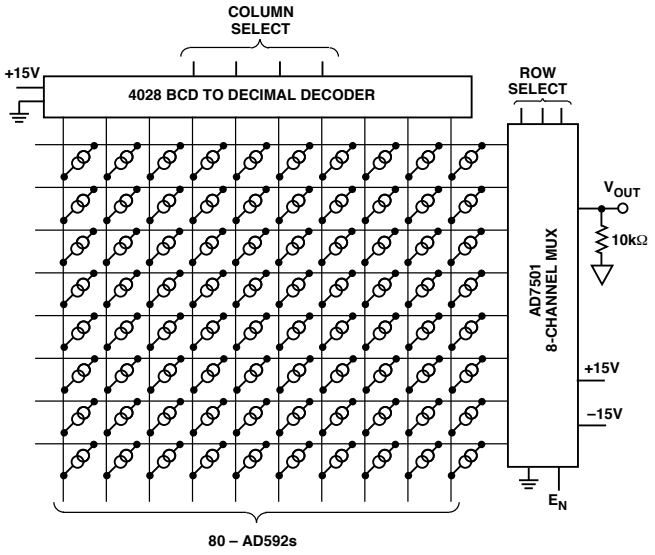

Figure 16. Matrix Multiplexer

To convert the AD592 output to °C or °F a single inexpensive reference and op amp can be used as shown in Figure 17. Although this circuit is similar to the two temperature trim circuit shown in Figure 6, two important differences exist. First, the gain resistor is fixed alleviating the need for an elevated temperature trim. Acceptable accuracy can be achieved by choosing an inexpensive resistor with the correct tolerance. Second, the AD592 calibration error can be trimmed out at a known convenient temperature (i.e., room temperature) with a single pot adjustment. This step is independent of the gain selection.

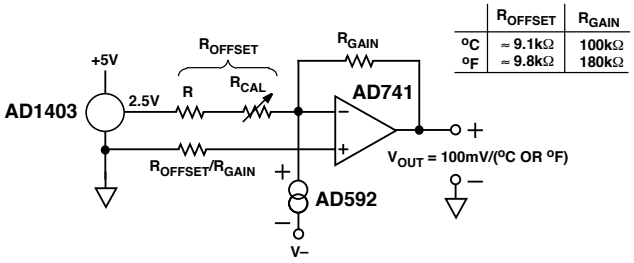

	R_{OFFSET}	R_{GAIN}
°C	≈ 9.1kΩ	100kΩ
°F	≈ 9.8kΩ	180kΩ

Figure 17. Celsius or Fahrenheit Thermometer

OUTLINE DIMENSIONS

Dimensions shown in inches and (mm).

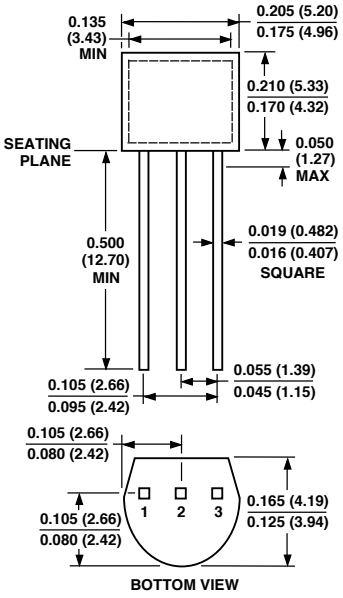

C819b–2–7/93

PRINTED IN U.S.A.

Appendix L

Technical Specifications - Data-Logger

DEVICE SPECIFICATIONS

NI USB-6210

M Series Data Acquisition: 16 AI, 4 DI, 4 DO Bus-Powered USB

The following specifications are typical at 25 °C, unless otherwise noted. For more information about the NI USB-6210, refer to the NI USB-621*x* User Manual available from *ni.com/manuals*.

Caution The input/output ports of this device are not protected for electromagnetic interference due to functional reasons. As a result, this device may experience reduced measurement accuracy or other temporary performance degradation when connected cables are routed in an environment with radiated or conducted radio frequency electromagnetic interference.

To ensure that this device functions within specifications in its operational electromagnetic environment and to limit radiated emissions, care should be taken in the selection, design, and installation of measurement probes and cables.

Analog Input

Number of channels	8 differential or 16 single ended
ADC resolution	16 bits
DNL	No missing codes guaranteed
INL	Refer to the *AI Absolute Accuracy* section
Sample rate	
Single channel maximum	250 kS/s
Multichannel maximum (aggregate)	250 kS/s
Minimum	0 S/s
Timing accuracy	50 ppm of sample rate
Timing resolution	50 ns
Input coupling	DC
Input range	±0.2 V, ±1 V, ±5 V, ±10 V
Maximum working voltage for analog inputs (signal + common mode)	±10.4 V of AI GND

CMRR (DC to 60 Hz)	100 dB
Input impedance	
Device on	
AI+ to AI GND	>10 GΩ in parallel with 100 pF
AI- to AI GND	>10 GΩ in parallel with 100 pF
Device off	
AI+ to AI GND	1,200 Ω
AI- to AI GND	1,200 Ω
Input bias current	±100 pA
Crosstalk (at 100 kHz)	
Adjacent channels	-75 dB
Non-adjacent channels	-90 dB
Small signal bandwidth (-3 dB)	450 kHz
Input FIFO size	4,095 samples
Scan list memory	4,095 entries
Data transfers	USB Signal Stream, programmed I/O
Overvoltage protection for all analog input and sense channels	
Device on	±30 V for up to two AI pins
Device off	±20 V for up to two AI pins
Input current during overvoltage condition	±20 mA maximum/AI pin

Settling Time for Multichannel Measurements

Accuracy, full-scale step, all ranges	
±90 ppm of step (±6 LSB)	4 µs convert interval
±30 ppm of step (±2 LSB)	5 µs convert interval
±15 ppm of step (±1 LSB)	7 µs convert interval

Typical Performance Graphs

Figure 1. Settling Error versus Time for Different Source Impedances

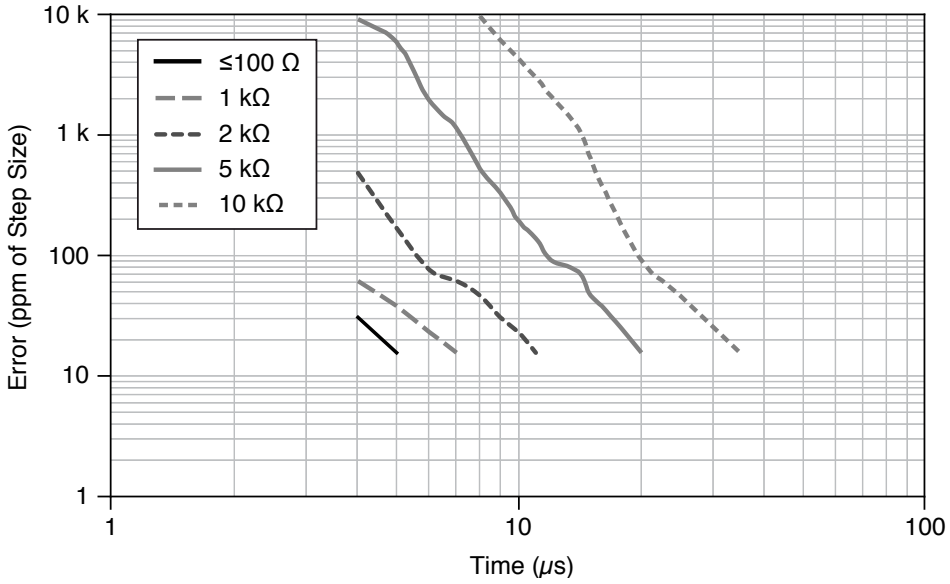

Figure 2. AI CMRR

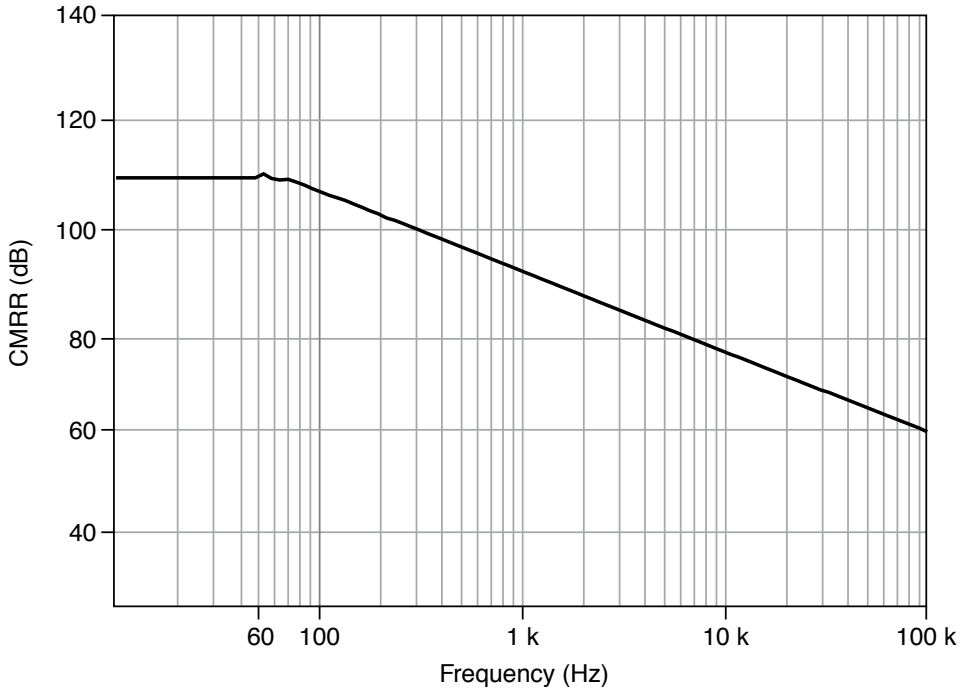

AI Absolute Accuracy

Note Accuracies listed are valid for up to one year from the device external calibration.

Table 1. AI Absolute Accuracy

Nominal Range Positive Full Scale (V)	Nominal Range Negative Full Scale (V)	Residual Gain Error (ppm of Reading)	Residual Offset Error (ppm of Range)	Offset Tempco (ppm of Range/°C)	Random Noise, σ (µVrms)	Absolute Accuracy at Full Scale (µV)	Sensitivity (µV)
10	-10	75	20	34	229	2,690	91.6
5	-5	85	20	36	118	1,410	47.2
1	-1	95	25	49	26	310	10.4
0.2	-0.2	135	40	116	12	88	4.8

Note Sensitivity is the smallest voltage change that can be detected. It is a function of noise.

Gain tempco	7.3 ppm/°C
Reference tempco	5 ppm/°C
INL error	76 ppm of range

AI Absolute Accuracy Equation

$AbsoluteAccuracy = Reading \cdot (GainError) + Range \cdot (OffsetError) + NoiseUncertainty$

$GainError = ResidualAIGainError + GainTempco \cdot (TempChangeFromLastInternalCal) + ReferenceTempco \cdot (TempChangeFromLastExternalCal)$

$OffsetError = ResidualAIOffsetError + OffsetTempco \cdot (TempChangeFromLastInternalCal) + INLError$

$NoiseUncertainty = \frac{\text{Random Noise} \cdot 3}{\sqrt{100}}$ for a coverage factor of 3 σ and averaging 100 points.

AI Absolute Accuracy Example

Absolute accuracy at full scale on the analog input channels is determined using the following assumptions:

- TempChangeFromLastExternalCal = 10 °C
- TempChangeFromLastInternalCal = 1 °C
- number_of_readings = 100
- CoverageFactor = 3 σ

For example, on the 10 V range, the absolute accuracy at full scale is as follows:

GainError = 75 ppm + 7.3 ppm · 1 + 5 ppm · 10 = 132 ppm

OffsetError = 20 ppm + 34 ppm · 1 + 76 ppm = 130 ppm

NoiseUncertainty = $\frac{229\ \mu V \cdot 3}{\sqrt{100}}$ = 68.7 µV

AbsoluteAccuracy = 10 V · (GainError) + 10 V · (OffsetError) + NoiseUncertainty = 2,690 µV

Digital I/O/PFI

Static Characteristics

Number of digital input channels	4 (PFI <0..3>/P0.<0..3>)
Number of digital output channels	4 (PFI <4..7>/P1.<0..3>)
Ground reference	D GND
Pull-down resistor	47 kΩ ±1%
Input voltage protection	±20 V on up to 8 pins[1]

PFI Functionality

PFI <0..3>/Port 0	
Functionality	Static digital input, timing input
Debounce filter settings	125 ns, 6.425 µs, 2.56 ms, disable; high and low transitions; selectable per input
PFI <4..7>/Port 1	
Functionality	Static digital output, timing output
Timing output sources	Many AI, counter timing signals

Maximum Operating Conditions

I_{OL} output low current	16 mA maximum
I_{OH} output high current	-16 mA maximum

Digital Input Characteristics

Level	Minimum	Maximum
V_{IL} input low voltage	0 V	0.8 V
V_{IH} input high voltage	2 V	5.25 V

[1] Stresses beyond those listed under *Input voltage protection* may cause permanent damage to the device.

Level	Minimum	Maximum
I_{IL} input low current (V_{in} = 0 V)	-	-10 µA
I_{IH} input high current (V_{in} = 5 V)	-	120 µA

Digital Output Characteristics

Parameter	Voltage Level	Current Level
V_{OL}	0.6 V	6 mA
V_{OH}	2.7 V	-16 mA
V_{OH}	3.8 V	-6 mA

General-Purpose Counters/Timers

Number of counter/timers	2
Resolution	32 bits
Counter measurements	Edge counting, pulse, semi-period, period, two-edge separation
Position measurements	X1, X2, X4 quadrature encoding with Channel Z reloading; two-pulse encoding
Output applications	Pulse, pulse train with dynamic updates, frequency division, equivalent time sampling
Internal base clocks	80 MHz, 20 MHz, 0.1 MHz
External base clock frequency	0 MHz to 20 MHz
Base clock accuracy	50 ppm
Inputs	Gate, Source, HW_Arm, Aux, A, B, Z, Up_Down
Routing options for inputs	PFI <0..3>, many internal signals
FIFO	1,023 samples
Data transfers	USB Signal Stream, programmed I/O

Frequency Generator

Number of channels	1
Base clocks	10 MHz, 100 kHz

Divisors	1 to 16
Base clock accuracy	50 ppm

Output can be available on any output PFI terminal.

External Digital Triggers

Source	PFI <0..3>
Polarity	Software-selectable for most signals
Analog input function	Start Trigger, Reference Trigger, Pause Trigger, Sample Clock, Convert Clock, Sample Clock Timebase
Counter/timer function	Gate, Source, HW_Arm, Aux, A, B, Z, Up_Down

Bus Interface

USB	USB 2.0 Hi-Speed or full-speed[2]
USB Signal Stream	4, can be used for analog input, counter/timer 0, counter/timer 1

Current Limits

+5 V terminal as output[3]	
Voltage	4.6 V to 5.2 V
Current (internally limited)	50 mA maximum, shared with digital outputs
+5 V terminal as input[3]	
Voltage	4.75 V to 5.35 V
Current	350 mA maximum, self-resetting fuse

Caution Do *not* exceed 16 mA per DIO pin.

Protection	±10 V

[2] If you are using an USB M Series device in full-speed mode, device performance will be lower and you will not be able to achieve maximum sample/update rates.

[3] These devices have a self-resetting fuse that opens when current exceeds this specification.

Power Requirements

Input voltage on USB port	4.5 V to 5.25 V in configured state
Maximum inrush current	500 mA
No load typical current	320 mA at 4.5 V
Maximum load	
Typical current	400 mA at 4.5 V
Suspend current	260 µA typical

Physical Characteristics

Enclosure dimensions (includes connectors)	16.9 cm × 9.4 cm × 3.1 cm (6.65 in. × 3.70 in. × 1.20 in.)
Weight	
Screw Terminal	206 g (7.2 oz)
OEM	73 g (2.5 oz)
I/O connectors	2 16-position combicon
USB connector	Series B receptacle
Screw terminal wiring	16 to 28 AWG
Torque for screw terminals	0.22 to 0.25 N · m (2.0 to 2.2 lb · in.)

Calibration

Recommended warm-up time	15 minutes
Calibration interval	1 year

Environmental

Operating temperature	0 ºC to 45 ºC
Storage temperature	-20 ºC to 70 ºC
Humidity	10% RH to 90% RH, noncondensing
Maximum altitude	2,000 m
Pollution Degree	2

Indoor use only.

Maximum Working Voltage

Maximum working voltage refers to the signal voltage plus the common-mode voltage.

Channel-to-earth ground	11 V, Measurement Category I

Measurement Category I is for measurements performed on circuits not directly connected to the electrical distribution system referred to as MAINS voltage. MAINS is a hazardous live electrical supply system that powers equipment. This category is for measurements of voltages from specially protected secondary circuits. Such voltage measurements include signal levels, special equipment, limited-energy parts of equipment, circuits powered by regulated low-voltage sources, and electronics.

Caution Do not use for measurements within Categories II, III, or IV.

Note Measurement Categories CAT I and CAT O (Other) are equivalent. These test and measurement circuits are not intended for direct connection to the MAINS building installations of Measurement Categories CAT II, CAT III, or CAT IV.

Safety

This product is designed to meet the requirements of the following electrical equipment safety standards for measurement, control, and laboratory use:

- IEC 61010-1, EN 61010-1
- UL 61010-1, CSA 61010-1

Note For UL and other safety certifications, refer to the product label or the *Online Product Certification* section.

Electromagnetic Compatibility

This product meets the requirements of the following EMC standards for sensitive electrical equipment for measurement, control, and laboratory use:

- EN 61326-2-1 (IEC 61326-2-1): Class A emissions; Basic immunity
- EN 55011 (CISPR 11): Group 1, Class A emissions
- AS/NZS CISPR 11: Group 1, Class A emissions
- FCC 47 CFR Part 15B: Class A emissions
- ICES-001: Class A emissions

Note In the United States (per FCC 47 CFR), Class A equipment is intended for use in commercial, light-industrial, and heavy-industrial locations. In Europe, Canada, Australia and New Zealand (per CISPR 11) Class A equipment is intended for use only in heavy-industrial locations.

Note Group 1 equipment (per CISPR 11) is any industrial, scientific, or medical equipment that does not intentionally generate radio frequency energy for the treatment of material or inspection/analysis purposes.

Note For EMC declarations and certifications, and additional information, refer to the *Online Product Certification* section.

CE Compliance CE

This product meets the essential requirements of applicable European Directives, as follows:

- 2014/35/EU; Low-Voltage Directive (safety)
- 2014/30/EU; Electromagnetic Compatibility Directive (EMC)
- 2011/65/EU; Restriction of Hazardous Substances (RoHS)

Online Product Certification

Refer to the product Declaration of Conformity (DoC) for additional regulatory compliance information. To obtain product certifications and the DoC for this product, visit *ni.com/certification*, search by model number or product line, and click the appropriate link in the Certification column.

Environmental Management

NI is committed to designing and manufacturing products in an environmentally responsible manner. NI recognizes that eliminating certain hazardous substances from our products is beneficial to the environment and to NI customers.

For additional environmental information, refer to the *Minimize Our Environmental Impact* web page at *ni.com/environment*. This page contains the environmental regulations and directives with which NI complies, as well as other environmental information not included in this document.

Waste Electrical and Electronic Equipment (WEEE)

EU Customers At the end of the product life cycle, all NI products must be disposed of according to local laws and regulations. For more information about how to recycle NI products in your region, visit *ni.com/environment/weee*.

电子信息产品污染控制管理办法（中国 RoHS）

中国客户 National Instruments 符合中国电子信息产品中限制使用某些有害物质指令(RoHS)。关于 National Instruments 中国 RoHS 合规性信息，请登录 `ni.com/environment/rohs_china`。(For information about China RoHS compliance, go to `ni.com/environment/rohs_china`.)

Device Pinout

Figure 3. NI USB-6210 Pinout

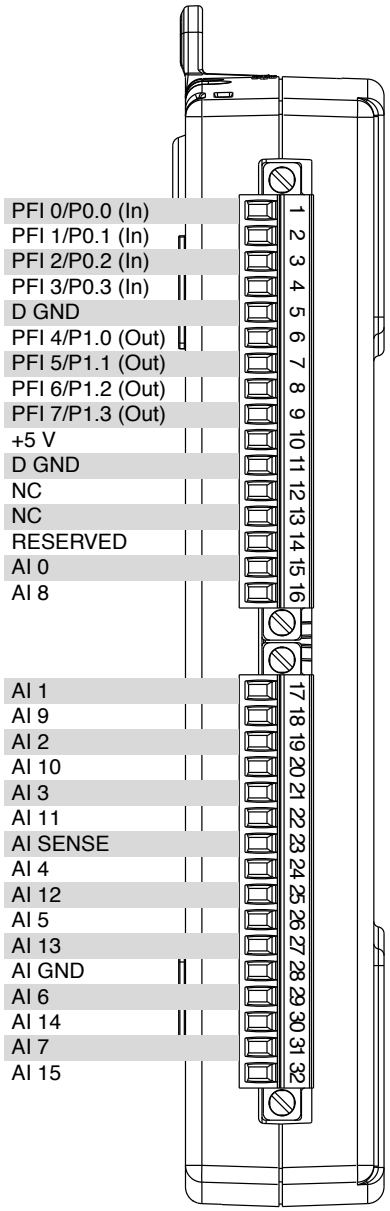

NC = No Connect

Appendix M

Technical Specifications - Cryostat

The right temperature worldwide

LAUDA WK class WK 1200

Circulation chiller

Cat. No. 100 V; 50 Hz / 115 V; 60 Hz: LWG 733

Description

Circulation chiller

1-line LED display for display of actual or set temperature and analogue pump pressure indication

User-friendly menu guidance with simplest 3-key operation

Electronic 2-point temperature control with hysteresis

Safety elements for refrigerant pressure, coil temperature. Level indication

Extremely powerful pressure pump

Adjustable bypass for pressure limiting

Programmable switching contact output

Filler opening at the front, drain tap

Automatic compressor on/off control

Air-cooled version

Technical data (according to DIN 12876)

Working temperature range	0 °C ... 40 °C

Ambient temperature range	5 °C ... 40 °C
Temperature control	± 0.5 °C
Cooling output at 20 °C	1.2 kW
Pump pressure max.	3.2 bar
Pump flow max.	40 L/min
Filling volume max.	23 L
Overall Dimensions (W x D x H)	450 x 550 x 790 mm

Product appearance and specifications are subject to change without notice.

PRINT THIS PAGE **EMAIL THIS PAGE**

LAUDA-Brinkmann, LP | 1819 Underwood Boulevard | Delran, NJ 08075
Phone: (856) 764-7300 | Fax: (856) 764-7307 | Email: info@lauda-brinkmann.com